AD-771 311

# AIRCRAFT VORTEX WAKE DESCENT AND DECAY UNDER REAL ATMOSPHERIC EFFECTS

P. B. S. Lissaman, et al

—

AeroVironment, Incorporated

Prepared for:

Transportation Systems Center

October 1973

AD-771 311

**Technical Report Documentation Page**

| 1. Report No. | 2. Government Accession No | 3. Recipient's Catalog No. |
|---|---|---|
| FAA-RD-73-120 | | |

| 4. Title and Subtitle | 5. Report Date |
|---|---|
| AIRCRAFT VORTEX WAKE DESCENT AND DECAY UNDER REAL ATMOSPHERIC EFFECTS | October 1973 |
| | 6. Performing Organization Code |
| 7. Author(s) *P.B.S. Lissaman, S.C. Crow, P.B. MacCready, Jr., I.H. Tombach, & E.R. Bate Jr. | 8. Performing Organization Report No. DOT-TSC-FAA-73-20 |
| 9. Performing Organization Name and Address<br>AeroVironment Inc.<br>660 South Arroyo Parkway<br>Pasadena CA 91105 | 10. Work Unit No. (TRAIS) R-3106/FA305<br>11. Contract or Grant No. DOT-TSC-523 |
| 12. Sponsoring Agency Name and Address<br>Department of Transportation<br>Federal Aviation Administration<br>Systems Research and Development Service<br>Washington DC 20591 | 13. Type of Report and Period Covered<br>Final Report<br>September 1972 - February 1973<br>14. Sponsoring Agency Code |

15. Supplementary Notes

*Under contract to: Department of Transportation
Transportation Systems Center
Kendall Square, Cambridge MA 02142

16. Abstract


Aircraft vortex wake descent and decay in a real atmosphere is studied analytically. Factors relating to encounter hazard, wake generation, wake descent and stability, and atmospheric dynamics are considered.

Operational equations for encounter hazard, wake generation, and atmospheric dynamics are given, including a brief description of a possible automatic meteorological system to provide atmospheric data for an airport wake forecasting program.

A new analysis for Crow Instability in ambient turbulence is given, expressing time-to-linkage as an explicit function of the turbulent dissipation. The analysis is well corroborated by flight tests although only limited data is available.

Wake descent in a stratified inviscid fluid is studied analytically providing new results for this problem. According to the present theory, the vortex span reduces upon descent into a stably stratified flow, causing the rate of descent to increase. Exact solutions are derived for vortex cell shapes in a uniformly sheared crosswind, showing that the upwind cell is greatly increased in size. It is believed that this may partly account for the observed unsymmetrical behavior (banking, etc.) in crosswinds.

A discussion of core bursting and turbulent wake entrainment during descent is given, with some tentative formulations for the latter. Full understanding of these two aspects must still be considered incomplete.

Finally, an assessment of the remaining problems is given, with recommendations for further analytical and flight test research.


| 17. Key Words | 18. Distribution Statement |
|---|---|
| Wake vortices, Atmospheric effects, Vortex transport and decay, Kolmorgorov Spectra | DOCUMENT IS AVAILABLE TO THE PUBLIC THROUGH THE NATIONAL TECHNICAL INFORMATION SERVICE, SPRINGFIELD, VIRGINIA 22151. |

| 19. Security Classif. (of this report) | 20. Security Classif. (of this page) | 21. No. of Pages | 22. Price |
|---|---|---|---|
| Unclassified | Unclassified | ~~223~~ 211 | $5.50/1.45 |

Form DOT F 1700.7 (8-72) Reproduction of completed page authorized

## PREFACE

There exists a massive body of literature on aircraft wake vortex research. As an aid for further work, a new bibliography has been prepared. The base of this list has been taken from the excellent listing given by McCormick, 1971: Aircraft Wakes: A Survey of the Problem (FAA Symposium on Turbulence, Washington, D. C.). This base has been complemented and updated by AeroVironment and is believed to be very comprehensive. The actual report refers to only a portion of these papers, and contains other references which are not directly concerned with vortex wakes. Thus, for ease of reading, a separate reference list has been prepared, containing only those papers quoted in this report.

It is pointed out that this is a first report, and by the nature of this particular subject, contains hypotheses and suggestions for which conclusive experimental data is still lacking. A second report will appear later in 1973 by which time more analytical and experimental data will be available. It is believed that this new research should settle some of the crucial questions identified in this report.

TABLE OF CONTENTS

## LIST OF ILLUSTRATIONS

LIST OF ILLUSTRATIONS (Cont.)

## LIST OF TABLES

# 1. INTRODUCTION

The hazards posed to following aircraft by the vortex wake system of a large airplane are well-known. In order quantitatively to assess the hazard, as an aid in designing wake avoidance systems, it is evidently necessary to know where the wake is, what its strength is, and what the danger to an encounter aircraft is. These three aspects are addressed in this report.

The hazard determination depends upon the strength of the wake and the response/control characteristics of the encounter aircraft. For a given wake this becomes a problem in aircraft dynamics, and the specialized aspects of this are not treated here, but in Section 3 simple danger indices are derived. The technology is available for the refinement of these indices, but in view of the uncertainties of wake strength and position, such extra precision may not be required.

The main thrust of this report is directed at the determination of wake strength and position. These characteristics are fundamentally connected with the initial parameters of the wake. Section 2 describes the mechanism of vortex sheet generation and roll-up. It is believed that this aspect, essentially an aerodynamic problem, is reasonably well understood and quantified.

After roll-up, we are concerned with the descent and decay of the wake in a real atmosphere. This atmosphere contains omnipresent turbulence, buoyancy, wind shears and wind gusts. Effects of these dynamic characteristics of the atmosphere on the vortex wake are very poorly understood and experimental data is limited. The major portion of this report, Sections 4 and 5, addresses itself to the principal elements of of this interaction, with the goal of arriving at quantitative expressions for these effects so that operational predictive equations can be derived.

Finally, to specify the atmospheric inputs, it is necessary to be able to infer or predict the turbulence, shear and other atmospheric dynamic properties from the basic meteorological observables. Section 4 shows how this may be done by using various earth boundary layer models and the large body of statistical meteorological data.

## 2. LIFT AND VORTEX GENERATION

The process of lift generation and vortex shedding on a continuous wing is well understood. Thwaites (1960) gives an excellent review of modern wing theory. We note that the determination of the spanwise and chordwise loading on a wing is not of concern here, but that a vast volume of literature treating this subject exists and modern lifting surface theory (as employed by all the major aircraft companies) gives a prediction of the wing characteristics and performances which correlates very well with experimental tests. For our purpose we are concerned with the way in which the trailing vortex core system is connected to the bound vorticity on the wing. For the moment, we will discuss a wing in attached flow with a continuous trailing edge; that is, where there are no special disturbances due to flaps or propulsion or fuselage attachments.

The vorticity on the wing itself is principally of spanwise orientation and associated with the wing boundary layer. If the wing is at zero lift this vorticity is shed oriented approximately parallel to the trailing edge and results in a low energy planar wake in which the velocity perturbations are mainly in the direction of the free stream, and represent a reduction in the free stream velocity associated with the viscous drag of the wing. The momentum loss in this wake can be directly connected to that in the boundary layer and is represented in an integrated form in the profile drag coefficient of the wing, $C_{Do}$. The downstream development in the non-lifting case consists of entrainment of outer flow air and a general coalescence of the wake cross-section from a sheet to an ellipse and finally a circle. However, these details are not important since we are interested in the lifting case, when the downstream development is dominated by the lift induced effects.

If the wing is lifting, an additional vorticity component is generated at the trailing edge. This vorticity is shed parallel to the local

velocity vector, that is, approximately in the direction of the free stream. It can be shown that the vorticity shed at each spanwise station is exactly equal to the gradient in spanwise lift at that station. It is this vorticity which rolls up to form the trailing vortex pair and with which the induced drag $D_i$ is associated. This vorticity creates (or is created by) the sidewash and downwash fields downstream of the wing and does not directly produce streamwise flows; however, as is shown later, viscous effects control the rollup of this vortex system and ultimately cause streamwise velocity perturbations which couple with the profile drag vorticity to create axial flows in the vortex core.

Continuing the analysis of classical wing theory, a number of significant (and exact) results can be developed for the relationships between spanwise loading, induced drag, and the final vortex position.

We write the spanwise circulation loading as

$$\Gamma = 2Ub \sum_{1}^{\infty} A_n \operatorname{Sin} n\theta \quad , \qquad n \text{ odd}$$

where $\cos\theta = \eta$ is the normalized span coordinate, U is the flight speed, and b the wing span. For symmetrical loadings only odd n is required. Then the center section circulation $\Gamma_o$ is given by

$$\Gamma_o = 2Ub \sum_{1}^{\infty} (-1)^{\frac{n-1}{2}} A_n$$

while the lift L and induced drag are given by the formulas

$$L = q\, b^2 \pi A_1$$

$$D_i = q\, b^2 \pi \sum_{1}^{\infty} n A_n^2$$

where q is the dynamic pressure $1/2\,\rho\,U^2$. A significant term in the downstream core development is the vortex span $b_v$. This can be shown to be equal to the centroid of the shed vorticity (for conservation of lift), and thus we obtain

$$b_v = \frac{\pi b}{4} \frac{A_1}{\sum(-1)^{\frac{n-1}{2}} A_n} = \frac{4}{\pi} \cdot \frac{L}{\rho U \Gamma_o}$$

These simple results are usually derived from lifting line theory, but it is worth noting that they are exact for all planar wings (even of low aspect ratio) providing that vorticity is shed only from the trailing edge.

It is usual to consider only elliptically loaded wings implying $A_n = 0$, $n > 1$. We remark that for any continuous loading the additional coefficients may be found by Fourier analysis and the more precise results determined. However, deviations from the elliptical loading for aircraft wings in the clean condition are usually small. As an illustration we quote results from Thwaites for a number of different untwisted planforms. We exhibit these as factors for comparison with the elliptical results. Thus for an untwisted elliptical wing we get

$$D_i = \frac{L^2}{q\pi b^2} \quad , \quad b_v = \frac{\pi b}{4}$$

while for the other wings we write

$$D_i = K_D \frac{L^2}{q\pi b^2} \quad , \quad b_v = K_v \frac{\pi b}{4} \quad .$$

Typical extreme cases are listed below for a wing of aspect ratio 6.

| | $k_D$ | $k_v$ |
|---|---|---|
| Straight Constant Chord Wing | 1.05 | 1.11 |
| Straight Pointed Wing (taper ratio 1) | 1.14 | .82 |
| 45° Swept Constant Chord Wing | ~ 1.08 | 1.12 |

We note that these cases give quite different spanwise vorticity loadings. Compared with the elliptical, the pointed wing has increased inboard loading. The swept wing has inboard loading significantly lower than that at about 60% span (the so-called saddleback loading), while the rectangular wing has relatively high tip loading. However, even in these extreme cases (within normal wing proportions) there is not very much difference in the final vortex span or the induced drag.

It should also be recalled that most aircraft wings are aerodynamically twisted so that the distribution at cruise will be nearly elliptical -- thus they will not exhibit such extreme loading distributions as the untwisted planforms noted above.

On these grounds we note that the elliptical assumption is certainly adequate for most practical wings for our purposes, especially in view of the much cruder assumptions inherent in analysis of the vortex wake development. However, if required, the precise determination of the global vortex properties can readily be made by the formulae above.

When the wing is in the dirty condition, with flaps extended, the remarks about elliptical loading no longer apply. However, the three equations for L, $D_i$ and $b_v$ still obtain and the calculations can still be conducted. With part span flaps the circulation distribution contains gradients which are logarithmically singular at the discontinuity, which means that many terms in the sine expansion must be used for an accurate determination of $D_i$ and $b_v$. This can be avoided by introducing

an additional circulation function capable of exactly matching the discontinuities in airfoil effective angle at the flap extremities. Using this stratagem a very accurate solution can be obtained with only a few terms. A modern development of this technique applicable to chord and twist discontinuities is given by Lissaman (1973). This method has been programmed and is available at NASA (Langley). It represents an exact solution for the problem discussed here.

The effect of inboard flaps is greatly to increase $k_D$ and to reduce $k_v$. These changes are such that the elliptical estimate is certainly no longer valid, and each flap type circulation loading should be analyzed as described above.

As an illustration of this effect, take a wing of aspect ratio 5 with 30% chord half-span inboard flaps deflected at $8^\circ$. Taking the lift distribution from a similar arrangement given by Bilanin and Widnall (1973) we obtain:

| | $k_D$ | $k_v$ |
|---|---|---|
| Straight Constant Chord Flapped Wing | 1.31 | .757 |

The circulation loading distribution of a wing defines all the properties of the inviscid vortex development. However, as pointed out above, for most vortex development purposes only a few characteristics of this distribution are required; the zero moment for the lift, and the center section bound vorticity for the centroid of lift. In addition, we require the induced drag which theoretically involves all moments and is actually quite strongly dependent on higher terms in the sine expansion

One further moment will prove useful; the moment of momentum, that is. the angular momentum of the fluid rotating around the vortex sheet. It has been shown by Betz (1933) that this can be conveniently evaluated by taking the second moment of the shed vorticity about any

spanwise position. A convenient position is the centroid of this vorticity. This term $M_m$ can also be expressed compactly in the Fourier coefficients as

$$M_m = \rho b^3 U^2 K_m$$

and $$K_m = \sum_1^\infty \frac{(-1)^{\frac{n+1}{2}} A_n}{n^2 - 4} - \frac{\pi^2}{64} \frac{A_1^2}{\sum_1^\infty (-1)^{\frac{n-1}{2}} A_n} .$$

Physically, $M_m$ has the dimensions of a moment, and represents the moment applied to the air about the centroid of vorticity by one side of the wing. It can quite easily be evaluated mechanically if the spanwise loading is known by taking the moment of this load about the centroid of vorticity.

We now note that we have developed expressions for the six major parameters of the trailing vortex sheet. These are the lift, the induced drag, the moment of momentum, the vortex span, the total bound vorticity, and the profile drag. The first five of these can be expressed directly from an analysis of the spanwise loading curve. Only four of these are actually independent in that $\Gamma_o$ can be determined from $b_v$ and $L$. The profile drag $D_o$ can readily be determined from standard drag determination methods. The total drag $D_T = D_o + D_i$.

Thus we can consider the vorticity sheet shed at the wing trailing edge to be determined (in a global sense) by $L$, $D_T$, $M_m$, $b_v$, $\Gamma_o$.

## Rollup and Development of the Vortex Sheet

After leaving the wing, the shed vorticity undergoes a series of complicated convolutions until it is finally diffused into the atmosphere. We can arbitrarily define four stages to this process, in which fairly distinct interactions occur. These are shown in Figure 2.1 and can be thought of as the Planar Sheet Stage, the Rollup Stage, the Viscous Vortex pair stage, and the Distributed Impulse stage. Our main interest is in the latter two. They are, of course, controlled by the initial conditions, which come from the Planar Stage discussed in the previous section.

After leaving the wing, various mutual inductions cause the vortex sheet to curl up at the tips and to form a scroll-like shape and initiate the rollup stage. Within about 20 spans this has developed into a viscous vortex pair of strength and span $\Gamma_0$, $b_v$ and having a finite core within which the vorticity is contained. Many authors (see Bibliography) have attempted to describe this rollup process but the proper analysis is still highly controversial. We will not specifically discuss these analyses here except to state that the results of numerical free vortex schemes should be regarded with caution. While these techniques in principal exactly treat the self-induced development of the trailing vortex sheet, the necessary discretization for computer operation may be expected to introduce instabilities and motions related more to the discretization and computer scheme than to the actual deformation of the vortex sheet. This is particularly true if the vortex sheet is modeled by a set of discrete line vortices. For our purposes we are not concerned with the details of the rollup process because this occurs so close to the wing.

The next stage is the viscous vortex development, which is discussed in more detail in a following chapter, and finally the decay to

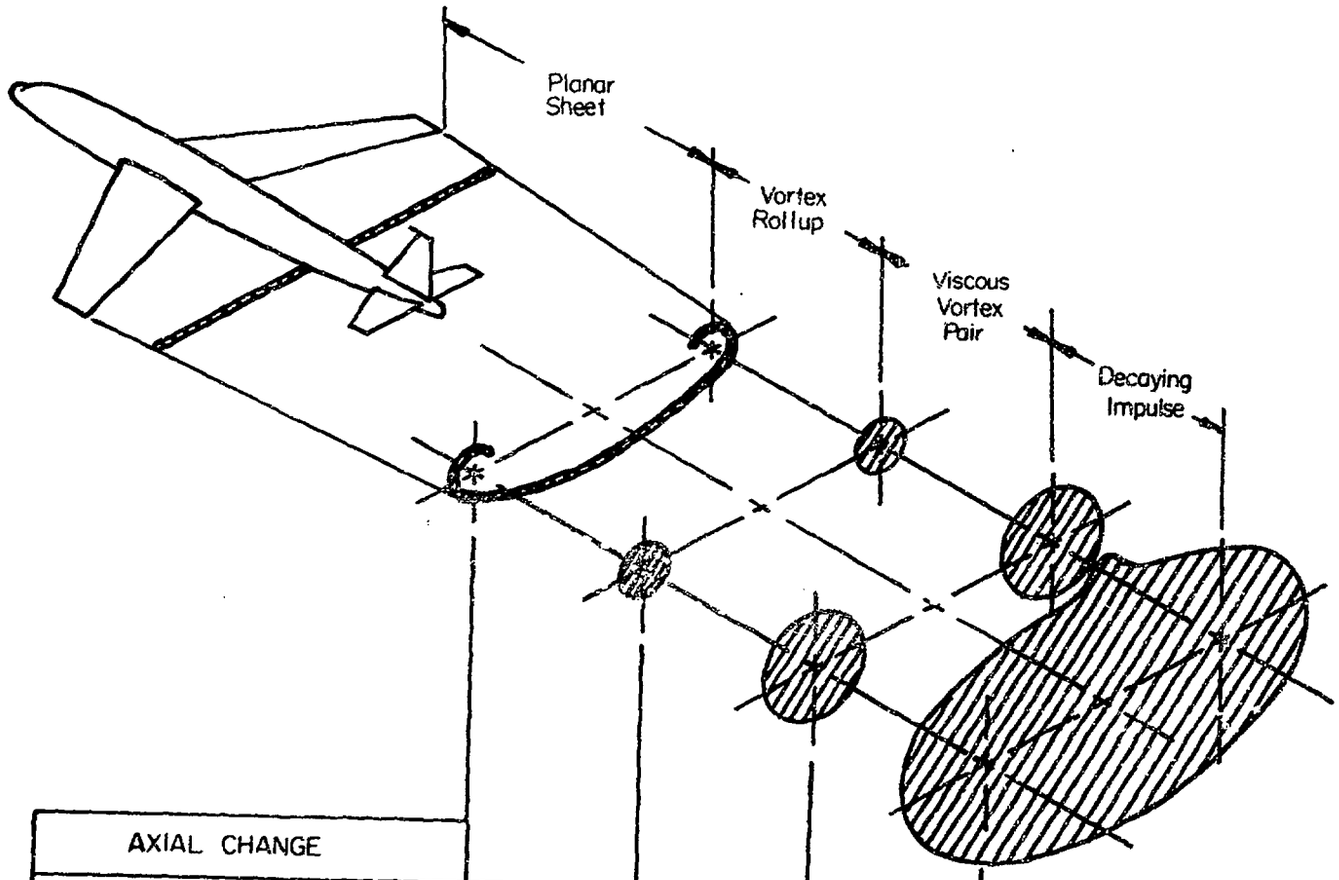


| AXIAL CHANGE | | | |
|---|---|---|---|
| Vortex Span, $\frac{db_v}{dz}$ | = 0 | = 0 | > 0 |
| Circulation, $\frac{d\Gamma}{dz}$ | = 0 | = 0 | < 0 |
| Total Head, $\frac{dH_L}{dz}$ | = 0 | < 0 | < 0 |

Figure 2-1. Stages of Wake Vortex Development

the distributed impulse (also considered in more detail in the Transport Section, 4).

To assist in the discussion of this development, we describe the various global invariants in the process. Evidently the lift and drag must be conserved throughout the development. Now we note the other terms; shed vorticity and moment of momentum are actually null for the entire wing and can be defined only for one half wing. However, provided there is no viscous interaction between the two sides (left and right) of the vortex system, then even in a viscous fluid we will find that $M_m$ and $\Gamma_o$ are conserved. We note by the kinematic condition of the solenoidal quality of vorticity, that even though the vorticity is diffused into originally irrotational flow, $\Gamma_o$ must be conserved until vorticity from the one core interacts with the other on the center line. The moment of momentum is conserved according to the same arguments. A physical interpretation of this is that no external torque can be applied to the vortex core and its surrounding flow system until appreciable vorticity has reached the center line. We comment here that as long as the flow on the center line is symmetrical even introducing viscous transfer in the equations will produce no shear along the center line since velocity gradients there are zero.

Thus during the rollup and the viscous pair stage a good assumption may be to conserve $M_m$ and $\Gamma_o$. In the final decaying impulse stage we will expect $M_m$ and $\Gamma_o$ to decay according to transfer processes, both of molecular viscosity and turbulence.

We have not discussed the variation of $H_o = p/\rho + \frac{1}{2} V^2$, the total head of the flow. This provides a local flow property (as opposed to global properties) which is useful to us. We note that at the wing trailing edge there is already a sheet of low energy air shed from the boundary

layer, having dimensions scaled by the span and the trailing edge boundary layer displacement thickness, and containing a total head deficit relating to the boundary layer momentum thickness. This wake will entrain external flow in the way normally associated with a non-lifting velocity deficit wake.

Of more interest is the entrainment and head loss due to the rotational flow associated with the sidewash and downwash flows connected to the induced drag. This effect features in the swirling viscous interaction which develops the axial flow in the vortex core. For convenience we define $H_L$ as the head loss connected with the lifting flow. It seems that this term becomes significant only in the vortex pair and decay stages.

It is noted that the global force and local energy relationships are not sufficient to solve for the details of the vortex development. However, they provide a useful insight into the processes occuring and can be very helpful in assessing different theoretical analyses, most of which contain direct or implicit statements relating to assumptions concerning these quantities.

## 3. THE ENCOUNTER HAZARD

Evidently, if conditions are such that an aircraft encounters a vortex wake while the wake is still in the organized state, consisting of two near-axial viscous vortices, the hazard will be a function of some parameters describing the strength and geometry of the wake, coupled with further factors relating to the control power and design load factors of the encounter aircraft. Other parameters in this situation are the flight path relative to the wake of the generating aircraft, and, of course, the proximity to the ground of the encounter.

Initially, we shall consider the case of the encounter aircraft entering the eye of one of the trailing vortices on a flight path approximately parallel to the vortex axis. In these circumstances a severe rolling moment will be induced on the encounter aircraft. It would at first appear that the magnitude of the rolling moment would be closely related to the core development, that is, the vortex age. However, when one assumes that the core will be less than 2/10 of the generating span, and that outside this the flow very closely approaches that of a horseshoe vortex, we see that much of the encounter aircraft wing for an encounter span of about 1/2 the vortex span, will be in the inviscid portion of the flow. Coupling this with the fact that the contributions to rolling moment vary directly with the spanwise position, we may expect that the actual size of the core will not be too important providing it is less than a certain fraction of the encounter span. On this basis, Crow (1971) has shown that the induced rolling moment will be proportional to $\Gamma_g / b_e^2$, where $\Gamma_g$ is the strength of the generator aircraft vortex and $b_e$ the span of the encounter aircraft. If it is then assumed that there is a certain maximum aileron induced roll rate of the encounter aircraft, $P_{max}$, one can assert that hazardous conditions will be obtained when the ratio of vortex induced roll to aileron rolling power exceeds a certain value. Writing the trailing vortex

strength in terms of lift coefficient, $C_L$ , span b , and aspect ratio, A we define this ratio below.

If the critical rolling rate of the encounter aircraft is $P_{max}$ (in radians per second), the non-dimensional danger factor D , expressing the hazard, can be written as

$$D = (b U C_L/\pi A)_g/(b^2 P_{max})_e$$

where the suffice g applies to the generator aircraft and e to the encounter aircraft. It has been estimated by Crow from Boeing tests by Condit and Tracy (1971) that a value for D of about unity is a good measure of critical hazard. If D exceeds this value, dangerous bank attitudes may be expected. At low altitudes a smaller D value will be appropriate since recovery time is reduced.

The danger factor has a very compact formulation and it will be noted that it contains no term relating to the distance behind the generator aircraft. This is a significant simplification and relates to the slow growth of the core and the invariance of the total circulation. A more detailed but still idealized analysis of the induced rolling moment conducted by Condit and Tracy (1971) shows the separation distance dependence. Taking the results of their numerical calculations, we see that the danger factor is in fact almost invariant with separation distance. For example, using dimensions appropriate to a B707 we find that the more precise analytical calculations will give a normalized reduction in induced rolling moment of about 2.5% per nautical mile behind the generator aircraft. These numbers are substantiated by flight tests on Boeing aircraft reported in the same paper.

It is noted that at first this appears to contradict the results of Bisgood, Maltby and Dee (1971) who use Squire's Theory to compute

wake dissipation and exhibit a theoretical curve showing a rather marked reduction in rolling rate with vortex age. This curve is for an assumed eddy viscosity of $.004\Gamma_o$ ($\Gamma_o$ being the vortex strength). However, the paper shows eddy viscosity inferred from flight measurement of core velocity peaks, indicating that the effective eddy viscosity according to this theory is more like $.0002\Gamma_o$ with some readings as low as $.00018\Gamma_o$. Using the value of $.0002\ \Gamma_o$ and conducting a similar analysis would show the reduction in rolling rate to be about 5% per nautical mile, which is more in line with the more modern and comprehensive Boeing tests.

Now, we should consider the other real factors associated with vortex entry in a near axial direction. These relate to control reversals as the encounter aircraft traverses the vortex laterally or enters the other vortex, as well as the coupled yaw-roll dynamics associated with the effect of the vertical stabilizer. Such excursions due to random oblique encounters will introduce hazard elements of more significance than those computable by simple axial vortex decay and thus justify ignoring the latter effect.

On these grounds it is believed that the danger factor D represents a useful criterion for the vortex hazard due to near axial encounters, and the assumption that D is invariant with separation distance is a significant and valid simplification. The critical value of D will depend on the aircraft ground proximity.

It must be remarked here that while the danger factor is invariant with vortex age or separation distance, its existence depends upon there being an organized viscous vortex; thus once the regular motion has been disrupted by sinuous or core instability the danger factor will change. This illustrates the importance of the understanding and prediction of the catastrophic instabilities.

The other critical mode, the encounter normal to the trailing vortices, is somewhat less simple to handle. In principle it involves the

same factors. The disturbance system will be described in terms of the peak vertical velocities and their spacing, while the response system now relates to the longitudinal transfer function of the encounter aircraft. Confining the analysis to the encounter with only one core of the vortex pair, it has been shown by Houbolt (1971) that the maximum normal acceleration N of the encounter aircraft can be written in a form involving the wing loadings and speeds of both aircraft, the aspect ratio of the generating aircraft and the transfer function of the encounter aircraft. This transfer function ($k_t$) is of course related to relative mass of the encounter aircraft as well as the ratio of its chord to the vortex core. A curve for this is given by Houbolt, which shows fairly weak variation with relative mass and core radius. We write Houbolt's equation in the same terms as the Crow axial danger factor, and assume a relatively high value of $k_t$ of .85 (to round off numbers), then obtain a transverse danger factor $D_T$ as

$$D_T = 20(UC_L/\pi A)_g/(NUC_L)_e$$

where N is the limit normal acceleration factor of the encounter aircraft. On this basis, a value of $D_T$ exceeding unity may be regarded as hazardous.

We now note that the ratio of these terms will indicate the relative severity of axial or normal encounter. Thus we obtain

$$D/D_T = b_g(NUC_L/20b^2 P_{max})_e$$

Noting that a normalized roll rate, $\frac{bP_{max}}{2V}$, of about .07 is usually attained, we can write this as

$$D/D_T = 0.35(NC_L)_e \, b_g/b$$

Now, taking representative transport aircraft values of $N \sim 4.5$, $C_L \sim .6$ we see that the ratio of the danger factors is approximately equal to the span ratio, showing that in all significant cases (smaller encounter aircraft) $D > D_T$ so that the axial encounter can be expected to be more hazardous.

# 4. VORTEX TRANSPORT

## 4.1 GENERAL

The trailing vortex pair creates an induced field which causes the vortex system to convect downwards. This vertical speed is relatively small compared to the flight speed. Making the classical assumptions of elliptical loading and inviscid rollup to a finite vortex pair, we obtain for the downwash velocity U*

$$U^*/U = 4C_L/\pi^3 A$$

We note for a typical wing of aspect ratio 6 that the downward motion may be about 1% of the flight cruise speed, increasing to 3 or 4% at the landing state.

This can be compared with the same ratio before the sheet has rolled up, which is about $(C_L/\pi)\{1/A + 1/\pi\}$ at the trailing edge, taking into account the bound vortex term, and about $2C_L/\pi A$ a few spans downstream. Thus for the first few spans the downwash may be about four times that of the final state; however, our interest is with the motion after the vortex pair has developed. Field observations have indicated that apparently in all cases the vortex descent rate is approximately constant for 30 - 40 seconds, then begins to reduce. Condit and Tracy (1971) report that in no cases have descents of more than about 1000 ft been observed, while the recent experiments of Tombach (1972) show a distinct reduction in transport velocity. However, we stress that definitive measurements of vortex descent rate are lacking. We discuss this further in the vortex decay section. It appears clear that after about 60 seconds the descent rate is not adequately described by the classical equations.

If the pair is immersed in a uniform crosswind, standard calculations indicate that the pair should simply be laterally convected with the crosswind, with no change in cell shape or vortex dynamics. This appears to be the case.

For a vertically non-uniform crosswind the situation is less simple. The pair is now immersed in a field containing a directed organized vorticity and one would expect various unsymmetrical effects such as vortex tilting to occur.

The simplest case, that of a uniformly sheared crosswind (linear wind profile), can be solved exactly in the inviscid case. This possesses a steady solution in a frame of reference fixed in the vortex cores, and for the inviscid model gives no banking or change in transport speed. This analysis is developed in a later section. It is simply noted here that the reason this problem can be solved is that although the external vorticity is redistributed by the vortex field, this does not introduce any unsteadiness in the flow since the redistribution does not change the uniform vorticity field in which the cell is immersed.

If one considers a field having a shear gradient, then even the inviscid problem becomes unsteady because of the redistribution of the non-uniform ambient vorticity. An unsteady model was utilized by Burnham (1972) in attempting to model the ground effect case with a non-uniform crosswind. A finite set of discrete vortices was introduced into the ambient field and permitted to convect with the flow. This model is an attempt to explain the observed rising of one of the vortices near the ground. It is believed that this model would give different quantitative vortex paths for different or more detailed models of the same crosswind field. We note too, that Bisgood, Maltby, and Dee (1971) modeled the vortex trajectory in ground effect with a non-uniform crosswind simply by computing the convection at each height and taking no account

of vorticity redistribution. This simple kinematic model gave excellent correlation with the observed vortex paths, at least for the few reported tests.

We note here that a large proportion of the tests conducted by Tombach exhibited unsymmetrical vortex response under crosswinds. This was normally observed in the vortex pair banking, and occasionally in the collapse of one vortex due to core bursting. Such behavior might be expected under the ambient conditions described, where interaction between the ambient and core vorticity could cause strong anti-symmetric effects both with respect to vortex transport and core development. Changes in core development could accelerate the instability of one element of the pair.

One of the more important effects of unsymmetrical core bursting might be expected to be the development of the solitary vortex. In a number of tests reported by Tombach it was observed that when only one vortex remained (or at least was visible) this vortex appeared to have a much longer life than usual, and did not show any signs of sinuous Crow Instability.

It appears that if these unsymmetrical effects are due to wind shear, then they should certainly be primarily attributable to the uniform shear case and that it should not be necessary to postulate a non-uniform shear to describe them. The basis for this is twofold, the first reason being that these effects have been observed at altitudes at which the uniform shear is weak and the shear gradient even weaker; the second that any viscous model will indeed give anti-symmetric behavior when immersed in a uniform shear field.

Thus while an inviscid uniform shear model will not give any vortex tilting, it is believed that the uniform shear is the dominant

effect and that a combined uniform shear/viscous decay model should be sufficient to account for vortex behavior in a general crosswind. This is described in Section 4.3

A further factor complicating the descent dynamics is the effect of flow stratification. The previous paragraphs have described the situation in a homogeneous fluid with the main effects due to entrainment or ambient organized vorticity. If the atmosphere is stratified as is frequently the case, one would certainly expect this to have some effect on the descent rate. At the moment, both the sense of the effect and its magnitude are controversial. Contrary to intuition, it appears that descent does not necessarily slow down in a stable stratification; that is, the cell is not necessarily retarded on penetrating the denser medium. Physically, this anomalous behavior is accounted for by the contraction of the vortex span -- the problem is whether the span does in fact expand or contract and at what rate. In a later section we develop a new theory which shows that an inviscid, stratified model does imply a span contraction and consequent acceleration of the downward descent. More details and an evaluation of these assumptions are made in the section.

It should always be recalled that in practically all cases the organized vortex pair motion is terminated by sinuous instability or by core bursting. This is the element which makes experimental data on descent rate so incomplete.

In the following sections we assume that an organized vortex pair motion exists and discuss in more detail three important cases: the descent in a homogeneous irrotational fluid, the descent in a homogeneous fluid of uniform rotation, and the descent in an irrotational fluid of uniform stratification.

Thus, if we consider the descent rate to be characterized by $U^* = U^*(Z, 1/T)$ where $Z$ is the ambient vorticity and $T$ the Brunt-Vaisala time (a measure of the stratification) we attempt to describe the problems

$$U^* = U^*(0, 0)$$
$$U^* = U^*(Z, 0)$$
$$U^* = U^*(0, 1/T)$$

Evidently a full analysis of the general problem cannot be achieved until the special cases above are understood and quantified. However, we note that a validation of the above cases may be difficult because it must depend on one of the atmospheric parameters approaching zero in the field test.

## 4.2 NEUTRAL IRROTATIONAL FIELD

After the wing vortex sheet has rolled up, the trailing system consists of a pair of vortices of finite rotational core area, but with the core radius a relatively small fraction of the vortex span. If this vortex pair is immersed in a still homogeneous inviscid flow, a well known classical solution exists under which the pair is convected downwards at a velocity $\Gamma_0/2\pi b$. The classical analysis shows that there is a closed recirculating mass of air, of roughly oval proportions, associated with the concentrated vortex pair, and that this cell is convected downwards at a uniform speed. Flow exterior to this cell never enters it. On this basis a long vortex pair, which may be regarded as substantially two-dimensional, will move downwards in an unbounded fluid with constant velocity for all times.

In real flows this situation does not persist indefinitely, and most experiments appear to show the rate of descent to reduce and finally approach zero. This is certainly due to diffusion of core vorticity by some combination of laminar and turbulent viscosity and will occur even in homogeneous (unstratified) flows. Much effort has gone into explaining and quantifying this effect, but the subject still remains controversial. Recently a new rational interpretation of this, coupled with careful observations, has been put forward by Maxworthy (1972) which greatly assists explanation of the effect.

Maxworthy conducted experiments with vortex rings in water, using various visualization techniques to identify where the flow went. When the vorticity was relatively well distributed in the ring he observed that the outer flow was entrained into the back of the cell, causing an increase in the cell volume. At the same time a portion of the cell vorticity was shed into the wake, removing both vorticity and momentum from the cell. The combined effect of this is to increase the cell size and to reduce its propagation velocity.

The mechanism of entrainment is important for our further development. Figure 4-1 shows a sketch of this flow field, in coordinates fixed at the core centers, so that the outer flow is represented by a uniform but unsteady flow from below. We note that the cell has a well defined stagnation point, A , and over the front portion, a well defined cell boundary, A-B . Across this boundary the pressure and velocity fields of inner and outer flows are continuous, the only discontinuity being between the inner vortical fluid and the outer irrotational flow. Due to both laminar and turbulent effects, this vorticity is transferred to the outer flow, and as a consequence the total head of the flow is reduced. Thus, after passing the maximum velocity point near B , the outer flow, contained approximately by the stream tube CD , is unable to recover sufficient velocity to rejoin the outer flow at the rear, but remains as part of the stationary cell. Thus the cell size is increased. At the same time, a neighboring stream tube EF acquires a smaller amount of vorticity and suffers less head reduction, so that is does depart from the cell at the rear, but at a lower than free stream total head. This portion develops into a wake behind the cell.

Thus the same process causes entrainment of the outer flow into the cell and a detrainment (removal) of some of the cell vorticity and momentum. A further process occurs on the centerline of the cell, AX. Here vorticity is annihilated by diffusion from the left and right cells. Thus three vorticity transfer mechanisms occur and the overall effect controls the cell dynamics.

Maxworthy showed that initially the vortex shedding to form the wake was extremely weak, since the cell vorticity at the boundary was quite weak. Thus, although the cell grew in size, it did not lose momentum, and the impulse I was conserved. In these circumstances the main vorticity loss occurred along the centerline and was small, and there was minimal wake momentum loss. During the later stages in growth history, when more vorticity is present near the boundary, the

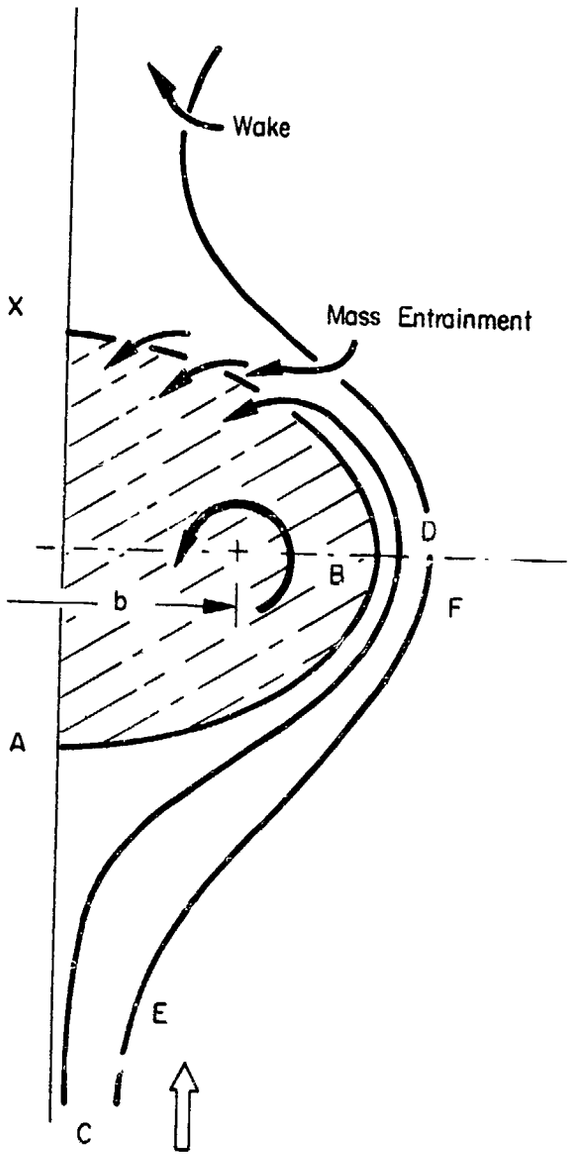


Figure 4-1. Viscous Effects on Vortex Cell.

wake develops; thus the impulse in the cell reduces while the cell size increases. Both these effects contribute to the reduction in speed and final complete annihilation of the cell momentum.

It must be noted that Maxworthy's experiments were conducted with vortex rings at extremely low Reynolds Numbers, when the flow was certainly laminar. Maxworthy has indicated in a private communication that further flow visualization tests with finite wings also exhibited a detrained wake. These experiments were also at very low Reynolds Numbers. It is, however, possible that during the later stages of development of an aircraft trailing vortex system that similar processes of mass entrainment and momentum detrainment occur. For laminar transfer the time scales would be too long to be of interest, but if the transfer is assumed turbulent, it may be possible to account for some of the observed effects. Thus it appears very probable that the later development of a vortex pair follows qualitatively the stages described by Maxworthy; with an additional initial stage which we will discuss. We therefore postulate three stages as shown in Figure 4-2.

Stage I - The Inviscid Cell. Here the vorticity is confined to well within the cell boundary. On the boundary itself there will be no laminar transfer (since there is no distortion) and turbulent transfer will have no net effect, since both inner and outer flow have the same total head. In these circumstances the inviscid cell model will be a good representation of the dynamics and we find that the time rates of change of cell size, $\dot{b}_v$, and impulse $\dot{I}$ are zero; so that the propagation velocity $U^*$ is constant.

Stage II - The Entraining Cell. As the core vorticity diffuses and approaches the cell boundary, the first process (of mass entrainment) occurs, represented by $\dot{b}_v > 0$, $\dot{I} = 0$. We find that the propagation velocity reduces from the inviscid value.

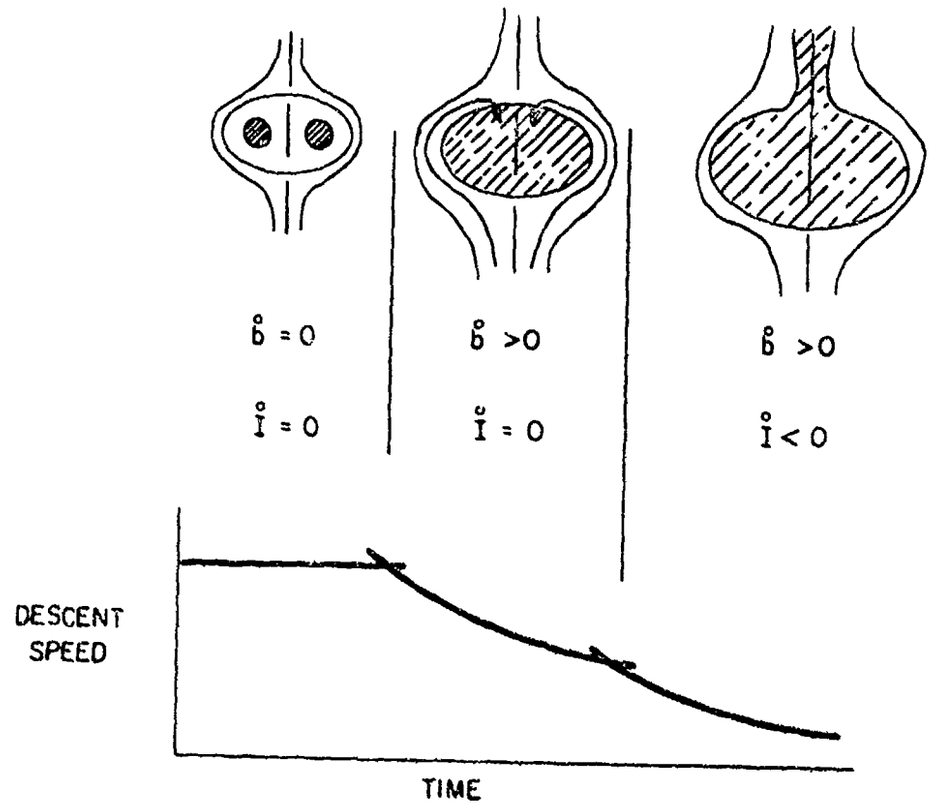


Figure 4-2. Vortex Cell Stages

Stage III - The Decaying Cell. During the later stages, substantial momentum and vorticity shedding occur, causing a wake to develop and giving $\dot{b}_v > 0$, $\dot{I} < 0$. Of course, various catastrophic instabilities may have developed before the complete decay has occurred.

1. Ordering of the Process

Maxworthy has made a laminar analysis of the last two stages for a ring vortex, and found excellent correlation with his experiments. He also includes an analysis for the two dimensional vortex pair for laminar diffusion. Here we continue this for turbulent diffusion.

To establish a turbulent transfer coefficient, we note that there will presumably be two turbulent scales at the cell boundary. During the initial stage we assume that ambient turbulence is the major term, since the inner flow near the cell boundary has very weak vorticity. If this is the case, the only turbulent parameter is $\epsilon$, the turbulent dissipation, and we can define an rms turbulent velocity $V_\epsilon$ for all scales smaller than the cell scale $b_v$ by

$$V_\epsilon \sim \epsilon^{1/3} b_v^{1/3}$$

In a later stage, we expect mechanically-generated turbulence due to the interior cell motion to dominate. Now we will take a turbulent velocity coupled to the cell velocity, so define another turbulent scale velocity

$$V_m \sim U^*$$

a. The Entraining Cell. Here we assume vorticity is entrained linearly with time as the layer progresses from A to B. Thus the height $\delta_e$ is given by

$$\delta_e = V_\epsilon t'$$

where t' is the time of travel. An estimate of t' is

$$t' = \pi b_v/(2U^*)$$

for the inviscid cell proportions. Now the unit density mass flow through BD is $2U\delta_e$, and taking the cell area to be about $\pi b^2$ and assuming all this mass is entrained, we obtain

$$\dot{b}_v \sim V_\epsilon \quad , \quad b_v \sim \epsilon^{1/2} t^{3/2}$$

Taking the total impulse to be that of the inviscid cell, $I = \Gamma b$, and the propagation speed $U^* = \Gamma/2\pi b$. Thus for I invariant we obtain

$$U^* = I/(2\pi\epsilon t^3)$$

We compare this with Maxworthy's result for laminar diffusion of kinematic viscosity, $\nu$, where he gives

$$b_v \sim (I\nu)^{1/5} t^{2/5} \qquad U^* \sim (I^3/\nu^2)^{1/5} t^{-4/5} \ .$$

The time dependence and the viscous terms appear in a similar fashion in both the turbulent and laminar cases, however in the turbulent case the departure from the inviscid cell results, as represented by the exponents, are much more distinct.

b. The Decaying Cell. In this case we admit both entrainment of mass and detrainment of momentum; thus the impulse is no longer conserved. We assume a turbulent velocity scale $V_T$ which will be defined later. Then, as before, we obtain the cell growth equation

$$\dot{b}_v = \alpha V_T$$

where $\alpha$ is some constant.

Now, to find the change in impulse, we estimate the reduction in circulation. We ignore vorticity annihilation on the interior cell centerline but attempt to compute the vorticity transferred to the wake by turbulence through the cell boundary. Dimensional arguments suggest that the cell vorticity goes like $\Gamma/b_v^2$ and the turbulent flux of vorticity through the boundary then becomes of the order $(\Gamma/b_v^2)\, b_v\, V_T$. Thus we obtain

$$\dot{\Gamma} = \beta \Gamma b_v V_T$$

where $\beta$ is another constant. Combining these equations with $\beta/\alpha = \gamma$ gives the result

$$\dot{\Gamma}/\Gamma = \gamma \dot{b}_v/b_v$$

independent of $V_T$, implying that $\Gamma \sim b_v^{\gamma}$.

If we now assume $V_T \sim U^*$ we obtain the results

$$b \sim t^{1/(2+\gamma)}$$

$$U^* \sim t^{-(1+\gamma)/(2+\gamma)}$$

$$I \sim t^{(1-\gamma)/(2+\gamma)}$$

We observe that for the impulse to decay, $\gamma > 1$ ; however, the reduction of propagation velocity will be less than that in the case of assuming turbulence coupled to the ambient dissipation. We note also an inherent contradiction in that if the mechanical turbulence is coupled to the $U^*$, then eventually it will reduce so that ambient turbulence again dominates.

## 2. Comparison of the Assumptions

We note that in this simple model we can assume that the impulse is conserved or not, and that the turbulent scale is either the ambient turbulent velocity or the propagation velocity. Thus we actually obtain four cases for similarity solutions. The ordering of the response is shown in the following table.

TABLE 4.1. THE ORDERING OF THE RESPONSE FOR FOUR CASES OF SIMILARITY SOLUTIONS

| Turbulent Mechanism | | Ambient | Mechanical |
|---|---|---|---|
| No Wake | $b_v$ | $t^{3/2}$ | $t^{1/3}$ |
| | $U^*$ | $t^{-3}$ | $t^{-2/3}$ |
| | $l$ | $t^{0}$ | $t^{0}$ |
| Wake | $b_v$ | $t^{3/2}$ | $t^{1/(\gamma+2)}$ |
| | $U^*$ | $t^{-3(\gamma+1)/2}$ | $t^{-(\gamma+1)/(\gamma+2)}$ |
| | $l$ | $t^{-3(\gamma-1)/2}$ | $t^{-(\gamma-1)/(\gamma+2)}$ |

We note that even on this simple basis, four different similarity solutions can be developed. It is possible that the stages with time progress from the ambient/no wake to mechanical turbulence/no wake case through the mechanical turbulence/wake case to the ambient/turbulence/wake case. However, this assumption, although sounding physically plausible, gives a non-monotonic variation in the propagation speed decay rate, which appears surprising. For example, if $\gamma = 1 + \delta$, we would find the propagation speed varied like $t^{-3}$, $t^{-2/3}$, $t^{-(2+\delta)/(3+\delta)}$, $t^{-3(1+2\delta)/2}$ as the different stages occurred.

We note here that, in fact, transfer must be due to some combination of the ambient and mechanically generated turbulence. A similarity solution does exist for the case $V_T = \epsilon^{1/3} b_v^{1/3} + \gamma U^*$ but only for $\gamma = -4/3$ which gives an increasing impulse! It is clear from the above equation that if the cell size increases with time and the velocity reduces (as appears to be the case for a descending vortex pair), then the ambient and mechanically generated turbulence cannot maintain the same ratio. This illustrates that similarity solutions can only be expected when one form of transfer dominates.

## 3. Dimensional Analysis

If we attempt simply to model the problem dimensionally, we find that there are three initial parameters, $b_o$, $U_o = \Gamma_o/2\pi b_o$ and $\epsilon$. A functional equation connecting U and t may be written as

$$U^*/U_o = f_m(\epsilon^{1/3} b_o^{1/3}/U_o,\ t/b_o U_o^{-1})$$

where we have used a mechanical time scale to normalize t and retain the parameter $\eta = \epsilon^{1/3} b_o^{1/3} U_o^{-1}$. This would provide a collapsing of data where ambient turbulence was insignificant. However, where ambient turbulence dominated, one would use an ambient time scale and write

$$U^*/U_o = f_a(\epsilon^{1/3} b_o^{1/3}/U_o,\ t/b_o^{2/3}\epsilon^{-1/3})$$

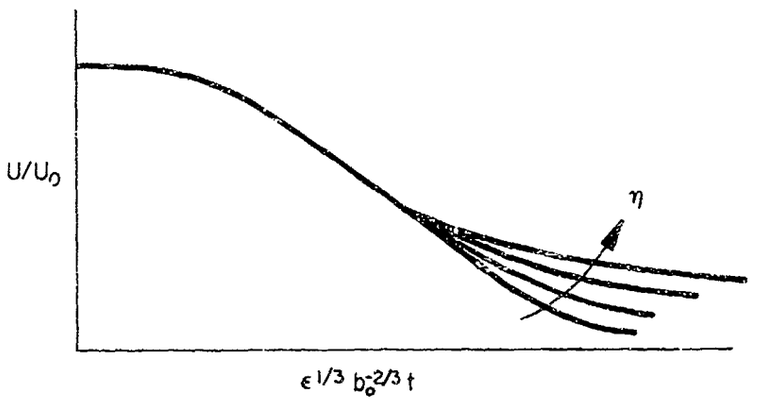


AMBIENT TURB. TIME SCALE

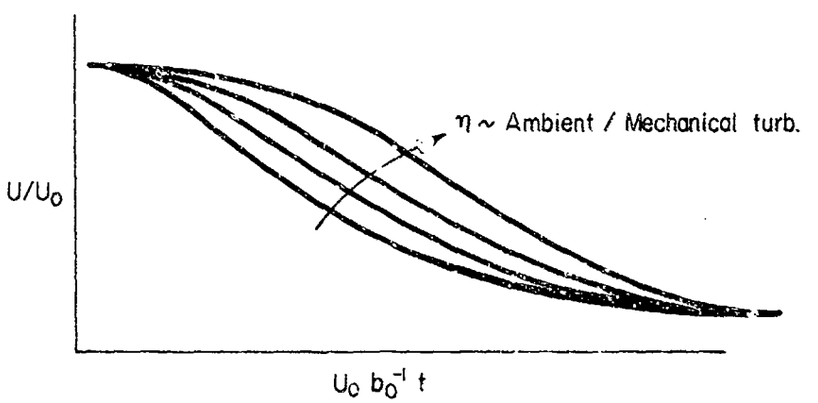


MECHANICAL TURB. TIME SCALE

Figure 1-3. Non-Dimensional Vortex Transport Curves.

Thus formulation will collapse data in regions where the ambient turbulence is important. A representation of this is shown in Figure 4-3 with the ambient/mechanical ratio $\eta$ as a parameter.

If data collapse of this sort is observed from proper analysis of flight tests, then the exponents of t described in the previous sections can be determined.

We note in passing that there is yet another time scale, that of viscous transfer. According to Maxworthy's experiments, this has the form $(b_o^3/U_o\nu)^{1/2}$. It appears that this scale is too large to be of concern to us; that is, the time involved for the problem to become a purely viscous one is beyond our range of interest.

## 4.3 NEUTRAL ROTATIONAL FIELD

### Statement of the Problem

Various explanations of the motion of vortices in a crosswind with shear have been given (Burnham, 1972; Harvey and Perry, 1971). These analyses were concerned with the vortex transport near the ground plane, where, typically, both vertical shear and vertical shear gradients are present when there is a crosswind. The objective of these works was to analytically model the observed unsymmetrical motion of the vortex pair as they descended into the wind shear region. Instead of both vortices leveling off at the expected height above the ground of $\lambda = b/2$, the upwind vortex sometimes drops below this value, and the downwind vortex levels off and then begins to rise to a distance greater than $b/2$. Thus, a tilting of the vortex pair results, superimposed on the lateral motion of the vortices caused by the uniform component of the crosswind, and the proximity of the ground plane.

Such analysis near the ground plane is unsteady both because of the redistribution of vorticity in the shear gradient of the external flow and the change in separation of the aircraft vortex pair due to the presence of the ground plane.

However, vortex tilting has been observed at sufficient heights above the ground (Tombach 1972), that ground effect need not be considered. Under these conditions, the problem can be treated in the classical sense of a descending vortex pair in steady flow. Also, at altitude, any severe vertical crosswind shear gradients would not be expected to be present, and the shear can be represented as a uniform vorticity field, again a steady flow situation. The problem may now be examined in a steady coordinate system, fixed to the vortex pair. The

solution to this problem will yield the streamlines of the external flow as well as the recirculating flow within the vortex cells. Since the vortex tilting phenomenon has been observed at altitude, such an analysis is expected to give a good inviscid representation of the effects of the flow asymmetry produced by a sheared crosswind interacting with the vortex pair and should form the basis for a more detailed viscous solution.

Analysis

A vortex pair with circulation $\pm\Gamma_o$ are located at $y = 0$ and $x = \pm b/2$ respectively. A vertical component of velocity $v = \Gamma_o/2\pi b$ is directed upward from below the vortex pair. The wind shear is represented as a horizontal velocity, $u = f(y)$ with $u = f(0) = 0$ to remove the effects of the contribution of the uniform component of the crosswind (for the steady coordinate system chosen).

Assuming a linear crosswind shear profile, $u = f(y) = K y$, from which $f(0) = 0$. This satisfies the condition of the removal of the uniform component of the crosswind. The details of the combined flows described above are presented in Figure 4-4.

The stream functions for each of the flows may easily be written separately as:

vortex flow:

$$\psi_1 = -\frac{\Gamma_o}{4\pi} \ell n \left[\frac{(x-b/2)^2 + y^2}{(x+b/2)^2 + y^2}\right]$$

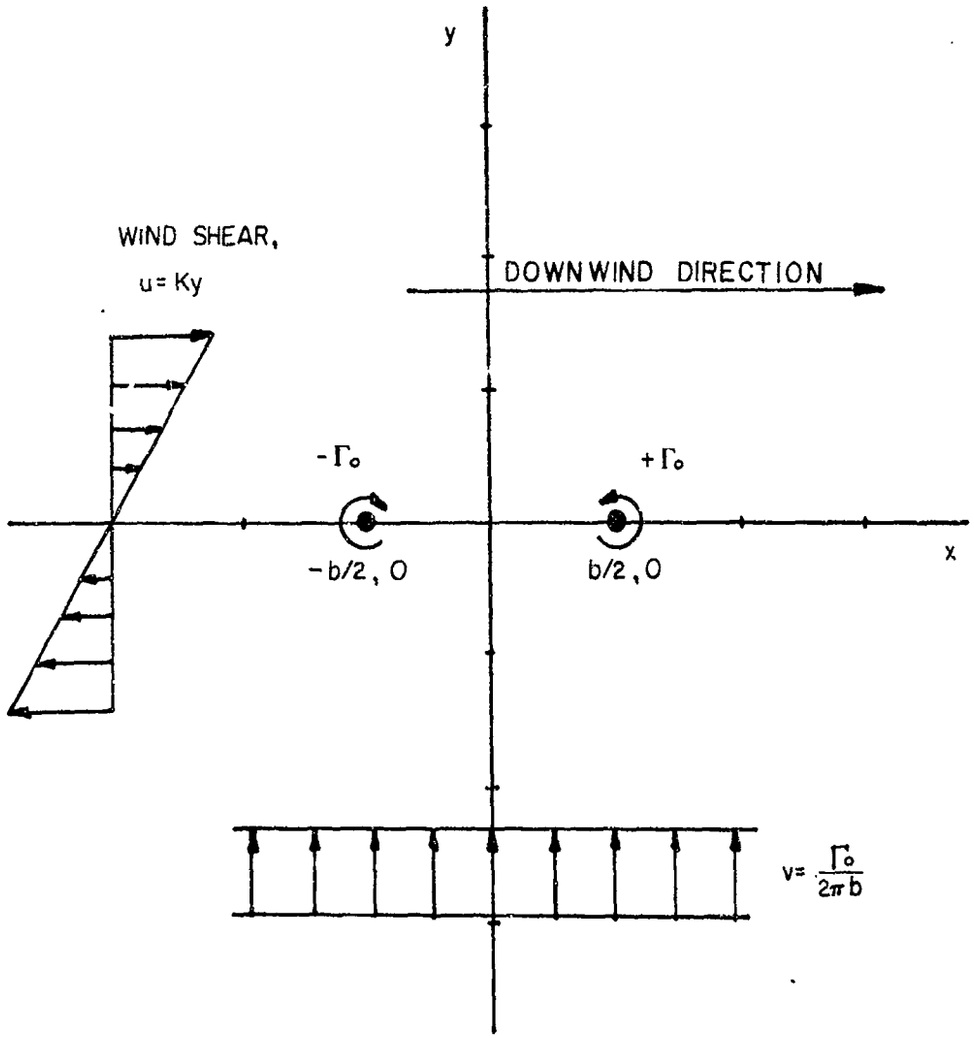


Figure 4-4. Coordinate System and Flow Geometry for Vortex-Pair in Uniform Cross-Flow.

uniform vertical flow:

$$\Psi_2 = -\frac{\Gamma_o}{2\pi b} x \ ,$$

and

shear flow:

$$\Psi_3 = \frac{K}{2} y^2 \ ,$$

from which the stream function $\psi$ for the complete flow field may be obtained.

By superposition:

$$\Psi = \Psi_1 + \Psi_2 + \Psi_3 \ ,$$

and

$$\Psi = \frac{K}{2} y^2 - \frac{\Gamma_o'}{2\pi b} x - \frac{\Gamma_o}{4\pi} \ln \left[ \frac{(x-b/2)^2 + y^2}{(x+b/2)^2 + y^2} \right] \quad . \quad (4\text{-}1)$$

Introducing the following dimensionless parameters,

$$X = \frac{x}{b/2} \ ,$$

$$Y = \frac{y}{b/2} \ ,$$

$$\Psi^* = \frac{4\pi}{\Gamma_o} \Psi \ ,$$

$$\sigma = \frac{K\pi b^2}{2\Gamma_o} \ ,$$

Eqn. 4-1 becomes:

$$\Psi^* = \sigma y^2 - x - \ell n \left[ \frac{(x-1)^2 + y^2}{(x+1)^2 + y^2} \right] \quad . \qquad (4-2)$$

Here, $\sigma$ is a non-dimensional shear parameter which relates the scale of the wind shear to the vortex parameters, $\Gamma_o$ and $b$. The vortices are located at $Y = 0$, $X = \pm 1$.

Before proceeding further it would be useful to calculate the order of magnitude of the shear parameter, $\sigma$, for subsequent evaluation of the streamlines, $\psi^*$, from Eqn. 4-2.

For a 727 aircraft,

$$\Gamma_o = 3400 \text{ ft}^2/\text{sec}$$

$$b_o = 108 \text{ ft}$$

$$b = (\pi/4) b_o = \pi(108)/4 = 84.78 \text{ ft}$$

$$\sigma = \frac{K \pi b^2}{2\Gamma_o} = 3.31 K \quad .$$

Typical values of shear near the ground (Zwieback, 1964) give a velocity of 18 ft/sec at 44 ft above ground, so that $K = u/y = 18/44 = .4 \text{ sec}^{-1}$. Stronger shears are possible closer to the ground or in gusty situations, so that it is not unreasonable to assume a range of $0 \leq K \leq 1$. This gives an upper limit on $\sigma$ of $\sigma = 3.31$. Eqn. 4-2 will be evaluated over a range of $\sigma$ from zero to 3.

Computation of $\psi^*$

Equation 4-2 gives the coordinates X, Y for the family of streamlines $\psi_n^*$ at constant $\sigma$ . Although the equation is in closed form, it is not easy to solve for X and Y for any given $\psi_n^*$ , especially when the value of $\psi_s^*$ , the stagnation point streamline, which also describes the bounding streamline of the recirculating vortex cells, is not known apriori.

The expression for $\psi^*$ was programmed on a Hewlett-Packard Model 9820A mini-computer using an x-y plotter for data output. After some experimentation with various inputs of $\psi^*$ and $\sigma$ , the pattern of the structure of the streamlines became clear. Figures 4-5, -6, -7, and -8 show the geometry of the stagnation, or dividing streamline of the vortex recirculation cells as well as several streamlines of the exterior flow for values of $\sigma = 0, 1, 2, 3$ respectively. In addition, Figure 4-9 is a "magnified" view of the streamlines in the immediate vicinity of the stagnation point for the case $\sigma = 3$ .

Discussion of Results

The obvious (and very striking) conclusion from Figures 4-5 through 4-8 is that as the strength of the wind shear increases, the size of the upwind vortex recirculation cell increases and the size of the downwind cell decreases. Presumably, for $\sigma$ large enough (a not very realistic case), the downwind cell would approach zero.

The problem treated here was assumed steady in all respects, including constant $\sigma$ . That is, the vortex pair was generated in a cross-wind shear field of constant $\sigma$ which remains constant as the vortex pair translates downwind. It is not clear from the present analysis what the

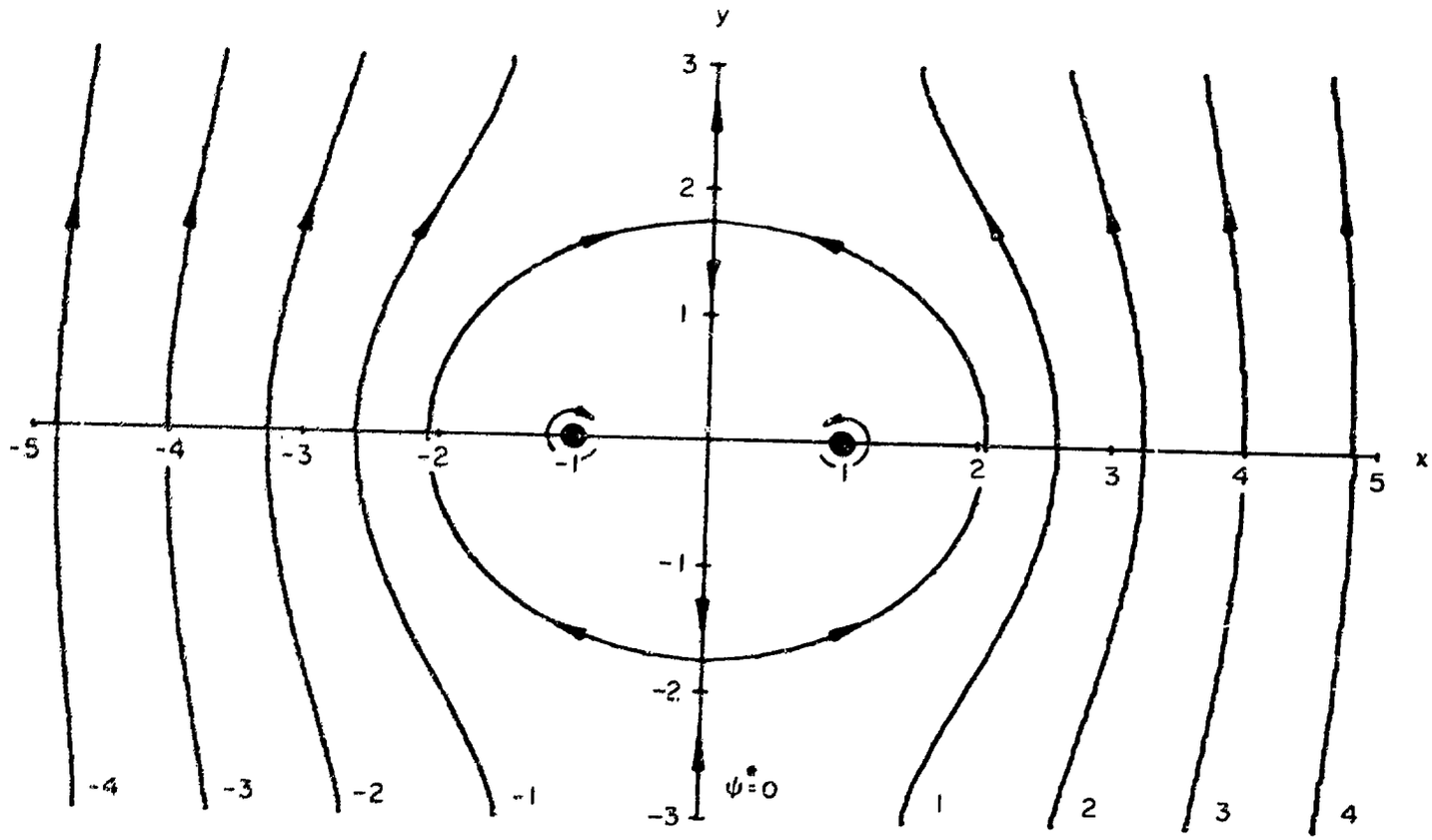


Figure 4-5. Streamlines in the Vicinity of a Vortex Pair with no Shear. Shear Parameter, $\sigma = 0$. Flow Directions and the Value of the Stream Function $\psi^*$ for each Streamline are Indicated.

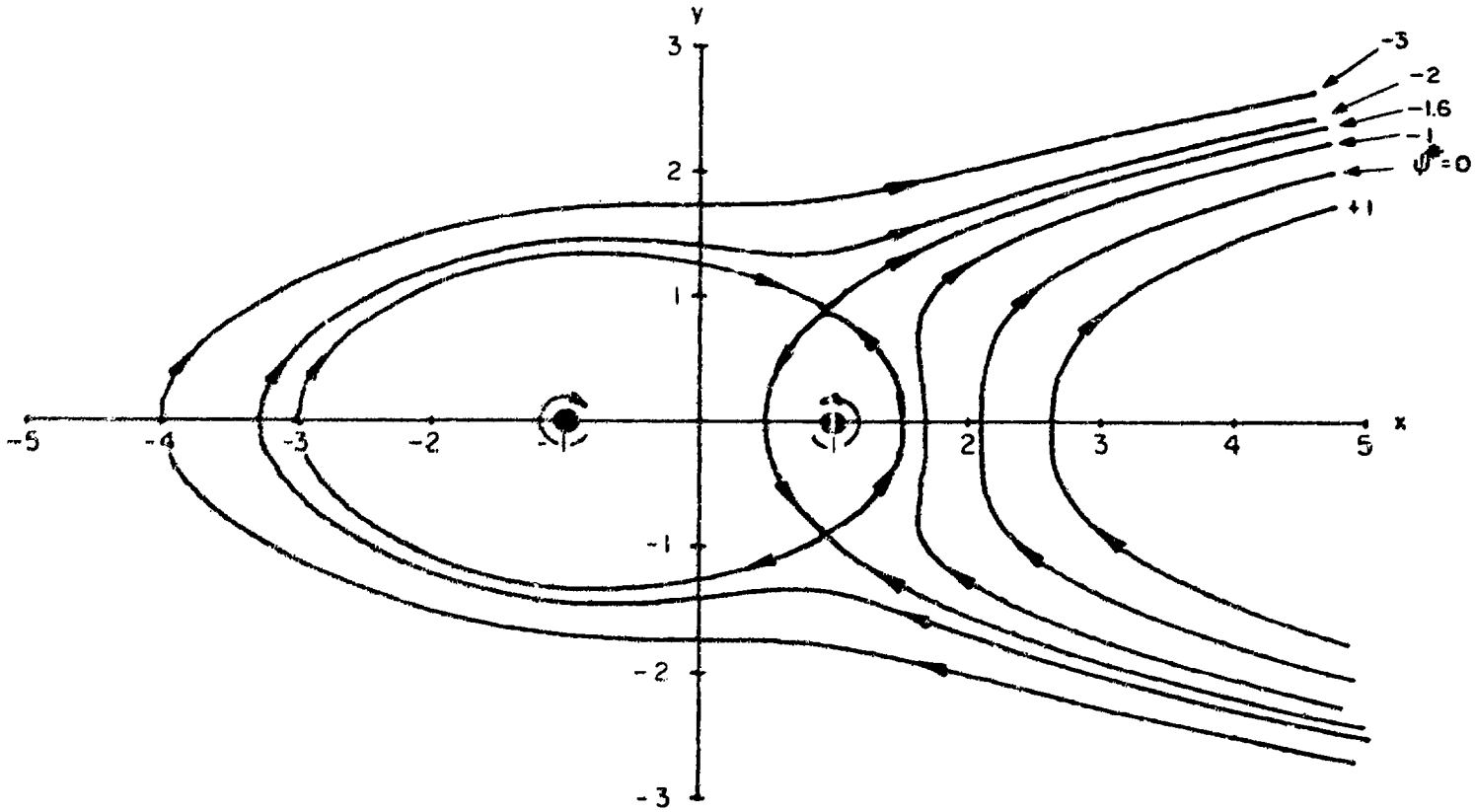


Figure 4-6. Streamlines in the Vicinity of a Vortex Pair in Light Shear. Value of the Shear Parameter, $\sigma = 1.0$. Crosswind from the left.

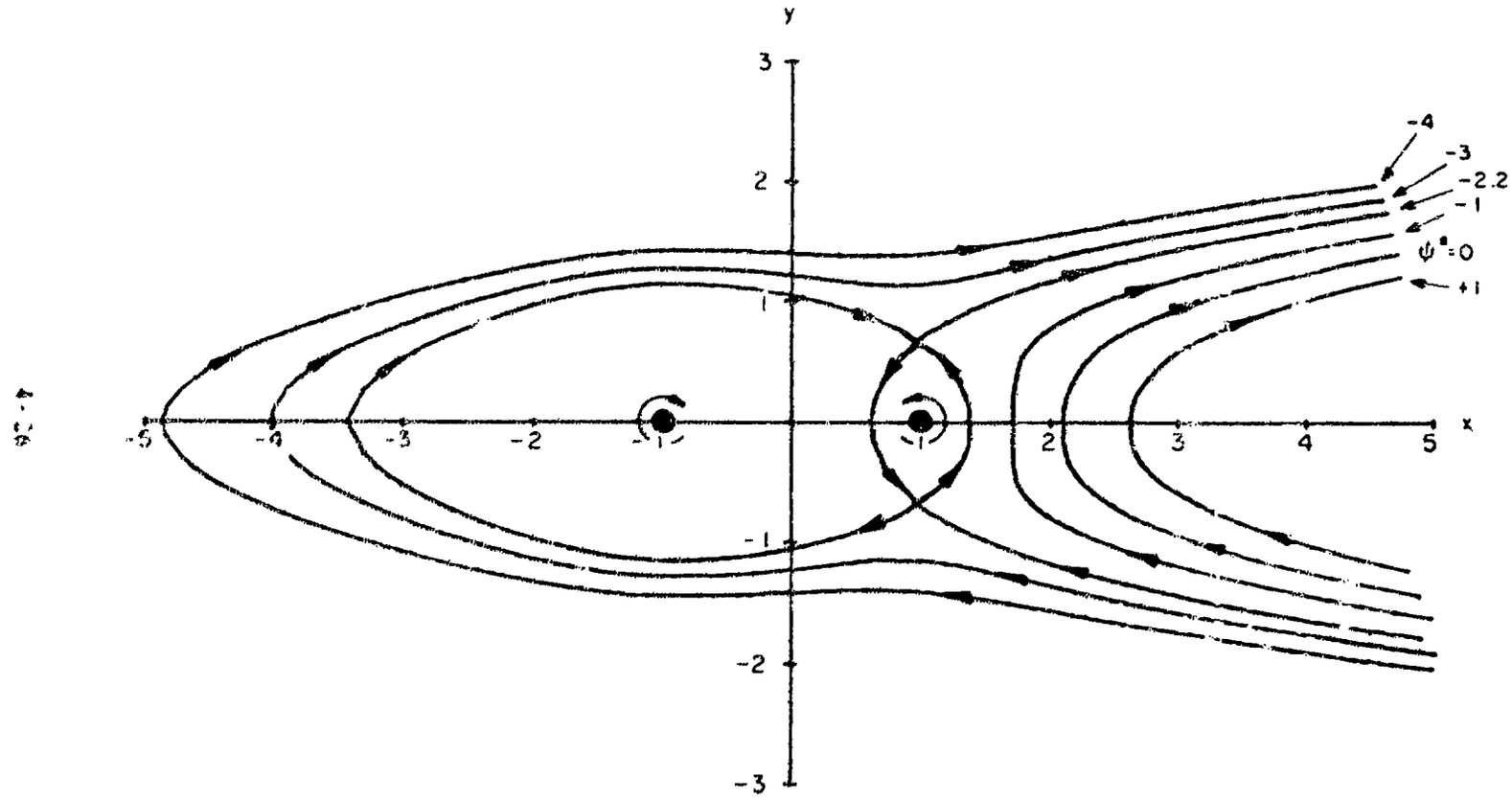


Figure 4-7. Streamlines in the Vincinity of a Vortex Pair in Moderate Shear. Value of the Shear Parameter, $\sigma = 2.0$. Crosswind from the Left.

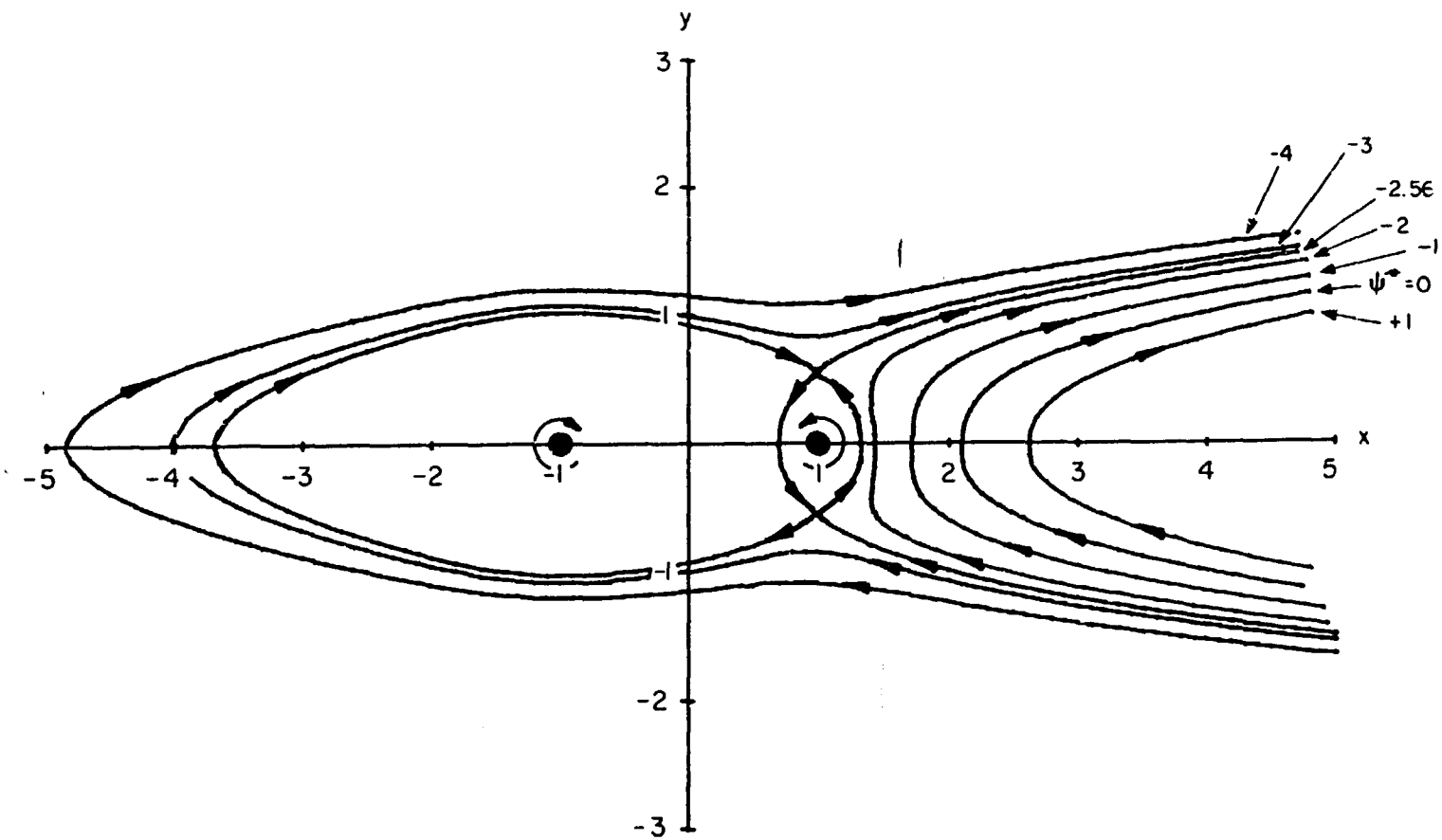


Figure 4-8. Streamlines in the Vicinity of a Vortex Pair in Heavy Shear. Value of the Shear Parameter, $\sigma = 3.0$. Crosswind from the Left.

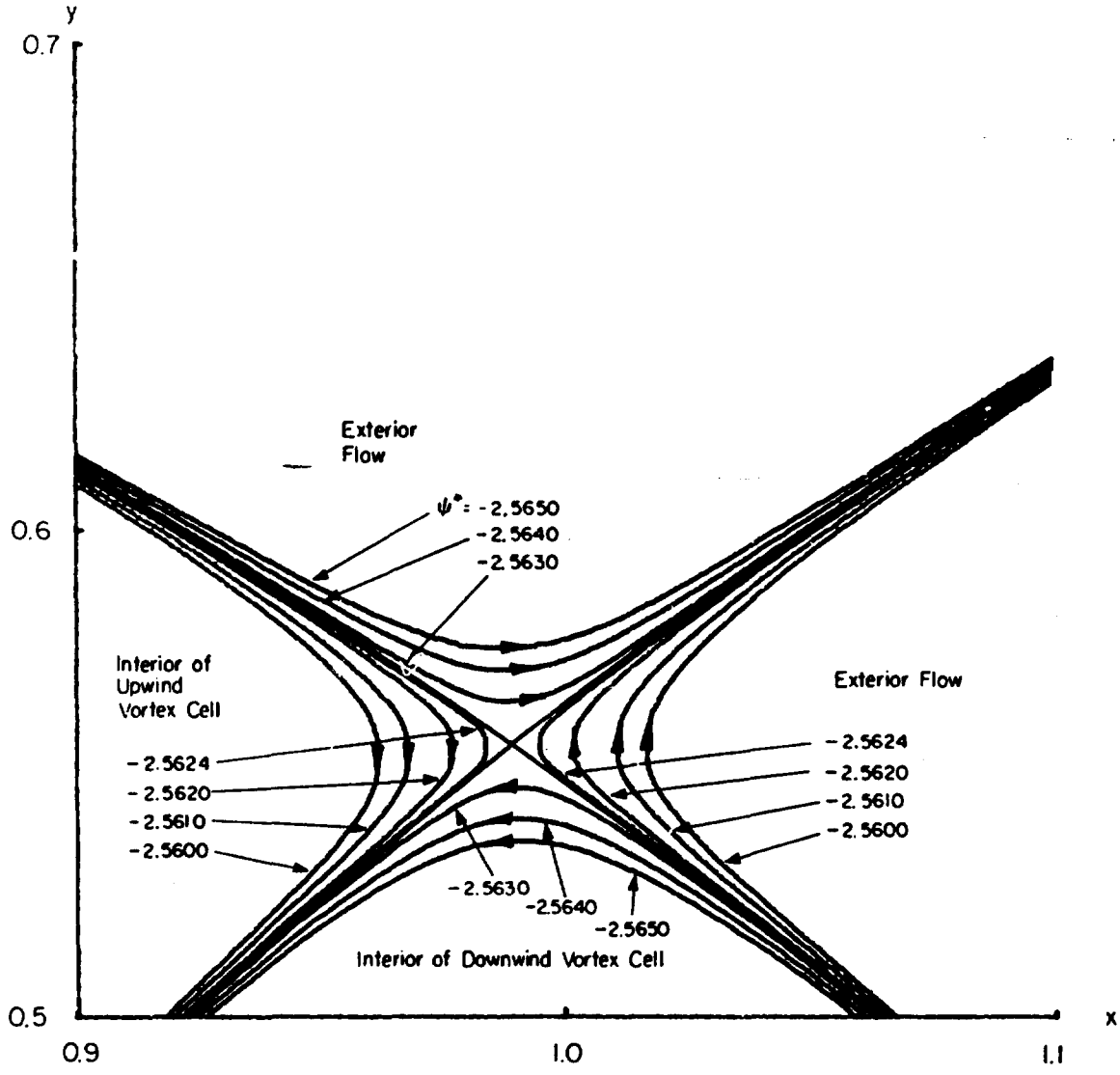


Figure 4-9. Streamlines in the Immediate Vicinity of the Top Stagnation Point for a Vortex Pair in Heavy Shear. Value of the Shear Parameter, $\sigma = 3.0$.

effects of changing $\sigma$ would be on the geometry of the flow, once established. However, it might be reasonable to speculate that Figures 4-5 through 4-8 give an instantaneous, steady view of the flow for each value of $\sigma$, and if $\sigma$ changes slowly, the flow field would change roughly in accordance with these figures. Thus, as $\sigma$ increases, the upwind cell would gradually increase in size and the downwind cell would gradually shrink.

Further analysis must be performed to verify this, but if the above assumption is reasonable, a method of predicting the flow geometry of a vortex pair descending into a crossflow with shear gradients would be possible.

It is not clear from the present analysis of the exact effects that a sheared crosswind has on vortex tilting. However, it is unquestionably the case that the wind shear produces asymmetry in the recirculating cells surrounding the two vortices. This asymmetry may explain the process whereby vortex tilting occurs. It should be remembered that the asymmetry always acts to increase the size of the upwind vortex recirculation cell and to reduce the size of the downwind cell, and that this effect is more pronounced as the strength of the wind shear is increased.

Section 4-2 describes the outward diffusion of the vortical core as the age of the vortex pair increases. The core diffusion is presumably related to vorticity gradients. Due to wind shear, the downwind vortex recirculation cell will be smaller than the upwind cell. The diffusing vorticity of the downwind vortex will thus reach the boundary of the inviscid cell before the similar situation occurs for the upwind vortex. Thus, vorticity associated with the downwind vortex will diffuse into the free stream flow and be swept away, reducing the vorticity and hence the circulation of that vortex. An asymmetry will then be produced

in the downwash velocities of one vortex with respect to the other.

Although the effect of these asymmetrical induction velocities should take into account the exact distribution of vorticity within the altered vortical cores, the sense in which the vortices translate with respect to each other should be straightforward.

If the circulation of the downwind vortex is decreased over that of the upwind vortex due to detrainment of vorticity, then its downwash velocity will be less than that of the upwind vortex. As a result, the upwind vortex will translate downward less rapidly than the downwind vortex. Tilting will occur with the sense that that the upwind vortex will rise with respect to the downwind vortex.

This result contradicts Burnham's observation that "the upwind vortex usually drops to a lower altitude than the downwind vortex." However, Burnham's work, and the experimental observations which he cites were all performed in ground effect at relatively low crosswind velocities. He states, "Both experimental observations and calculations indicate that other phenomena occur at much higher crosswind speeds (e.g., 30 fps instead of the 10 fps considered here)."

Future work needs to be performed to adequately describe the mechanism which initiates vortex tilting. It seems reasonable from the present analysis that the asymmetry in the flow fields surrounding the vortex cores forms an excellent point of departure for such further investigation. The assumption of a uniform shear was sufficient to indicate this asymmetrical behavior. Including the effects of shear gradients in future work would undoubtedly refine the results somewhat, but their effects should probably be small and would produce results in the same sense indicated by the present analysis.

For a sufficiently large vortex age, the core diffusion process would continue to a point at which vorticity detrainment from the downwind vortex (with shear flow) would result in sufficient reduction of its circulation that for all practical purposes, it would cease to exist. This would not be the case for the upwind vortex, considering its larger cell size. This process would proceed more rapidly for larger $\sigma$ . Indeed, for a locally large value of $\sigma$ such as might exist in a gust with high shear rate, the above process would occur catastrophically -- a possible explanation for core bursting. For both the case of the slower detrainment rate and the catastrophic situation, the remaining vortex would be the upwind vortex.

Concluding Remarks

The calculation of the family of streamlines $\psi_n^*$ for a given value of shear $\sigma$ is tedious. The only really necessary streamline to obtain is that which describes the boundary of the recirculation cells, $\psi_b^*$ . However, the value of $\psi_b^*$ is identical to the value of the stream function at the stagnation point $\psi_s^*$ . $\psi_s^*$ may be solved in terms of $\sigma$ explicitly and presented graphically or in tabular form. Substitution of $\psi_s^* = \psi^*(\sigma)$ in Eqn. (4-2) will then give the shape of the recirculation cells for any desired value of $\sigma$ .

The conditions for the calculation of $\psi_s^*$ are:

$$\psi_s^* - f_1(X_s, Y_s, \sigma) = 0 \quad , \tag{4-3}$$

$$u = \left.\frac{\partial \psi^*}{\partial y}\right|_s = f_2(X_s, Y_s, \sigma) = 0 \quad , \tag{4-4}$$

$$v = -\left.\frac{\partial \psi^*}{\partial x}\right|_s = f_3(X_s, Y_s) = 0 \quad , \tag{4-5}$$

where the subscript $s$ implies that the quantities are to be evaluated at the stagnation point. Equation (4-3) is identical to Eqn. (IV- 2) evaluated at $s$ .

The simultaneous solution of Eqns. (4 - 3, 4, 5) will yield the values of the three unknowns, $X_s$, $Y_s$, $\psi^*_s$ in terms of $\sigma$ , of which only $\psi^*_s$ is of interest. The simultaneous solution of these equations is also not exactly easy, but can be performed in a straightforward manner using computer techniques.

The cell boundary streamline will be given by the expression:

$$-\Psi^*(\sigma) + \sigma Y^2 - x - \ell n \left[\frac{(x-1)^2 + y^2}{(x+1)^2 + y^2}\right] = 0 \ , \qquad (4-6)$$

from which the shape of the recirculating cells may be calculated or plotted by computer. The shape, size, or area of the recirculating cells may thus be obtained as continuous functions of the wind shear, $\sigma$ , within the accuracy of the computational methods used.

## 4.4 WAKE TRANSPORT IN A STRATIFIED FIELD

If a vortex wake descends through a stably stratified atmosphere, as is usually the case, then it becomes buoyant as it descends because its density increases at a slower (adiabatic) rate than the ambient density. A wake could also conceivably acquire buoyancy at the time of its generation, from hot engine exhaust gases mixed into it. In either case, the buoyancy thus generated acts to decrease the overall wake impulse and (possibly) circulation, although any mixing between the wake and its surroundings would tend to dilute the buoyancy and to decrease these effects.

### 4.4.1 EXPERIMENTAL OBSERVATIONS

Observations of wakes generated by full-size aircraft tend to suggest that stratification may have an effect on wake transport. Specifically, a study of the dissemination of particles released from aircraft (Smith and Wolf, 1963; Smith and MacCready, 1963) included some observations of wake descent from a variety of aircraft. Tests with aircraft up to DC-3 size gave typical descent distances of 25 to 100 feet over land, with the wake descending initially at the theoretical speed, but then broadening and slowing up. On the other hand, similar measurements over the ocean sometimes, but not always, indicated wake descents of 600 feet. A possible explanation was that turbulence slowed the wake's motion and helped spread it and that a stable atmosphere further impeded descent. Both stability and turbulence are usually less over the ocean than over land, thus resulting in longer vortex life and descent.

Another study (FAA Task Force, 1971) found that the vortices generated by jumbo jet aircraft began descending at 400 to 500 feet per minute, but that fully developed wakes were generally not found more than 1000 feet below the altitude of the generating aircraft.

Leveling off, combined with start of breakup usually began after a descent of 800 to 900 feet and the vortex spacing appeared to remain constant until breakup. Occasional descents of 1100-1200 feet, with no noticeable slowing of descent speed, were measured during the same study by Andrews, et al (1972). In contrast, in one case the wake from a cruising C-5A (Mach no. = 0.8) was measured at 500 feet below the aircraft at 3 miles behind it, and remained at that level for more than 40 miles.

During a British study of wakes behind jet transport aircraft (Rose and Dee, 1965) wake descents of up to 800 feet were measured during the first 150 seconds of wake life and no general leveling-off trend was observed. Quantitative measurements of vortex spacing were obtained in another British study (Bisgood, et al, 1971) where the vortex spacing behind a delta-wing aircraft was observed to grow to about 3 times the initial spacing in about 45 seconds.

The descent of the wake generated by a lightplane in a variety of meteorological conditions was measured by Tombach (1972, 1973). He found that the descent speed of the wake was constant for about 20 seconds in a stable atmosphere, after which the descent was slowed and often stopped. There seemed to be no noticeable differences in wake behavior at different atmospheric stratifications, however, but the dominant factor governing wake descent was probably a banking of the plane of the vortices (which was discussed earlier).

Tombach also attempted to measure vortex spacing as the wake descended. The same banking tendency complicated the interpretation of the data, but he noted that slight increases in vortex spacing could be observed in the few cases when the wake remained relatively level. Considerable increases in spacing were noted for wakes which had banked well out of the horizontal plane.

The observations by Tombach showed that the smoke-marked vortex wake sometimes rose again after its descent had stopped. Whether the cause for this is atmospheric upcurrents or buoyancy is not known.

A few laboratory experiments have been performed to study the motion of buoyant vortex pairs. Most of these have been concerned with line thermals, where the buoyancy of the thermal is such as to increase the total circulation around each vortex. When in a homogeneous medium and well developed, i. e., when the vortex motion is well organized, these thermals are observed (Richards, 1963; Tsang, 1971) to grow in scale as $\Delta \rho^{1/3} t^{2/3}$, where t is time (with $t = 0$ at the extrapolated point when the vortex pair would have been of zero size) and $\Delta \rho$ is the density difference between the thermal and the ambient fluid at the time of release. Their speed of advance has been found to slow as $\Delta \rho^{1/3} t^{-1/3}$. This entrainment of the ambient fluid is observed to erode the buoyant driving force and to eventually bring the growing thermal to a halt. Extension of such results to the vortex wake problem is not straightforward, however, because (1) the buoyancy opposes the motion of the vortex wake, and (2) the impulse of the thermal is coupled to its initial buoyancy, whereas the impulse of the vortex wake is totally unrelated to its initial buoyancy (which is often zero).

One set of laboratory experiments to study the motion of a vortex pair with initial impulse in a stratified medium was performed by Tulin and Shwartz (1971) (with a related experiment by Birkhead, et al, 1969). They generated an impulsive vortex pair in a stratified water tank and observed its motion, which looked like that shown in Figure 4-10. (The figure has been redrawn to correspond to the direction of motion of an aircraft wake). The total vertical travel of the wake was about 4 vortex spacings (which is of comparable magnitude to the aircraft results quoted earlier) before the stratification dominated

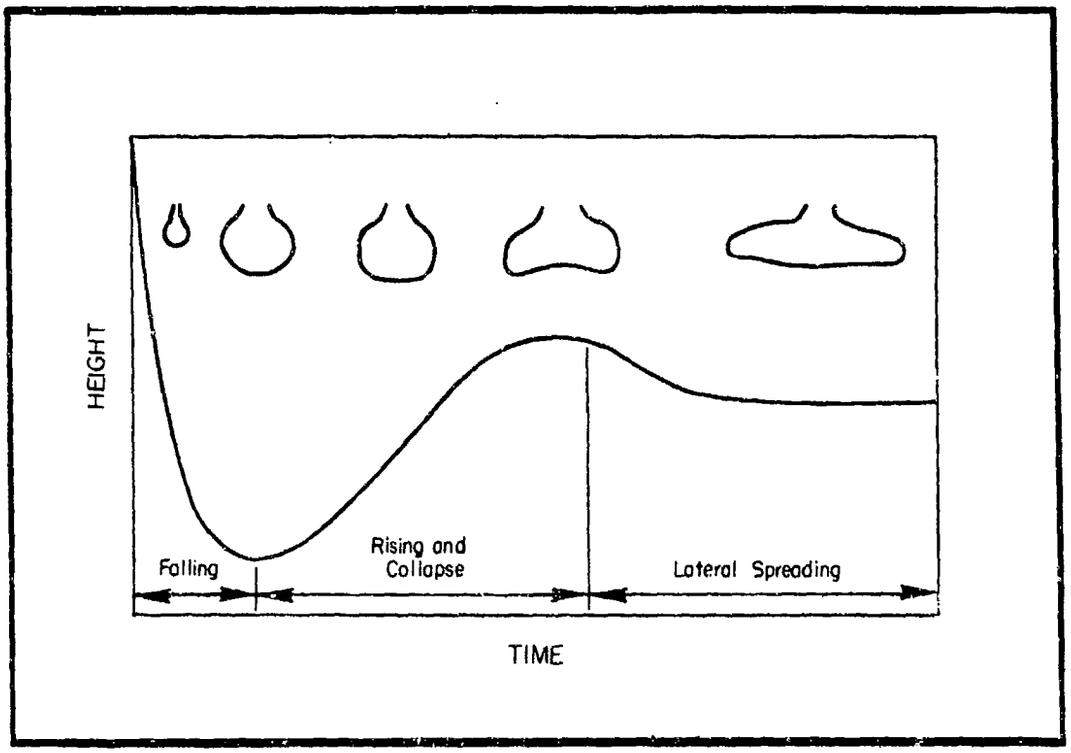


Figure 4-10. Trajectory of a Vortex Pair in a Linearly Density Stratified Medium (from Tulin and Shwartz, 1971). The Upper Sketches Show the Observed Cross Section of the Wake.

the motion and caused the wake to reverse direction and collapse. This process took place in a characteristic time which is proportional to the Vaisala period $T_1 = (g/\rho\, d\rho/dy - g^2/a^2)^{1/2}$ where $\rho$ is the atmospheric density and $a$ is the speed of sound, with the proportionality factor depending on the initial strength of the vortices, which in turn is represented by another time $T_2 = b_v/V$ where $V$ is the descent speed and $b_v$ is the vortex spacing. According to Tulin and Shwartz, if $T_2 < T_1$, the vortices dominate the motion, while if $T_2 > T_1$ the stratification dominates it. Since $T_2$ increases if the wake descends and grows, their experiments show that stratification must invariably dominate the motion unless some instability has first destroyed the vortices.

The Tulin and Shwartz data appear to be of good quality, but some reservations exist about their applicability to the aircraft wake problem. The method of vortex generation, with an impulsive motion of a piston pushing fluid through a slit, does not generate a pure vortex pair, but adds a wake behind the moving vortex pair. (This problem is a well known one in vortex ring generation also). Since the total vortex wake motion from the wall orifice is only a few times the wake size, the effects of the wall and of the wake trailing behind the vortices might be significant. It should be noted also, that the stratification was quite strong, with the Vaisala period T ranging from 1-4 seconds (as compared to typical atmospheric values around 100 sec.). However, the ratio $T_2/T$ is initially of order 1/10 for both their experiments and for full scale wakes in the atmosphere, which indicates comparable scaling of vortex strength versus buoyancy.

In summary, the experimental picture is somewhat fuzzy. The evidence to show that wake descent stops in a stratified atmosphere is not conclusive, but the suggestion is there. Similarly, vortex spacing seems to vary little with descent, or possibly to increase, but again the experimental evidence is not extremely strong. Using the

knowledge of wake behavior, limited and confused as it may be as a foundation, let us now look at efforts to approach the problem analytically.

## 4.4.2 PREVIOUS THEORETICAL MODELS

The theories which have been developed to describe the motion of a vortex wake in a stably stratified atmosphere are numerous, include various types of modeling approaches, and give a variety of contradictory conclusions. The state-of-the-art is summarized below in Table 4-2. As shown in the table, the models suggest two main types of behavior -- a slowing of wake descent with an increase of vortex spacing, or an acceleration of wake descent accompanied by a decrease in vortex spacing.

TABLE 4-2. COMPARISON OF THEORETICAL MODELS FOR DESCENT OF A VORTEX WAKE IN A STABLY STRATIFIED ATMOSPHERE.

| Author | Vortex Spacing | Descent Speed | Buoyancy-generated Vorticity |
|---|---|---|---|
| Costen (1972)** | | | |
| Weak stability | Decreases | Increases | No effect |
| Strong stability | Increases (?)* | Stops (?)* | -- |
| Kuhn & Nielsen (1972) | Decreases | Increases | Partly entrained |
| Saffman (1972) | Increases | Stops | Entrained |
| Scorer & Davenport (1970) | Decreases | Increases | Detrained |
| Tombach (1971) | | | |
| Strong stability | Increases* | Stops* | Entrained |
| Weak stability | Decreases | Increases | Entrained |
| Tulin & Shwartz (1971) | Increases | Stops | Entrained & annihilated |

* See discussion in text.

**Costen's model is a buoyant core model. All others are models for a buoyant wake oval.

In order to assess the credibility of the various models each of them will be discussed briefly below. Since there has been a slight evolutionary trend, they will be presented in a generally chronological order.

The first two modeling approaches (Scorer and Davenport, 1970; Tombach, 1971) are both based on the assumption that the effect of buoyancy is to change the classical hydrodynamic impulse of the vortex pair and its accompanying fluid. Both assume that the buoyancy effects take place rather slowly, so that the instantaneous shape of the oval cylinder of accompanying fluid is the same as that of the classical wake in a uniform medium, and hence the wake size scales with the vortex spacing. The basic equations of motion are thus

$$\frac{dI}{dt} = \rho_o F$$

and

$$\frac{dF}{dt} = -Av/T^2$$

where $I \approx 2 \rho_o \Gamma b$ is the impulse per unit length of wake, $\rho_o$ is the initial density, $F = g A \Delta\rho/\rho_o$ gives the buoyancy, A is the cross-sectional area of the wake oval, the Vaisala period T gives the stability, and v is the descent speed of the wake.

Scorer and Davenport assume the circulation to be constant. They find a single solution in which the vortices converge and accelerate downward in a stable atmosphere. They compute numerically the internal streamline patterns for this case and suggest that the detrainment is indeed a stable process and that the circulation is, in fact, constant because the vorticity generated by the buoyancy at the boundary of the wake oval is continually

detrained as a curtain above the descending oval. After a time, however, they state that some of this fluid and vorticity is mixed into the wake, which results in its eventual destabilization and destruction.

The idea of detrainment has some experimental support. Photographs of contrails made from the side (Smith and Beesmer, 1959) show a curtain of condensed vapor extending above the wake up to the flight level of the generating aircraft. These same contrail observations, as well as low altitude measurements by Smith and MacCready (1963), suggest however that the vortex separation increases at least slightly as the wake descends instead of decreasing as the theory predicts. This troublesome point will reappear again in later analyses, so it should be pointed out here that buoyancy may indeed cause the vortices to converge and accelerate even though such behavior has not been observed experimentally. Since none of the analyses consider either turbulence or viscosity, both of which are omnipresent in the atmosphere, it is quite possible that other mechanisms overwhelm the buoyancy effect and cause the observed behavior.

Saffman (1972) points out that the Scorer and Davenport analysis does not properly treat the dynamical effect of the vorticity generated at the interface between the accompanying fluid and the denser surrounding atmosphere. As he shows, this vorticity must be included in the calculation of the impulse of the wake. The error in neglecting it may be small, however, if the generated vorticity is totally annihilated on the centerline by interaction with its counterpart of opposite sign from the other side of the oval. This is equally true for entrained or detrained vorticity.

There are several confusing mathematical errors in the Scorer and Davenport paper which affect its readability, but do not alter any of its conclusions. Specifically, the right sides of their equations (5)

and (11) should both be multiplied by (-1). The quantity $\eta$, which they call the vorticity, is really the vortex sheet strength, i.e., the circulation per unit length of sheet (which is the vorticity integrated across the sheet thickness). Their equations (17) for the "non-dimensional" vorticity" $\Phi$ do not give a dimensionless value. The corrected expressions should be

$$\frac{\partial \Phi}{\partial \xi} = \frac{k}{4\pi R} \cdot \frac{w}{uq} \quad , \quad \frac{\partial \Phi}{\partial \zeta} = \frac{k}{4\pi R} \frac{1}{q} \quad .$$

If these equations are used, then the expression in Eqn. (16) is correct.

In contrast to the constant circulation postulated by Scorer and Davenport, Tombach (1971) considered the possibility that buoyancy-generated vorticity would decrease the overall circulation around each vortex, by allowing their circulation to vary at a rate proportional to the ambient density gradient. The approach used followed that of Turner (1960) for rising buoyant vortex pairs. In addition to the geometric similarity assumption made by Scorer and Davenport, Tombach also assumed that the overall entrainment and mixing process could be characterized by a single parameter which is represented as a length in the Bjerkness circulation equation, with the rate of change of the circulation of a vortex being proportional to this length. He also assumed that this length scales with all the other lengths in the wake, which then results in the rate of change of circulation being related to the wake scale and the atmospheric stability, and suppresses any explicit display of the effect of the wake buoyancy. Although a similar assumption was used by Turner (1960) and is supported by experiments by Woodward (1959) with thermals, it is not a valid one to make initially when the vortex wake has no buoyancy and thus is not generating any vorticity. Thus the Tombach model does not properly describe either the initial behavior of the wake nor can it properly treat it at very long times when the oval height could be sufficiently great so that gravitational effects on its shape have to be considered.

In the intermediate time intervals, the model suggests that two distinct types of wake behavior may be possible, with the choice of which behavior will occur being determined by the initial vortex strength, the atmospheric stability, and the degree and manner of entrainment (which at present cannot be quantified). If the initial vortex strength is weak enough and/or the stability great enough, the model says buoyancy rapidly erodes the circulation, and the residual impulse can only be accommodated by an increase in the vortex separation and a slowing down of the wake descent. The motion is much like that of a vortex pair descending into ground effect.

On the other hand, if the vortex is strong or the stability weak, then there is residual circulation remaining when the impulse has been eliminated by the buoyancy, and the kinematical consequence is a rapid convergence of the vortices with an accompanying downward acceleration, similar to that predicted by Scorer and Davenport. The index determining which behavior will occur, denoted by $Q$ , is given by

$$Q \sim T\Gamma_o/b_o^2$$

where $T$ is the Vaisala period, $\Gamma_o$ is the initial circulation of one vortex, and $b_o$ is the initial vortex spacing. The proportionality factor depends on the entrainment details. Small $Q$ ($<\pi/2$) corresponds to the first type of motion mentioned, while large $Q$ ($>\pi/2$) corresponds to the second type.

As one would expect, the time scale of the motion is found to be proportional to $T$ , hence the greater the stability the more rapidly the motions described above take place. The vertical length scale is proportional to $T^{2/3}$, thus as the atmospheric stability is increased the vertical extent of the motion will decrease.

In the same way as for the Scorer and Davenport model, Saffman states that the Tombach model is also in error because it equates the change in the wake impulse to the buoyancy force, which is correct only if the Boussinesq approximation holds (i.e., if the density difference between the wake and the environment are small) and if all the vorticity generated by the buoyancy is included in the computation of the impulse. He claims that the latter requirement was not satisfied in the analysis. However, the Tombach analysis does take into account the change in impulse due to the buoyancy generated vorticity according to the Bjerkness equation. It does assume, however, that it is possible to approximate the impulse of the wake, including the new vorticity, by the impulse of a geometrically identical wake with all of the vorticity, old and new, concentrated in the two vortex cores. This approximation will probably result in errors after the wake has acquired considerable buoyancy, although by that time the model may no longer be valid for a variety of other reasons.

Although qualitatively similar, the Tombach large-Q solution cannot be matched to the Scorer and Davenport solution. Scorer and Davenport assume constant circulation, but permit detrainment of mass from the wake oval. On the other hand, Tombach requires that any mass transfer must affect the circulation, hence the assumption of constant circulation (which requires that his entrainment parameter $s = 0$) would automatically require no entrainment or detrainment.

Costen (1972) points out that the portion of the Tombach model for which the circulation decreases more rapidly than the impulse is impossible. This conclusion is derived by taking the ratio of Tombach's equations (3) and (9), which give (in his notation)

$$\frac{d \log \Gamma}{d \log M} = \frac{1}{\Gamma} \frac{d\Gamma}{dt} \cdot \left(\frac{1}{M} \frac{dM}{dt}\right)^{-1} = \frac{2h}{q} \cdot \frac{\rho - \rho''}{\rho - \rho'}$$

where hb is the height of the wake oval (b is the vortex semi-span for his analysis), the wake cross-sectional area is $qb^2$ , $\rho$ is the ambient density, $\rho'$ is the average wake density, and $\rho''$ is the average wake density along the axis of symmetry between the vortices. Numerical values of the constants are $h = 3.46$ and $q \approx 11.62$ , giving

$$\frac{d \log \Gamma}{d \log M} \approx .6 \frac{\rho - \rho''}{\rho - \rho'}$$

and since one would expect $\rho \geq \rho'' \geq \rho'$ , this gives

$$\frac{d \log \Gamma}{d \log M} \leq .6$$

Thus the only self-consistent solutions of Tombach's equations are those for which $\Omega < \pi/2$ , i.e., the converging and accelerating solutions.

Another theory was developed by Tulin and Shwartz (1971) in which they modeled the vortex system by separate velocity scaling of the flows internal and external to the wake oval, with a shear layer at the boundary between the two flow fields. Based on experiments they performed in a water tank, they conclude that the wake entrains the vorticity generated at this shear layer (in contrast to the detrainment postulated by Scorer and Davenport) but that the ingested vorticity is mainly canceled out at the wake centerline through mixing with vorticity of the opposite sign from the other side of the wake. Consequently, they model a turbulent wake in a stratified medium by assuming conservation of volume, mass, and energy and neglecting vorticity and momentum. They then find completely similar solutions which depend on four parameters -- the initial buoyancy of the wake, the stability of the fluid, the dissipation of kinetic energy, and the ratio of kinetic to potential energy. The latter two parameters are assigned values based on their experiments, which were discussed earlier.

Tulin and Shwartz give formulas for vortex wake motion in a stratified medium, which are too complex to present here, and present excellent correlations between their formulas and experiments. Their model predicts that a wake will slow down and stop its descent in a stratified fluid and that the vortex separation will increase as the wake descends. The descent in a homogeneous fluid has the behavior $z \sim t^{1/2}$ and $b \sim t^{1/2}$. In a stably stratified fluid, the descent slows down more quickly and the spreading is more rapid, but similarity no longer holds when the wake has come to rest. The nature of the motions they observed experimentally and their model endeavors to describe was shown earlier in Figure 4-10.

In the Tulin and Shwartz formulation, as well as in those discussed above, the time scale of the motion is proportional to the Vaisala period $T$. For those models which predict a stopping of wake descent, this then means that the time required for the wake to descend to its lowest level is proportional to $T$.

Saffman (1972) has presented a model which indicates that a vortex system in a stable environment descends with the vortex spacing remaining constant if there is no entrainment, and increasing if entrainment is assumed proportional to the density difference between the wake and environment. In either case, the wake descent is stopped by the stability and it subsequently oscillates vertically. To find these solutions, Saffman solves the Laplace equation for the potentials inside and outside the wake volume, with the constraint that there is no change in wake volume (except due to entrainment, which he treats separately). His criticisms of the Scorer and Davenport, and Tombach, models have already been reviewed, and his formulation was designed to overcome the deficiencies he described.

Saffman points out that it is "by no means certain" that turbulent mixing, caused by the Kelvin-Helmholtz instability of the wake-atmosphere

interface, must occur when the motion is generated aerodynamically and buoyancy effects are (at least initially) a small perturbation. As was pointed out earlier, this is a different situation from the line thermal case, where the motion is generated by buoyancy. Since the experimental evidence obtained to date does allow not allow one to assert with any confidence that significant turbulent mixing does take place, he considered both non-entraining and entraining cases for completeness.

Work by Kuhn and Nielsen (1972) attempts to model the entrainment differently than Tombach or Scorer and Davenport. One shortcoming of the Tombach model was the assumption that the rate of change of circulation was proportional to the scale of the wake. This is erroneous at small times if the wake has no initial buoyancy, since then one should have no generation of vorticity. Kuhn and Nielsen use a variable entrainment length, proportional to the density difference between the entrained fluid and the ambient fluid, with the entrained fluid density being a weighted average of the ambient density, the density in the vicinity of the vortex, and the density in the region into which the outer fluid is entrained. The effect is to make Tombach's entrainment parameter s into a variable which has value zero initially.

Kuhn and Nielson thus model the entrainment so that part of the buoyancy generated can be entrained and part of it detrained, with the proportions of each being governed by an unknown wake mixing parameter. Their analysis shows the wake accelerates as it descends and the vortex spacing decreases. Increased values of the wake mixing parameter reduce the rates of descent and convergence, while the addition of heated air to the wake, but outside the vortices, is found to cause a leveling-off and spreading of the wake. Saffman's criticisms about the proper formulation of the impulse to include the entrained vorticity apply here also.

Yet another model by Costen (1972) finds that buoyant vortex cores (different from the buoyant wake considered in the other models) will accelerate and close together as they descend in a neutral atmosphere. He concludes that stable atmospheric stratification will accelerate the effect. Costen also suggests that a strong inversion layer might retard the vortex motion and cause their spacing to increase, but does not present any support for this inference.

In summary, the analytical situation with respect to the effects of stratification is not clearer than the experimental one. In fact, if one arrives at a consensus based solely on the number of models which predict the same behavior, one would conclude that buoyancy causes the wake to accelerate downward and the vortex spacing to decrease. This appears to be in contradiction to the experimental observations, which suggest the opposite behavior. Both the theories and the experiments may be correct however, with the differences being due to factors such as entrainment (due to, say, ambient turbulence) which were not considered in the models. In fact, all of the models which predict the slowing down and spreading out behavior do include entrainment as a factor.

There are fundamental questions which arise about the formulations of these models, however, some of which were raised during the discussion. All of the models contain simplifying assumptions about the distribution of vorticity and of buoyancy, in order to make a tractable problem. In many cases the effect of such assumptions is not really known, nor is there empirical evidence to support or refute their validity.

As part of the current study, AV has developed a more rigorous description of the effects of buoyancy on a wake descending through

an inviscid, non-turbulent, incompressible, stratified fluid. It also concludes that the effect of buoyancy is to contract the vortex spacing and accelerate the wake motion. The analytical derivation of this conclusion is presented in the next subsection, in which the model is described in detail. Extension of the derivation to a compressible stratified medium is straightforward, and requires only that the potential temperature or potential density gradient be used in the computation of the Vaisala period.

## 4.4.3 NEW THEORY FOR TRAILING VORTICES IN A STABLY STRATIFIED ATMOSPHERE

### Nature of the Theory

The new theory is based on two approximations, best illustrated by dimensional reasoning. We focus attention on the x-y plane and imagine that an aircraft passes through the origin of the coordinates at time $t = 0$. The aircraft generates a pair of vortices of circulation $\pm \Gamma$ and initial separation $2s_o$, and the vortices descend along the y-axis according to some displacement history $y(t) < 0$. The displacement $y(t)$ can be transformed into a spatial trajectory $y(z/U)$, where U is the speed of the aircraft and z is distance behind, but non-steady motion in the x-y plane is a more convenient point of view for the present analysis.

If the atmosphere were of uniform density, then the vortex spacing would remain constant, and the pair would descend according to the formula

$$y = - \frac{\Gamma}{4\pi s_o} t \quad .$$

But we are interested in the case where the ambient density $\rho_o$ is a function of y, say

$$\rho_o(y) = \rho_o + y \frac{d\rho_o}{dy} + \cdots \cdots \quad ,$$

where $d\rho_o/dy$ is negative in a stable atmosphere, and the first two terms of the Taylor series describe the density variation with sufficient accuracy near the vortices. Stratification implies that y may depend on

$\rho_o$ , on $d\rho_o/dy$ , and on the acceleration of gravity $g$ , as well as on the vortex parameters introduced already. Thus, $y = y\,(t, \Gamma, s_o, \rho_o, d\rho_o/dy, g)$ , which can be simplified by dimensional analysis as follows:

$$y = \frac{\Gamma}{4\pi N s_o}\; y^*\,(Nt, NT, s_o/g\,T^2) \quad .$$

N is the Brunt-Vaisala frequency for atmospheric gravity waves,

$$N = \sqrt{-\frac{g}{\rho_o}\,\frac{d\rho_o}{dy}} \quad ,$$

and T is the time required for the vortex pair to induct itself downward a distance $s_o$ in the absence of stratification:

$$T = \frac{4\pi s_o^2}{\Gamma}$$

$y^*$ is the dimensionless trajectory of the vortex pair, depending on the dimensionless time $Nt$ , and on two dimensionless parameters $NT$ and $s_o/gT^2$ . The possibility must also be admitted that the spacing $2s$ between the vortices changes as the pair descends into a stably stratified atmosphere, so

$$s = s_o\, s^*(Nt, NT, s_o/g\,T^2)$$

by similar dimensional reasoning. Note that the kinematic viscosity $\nu$ does not appear in the arguments of $y^*$ and $s^*$ . The Reynolds number $\Gamma/\nu$ is enormous in practical situations, say $10^8$, and the theory accounts for the effect of stratification without reference to viscous or turbulent diffusion.

The parameter NT is a measure of the strength of the stratification relative to the internal dynamics of the vortex pair. If NT is small, then the vortices travel downward many times their own separation within a single period of the gravity waves that they generate. The parameter $s_o/gT^2$ measures the ratio of fluid acceleration induced by the vortices to the acceleration of gravity. Local acceleration of a fluid particle operating on the density gradient within it generates vorticity. If $s_o/gT^2$ is small, the vorticity arising in the flow surrounding the original vortex pair is mainly the result of gravity acting on density gradients. To estimate NT and $s_o/gT^2$, recall that

$$N = \sqrt{\gamma}\,\frac{g}{c} \approx 0.035 \text{ sec}^{-1}$$

for an isothermal atmosphere, where $\gamma$ is the ratio of specific heats, $c$ is the adiabatic speed of sound, and the numerical estimate is based on $\gamma = 1.4$ and the sea-level value $c = 1100$ ft/sec. An isothermal atmosphere is untypically stable, so $0.035 \text{ sec}^{-1}$ can be taken as the practical upper limit of N. A Boeing 747 generates vortices of strength $\Gamma = 9000 \text{ ft}^2/\text{sec}$ and spacing $2s_o = 110$ ft during approach to landing (Crow and Olsen, 1969), so the parameters entering the stratification problem are of order

$$NT = 0.15$$

at most, and

$$\frac{s_o}{gT^2} = 0.10 \quad .$$

The theory is designed to exploit the fact that both parameters are much smaller than unity. In fact, the acceleration parameter $s_o/gT^2$ is much

less important to the structure of the theory than NT , so the trajectory and vortex separation will emerge as a one-parameter family

$$y = \frac{\Gamma}{4\pi N s_o} \, y^*(Nt, NT) \quad ,$$

$$s = s_o s^*(Nt, NT) \quad ,$$

with

$$NT << 1 \quad .$$

The idea of weak stratification is acceptable enough, but it leads to mathematical conclusions that seem to defy intuition. The point of view taken here is that the conventional intuition is appropriate, if at all, to the limit $NT >> 1$ opposite to the limit of aeronautical interest. Most previous theories imply that the recirculation cell surrounding the vortices becomes buoyant as it descends into heavier fluid and bounces upward after a time of order $N^{-1}$, as though the cell were a gas-filled balloon (cf. Saffman 1972). Those theories originate from the work of Turner (1960), who was concerned with vortices generated from rest by buoyancy. But here the wake is assumed to descend too fast for buoyancy to generate significant local vorticity. The vorticity responsible for altering the trajectory of the wake arises slowly, primarily in a region above the wake called the buoyant upwash. The flow induced by the upwash draws the vortices together and diminishes the volume of their recirculating fluid. Ultimately the vortices diffuse into one another, while the upwash relaxes into Boussinesq gravity waves, which carry the impulse of the aircraft wake to infinity.

## Hydrodynamic Drift

The passage of a vortex pair leaves no residual velocity disturbance in an ideal fluid. Fluid particles, however, suffer a net downward displacement during the passage, called drift in the hydrodynamic literature. Figure 4-11. illustrates the drift of fluid particles above the closed recirculation cell of the trailing vortices. The heavy lines in the drawing can be regarded as filaments of ink, inscribed horizontally in the x-y plane prior to the start of vortex motion. The filament BB below the recirculation cell as yet is hardly disturbed, but the filament AA has been stretched around the cell and sucked downward behind it. As time passes the filament approaches an asymptotic displacement h(x) , which is permanent in an unstratified fluid. The drift h(x) was introduced by Darwin (1953), who showed that the integral

$$\rho_0 \int_{-\infty}^{\infty} h(x)\, dx$$

is an apparent mass, in this case the apparent mass of the fluid outside the recirculation cell. The drift h(x) diverges logarithmically at x = 0 owing to the stagnation point of the recirculation cell, but the integral is finite.

No analytical solution for the drift of a vortex pair is known, but h(x) can be computed numerically from the construction of Figure 4-12. For the moment the coordinates x-y are fixed to the vortices, so the flow outside the recirculation cell is steady, with an upward velocity $V = \Gamma/4\pi s$ at infinity. Fluid particles P and Q move on separate streamlines, P passing close to the recirculation cell and Q remaining indefinitely far away. Suppose P and Q come from the same stratum y far below the vortices and are presently

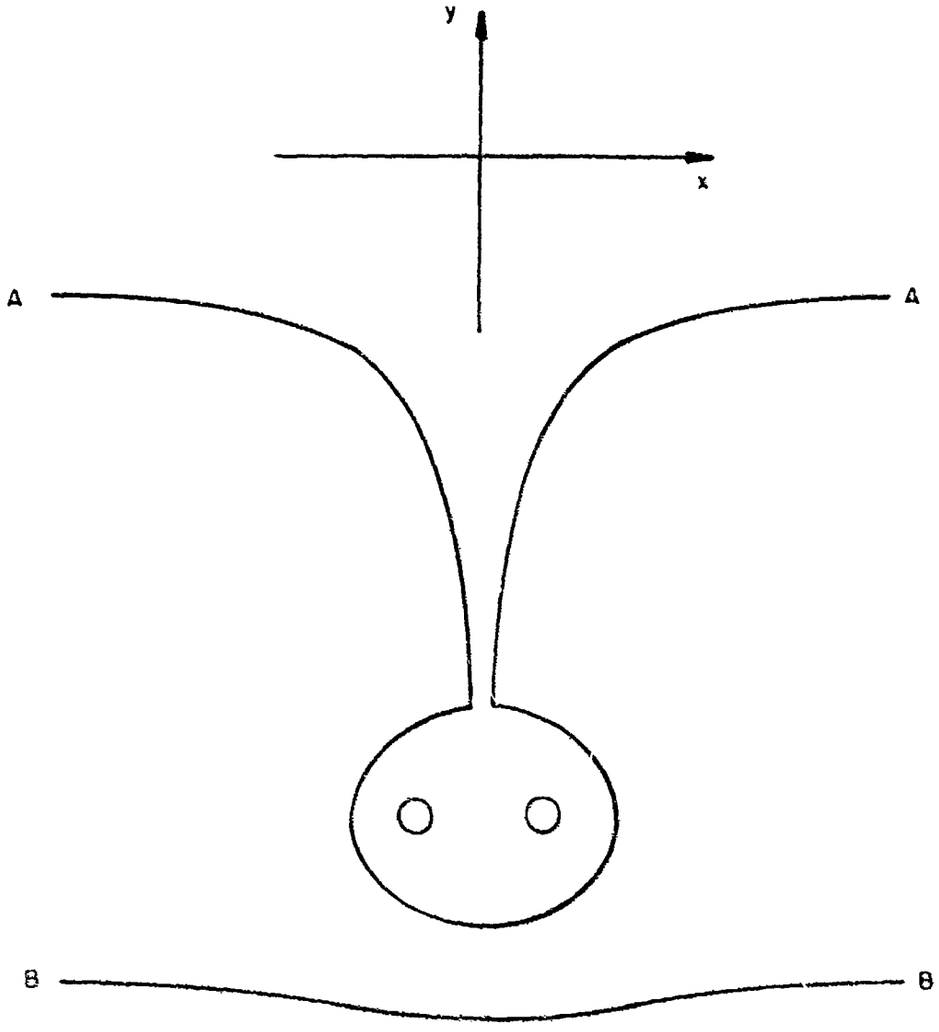


Figure 4-11. Formation of Drift Behind a Vortex Pair

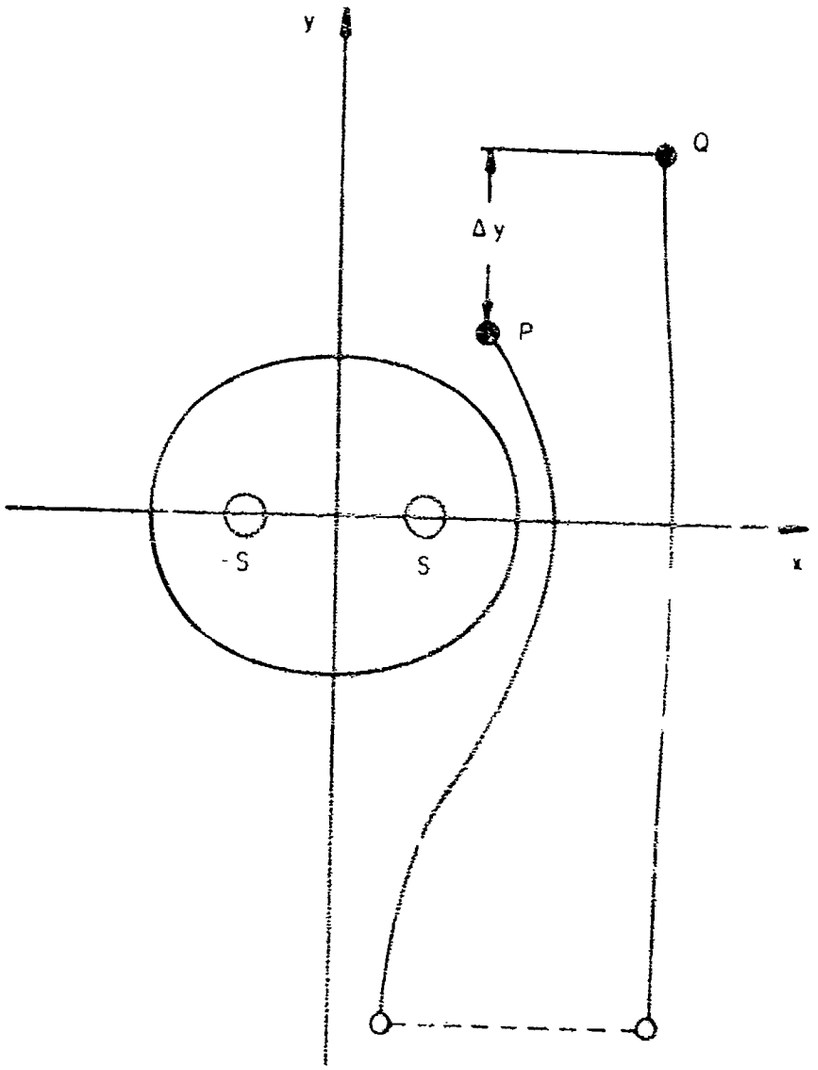


Figure 4-12. Calculation of Drift

separated a distance $y$ vertically. Then

$$\frac{d\Delta y}{dt} = V - v(\Psi, y) \quad ,$$

where $v$ is the vertical component of velocity at $P$, $\Psi$ is the stream function identifying the streamline on which $P$ is moving, and $y$ is the current location of $P$. Moreover,

$$\frac{d\Delta y}{dy} = \frac{d\Delta y}{dt}\,\frac{dt}{dy} = \frac{V-v}{v} \quad ,$$

so

$$h = \int_{-\infty}^{\infty} \left[\frac{V}{v(\Psi, y)} - 1\right] dy \quad , \qquad (4\text{-}7)$$

which gives the ultimate displacement of a particle on the streamline $\Psi$. The stream function for the flow around a pair of vortices located at $x = \pm s$, $y = 0$ is given by the formula

$$-\Psi(x, y) = -V\left\{ \ell n \left[\frac{y^2 + (x-s)^2}{y^2 + (x+s)^2}\right] + x \right\} \quad ,$$

which can be solved for $x(\Psi, y)$ by iteration. The resulting value of $x$ can be substituted into the formula

$$v = -\frac{\partial \Psi}{\partial x} = V\left[\frac{2(x-s)s}{y^2+(x-s)^2} - \frac{2(x+s)s}{y^2+(x+s)^2} + 1\right]$$

to determine $v(\Psi, y)$. The procedure is repeated for each step of the integration 4-7, resulting in numerical values of the drift $h(x) = h(-\Psi/V)$.

The drift is best presented as a universal function $\eta(\xi)$, where

$$h = s(t)\eta(\xi) \quad , \quad \xi = \frac{x}{s(t)} \tag{4-3}$$

Here we take account of the fact that the separation $2s(t)$ between the vortices may change slowly with time, but the <u>shape</u> of their recirculation cell and the <u>shape</u> of the drift they leave behind will be invariant.

Figure 4-13 is a plot of the dimensionless drift $\eta(\xi)$. The function was obtained numerically by the procedure outlined above. Semi-logarithmic coordinates are used to emphasize the asymptotic behavior of $\eta$ for small $\xi$, and in fact the asymptotic expression

$$\eta = 1.073 - 2.298 \ln|\xi|$$

is rather accurate throughout the range $0 < |\xi| < 1$. A quantity of major importance in the theory of wake descent is the integral

$$D = \int_{-1}^{1} \eta(\xi)\, d\xi = 8.184 \quad , \tag{4-9}$$

which also was evaluated numerically. It is a curiosity of the theory that the influence of stratification depends upon the part of the drift between the vortex cores, as further analysis will show, rather than upon the integral.

$$\int_{-\infty}^{\infty} \eta(\xi)\, d\xi$$

proportional to the apparent mass of the recirculation cell.

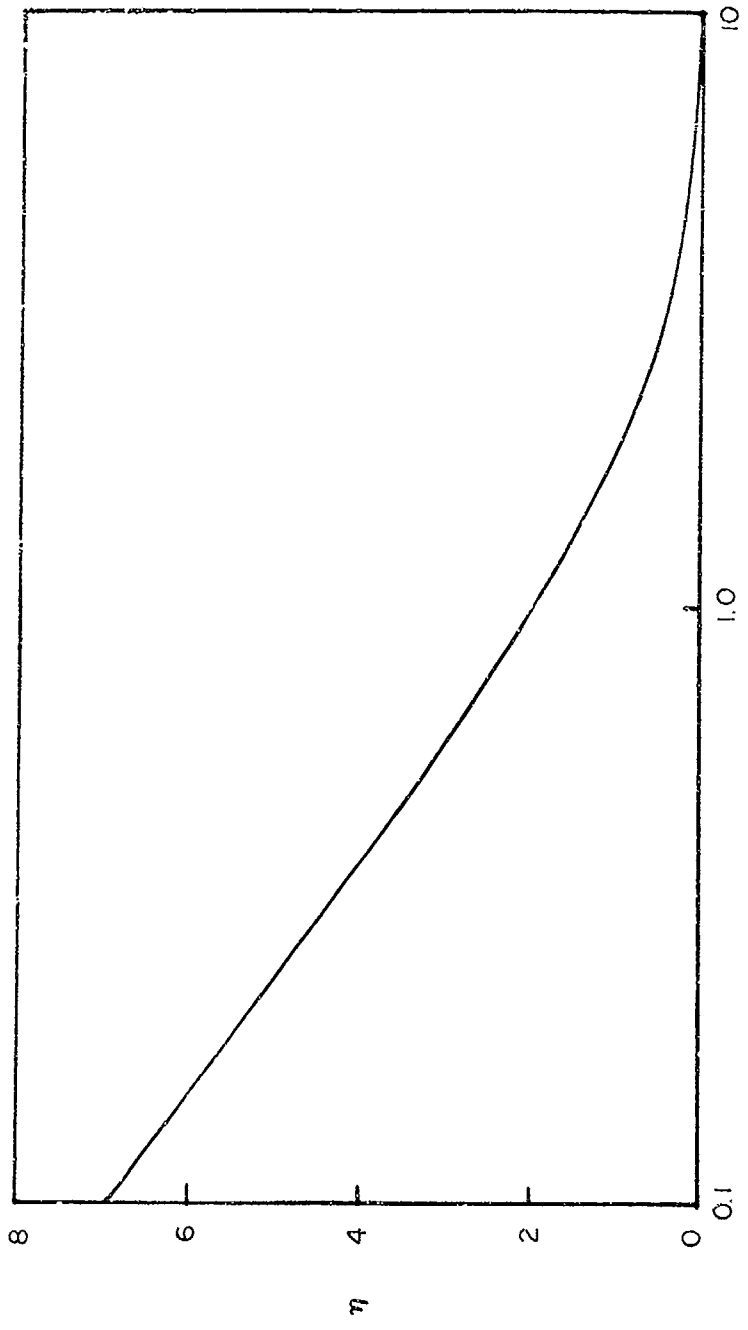


Figure 4-13. The Dimensionless Drift, $\eta(\xi)$.

## Buoyant Upwash

Drift would have no dynamical consequences in a neutrally stable atmosphere. The flow velocity would relax to zero after the passage of the wake, and fluid particles would remain permanently depressed. When the atmosphere is stratified, however, the drift results in a density distribution that cannot persist. The density distribution immediately above the wake is illustrated in Figure 4-14, where the darker bands represent the heavier strata of fluid. The wake leaves behind a density field

$$\rho(x, y) = \rho_o(y) + h(x) \frac{d\rho_o(y)}{dy} \quad . \tag{4-10}$$

By our sign convention h is positive, and $d\rho_o/dy$ is negative in a stably stratified atmosphere, so the density is reduced behind the vortex pair.

The next dynamical stage is that the depressed light fluid buoys upward. The initial buoyant motion is best treated in terms of the vorticity equation, which can be written as

$$\frac{D\underset{\sim}{\zeta}}{Dt} = \frac{\nabla\rho}{\rho} \times (\underset{\sim}{g} - \frac{D\underset{\sim}{u}}{Dt}) \tag{4-11}$$

for two-dimensional flow (vortex stretching is absent). Here $\underset{\sim}{\zeta}$ is the vorticity aligned in the z-direction, and $D\underset{\sim}{\zeta}/Dt$ is the rate of change of vorticity following a fluid particle. The right-hand side is the Bjerkness force, coupling the density gradient $\nabla\rho$ to the acceleration of gravity $\underset{\sim}{g}$ diminished by the particle acceleration $D\underset{\sim}{u}/Dt$. The ratio of $D\underset{\sim}{u}/Dt$ to $\underset{\sim}{g}$ is of order $s_o/gT^2$, a small parameter according to Section 1, so the particle acceleration can be neglected compared with gravity in Eqn. (4-11).

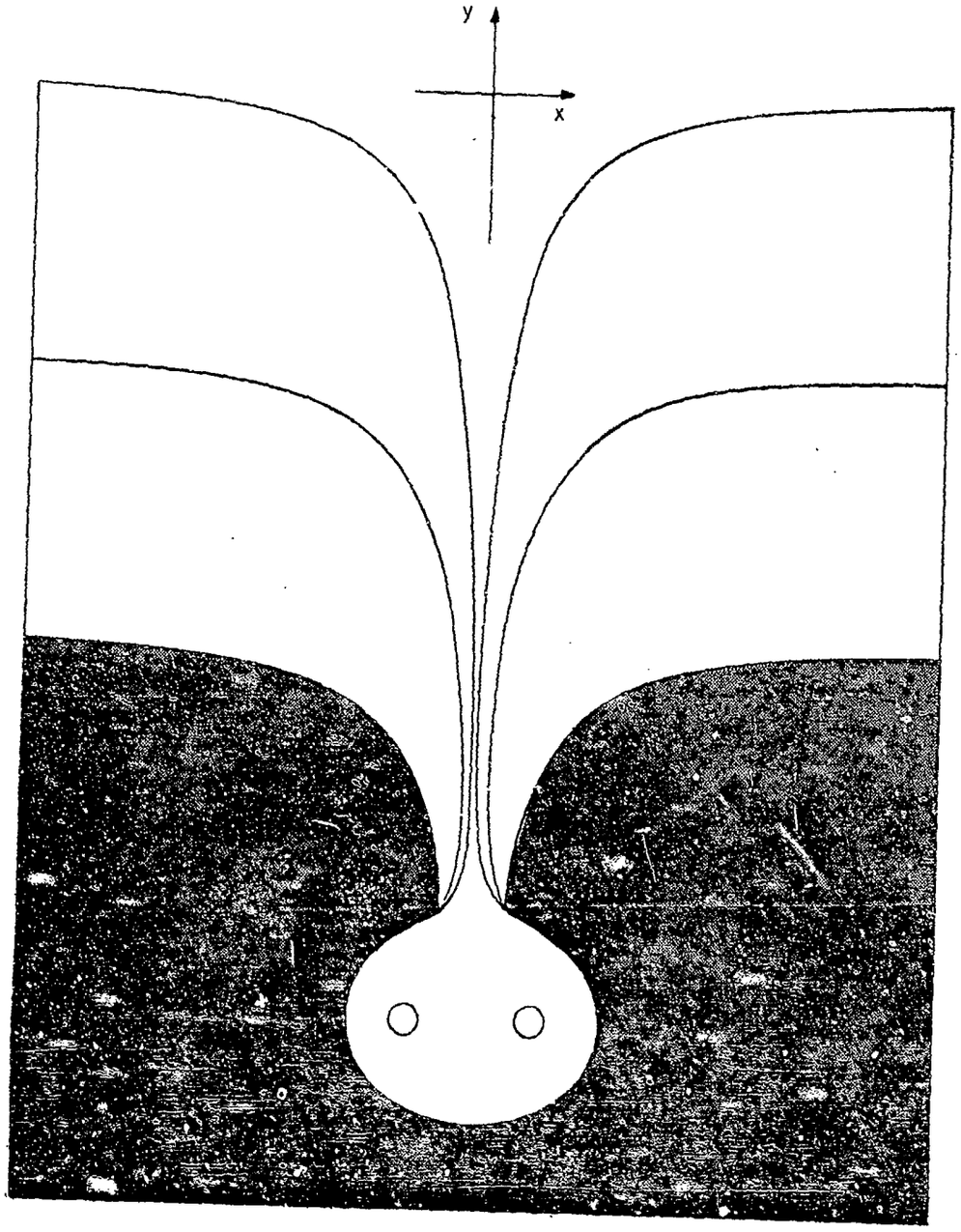


Figure 4-14. Density Field Above the Wake.

Suppose the current time is $t$, and the trailing vortices passed level $y(\tau)$ at some previous time $\tau$. If the time difference $(t-\tau)$ is short compared with the inverse of the Brunt-Vaisala frequency $N$, then the vorticity $\zeta$ is in the initial stage of growth described by the linearized version of Eqn. (4-11), namely

$$\frac{\partial \zeta}{\partial t} = - \frac{g}{\rho_o} \frac{\partial \rho}{\partial x} ,$$

where the cross-product has been performed, and $\rho_o$ has been substituted for $\rho$ with sufficient accuracy in the denominator. By virtue of Eqn. (4-10).

$$\frac{\partial \zeta}{\partial t} = - \frac{g}{\rho_o} \frac{d\rho_o}{dy} \frac{dh}{dx} = N^2 \frac{dh}{dx} ,$$

and from Eqn. (4-8),

$$\frac{\partial \zeta}{\partial t} = N^2 \eta' \left[\frac{x}{s(\tau)}\right] ,$$

where the prime denotes differentiation with respect to the dimensionless argument of $\eta$. The vorticity equation can be integrated from the time of wake passage $\tau$ to the current time $t$, with the result that

$$\zeta[x, y(\tau)] = N^2 (t-\tau) \eta' \left[\frac{x}{s(\tau)}\right] \qquad (4-12)$$

as long as

$$N(t-\tau) << 1 .$$

The ordinate y is given the argument $\tau$ as a reminder that we are dealing with the stratum y penetrated by the vortex pair at time $\tau$, when the vortex cores were separated a distance $2s(\tau)$.

The drift $\eta(\xi)$ is positive and decreases symmetrically around $\xi = 0$, so the vorticity $\zeta$ is antisymmetric and negative for positive x. The vorticity distribution (Eqn. (4-12) thus represents an upwelling of gathering strength behind the original vortex pair. Figure 4-15 depicts the vertical component of velocity within the upwelling flow. From the vantage point of the vortex pair, the flow appears as a concentrated upwash whose strength increases linearly with distance upward, a buoyant upwash. Figure 4-16 shows instantaneous streamlines induced by the buoyant upwash. The induced flow tends to draw the trailing vortices upward and together.

## Induction by the Buoyant Upwash

The trailing vortices move under their own induction and the induced field of the buoyant upwash. Suppose the right-hand vortex is located at $x = s(t)$ and $y = y(t)$. Then it moves according to the equations

$$\frac{dy}{dt} = -\frac{\Gamma}{4\pi s(t)} + v \quad , \tag{4-13a}$$

$$\frac{ds}{dt} = u \quad , \tag{4-13b}$$

where $\Gamma/4\pi s(t)$ is the downward speed induced by the left-hand vortex, u is the x-component of velocity induced by the upwash, and v is the y-component. Both u and v are to be evaluated at $x = s(t)$, $y = y(t)$.

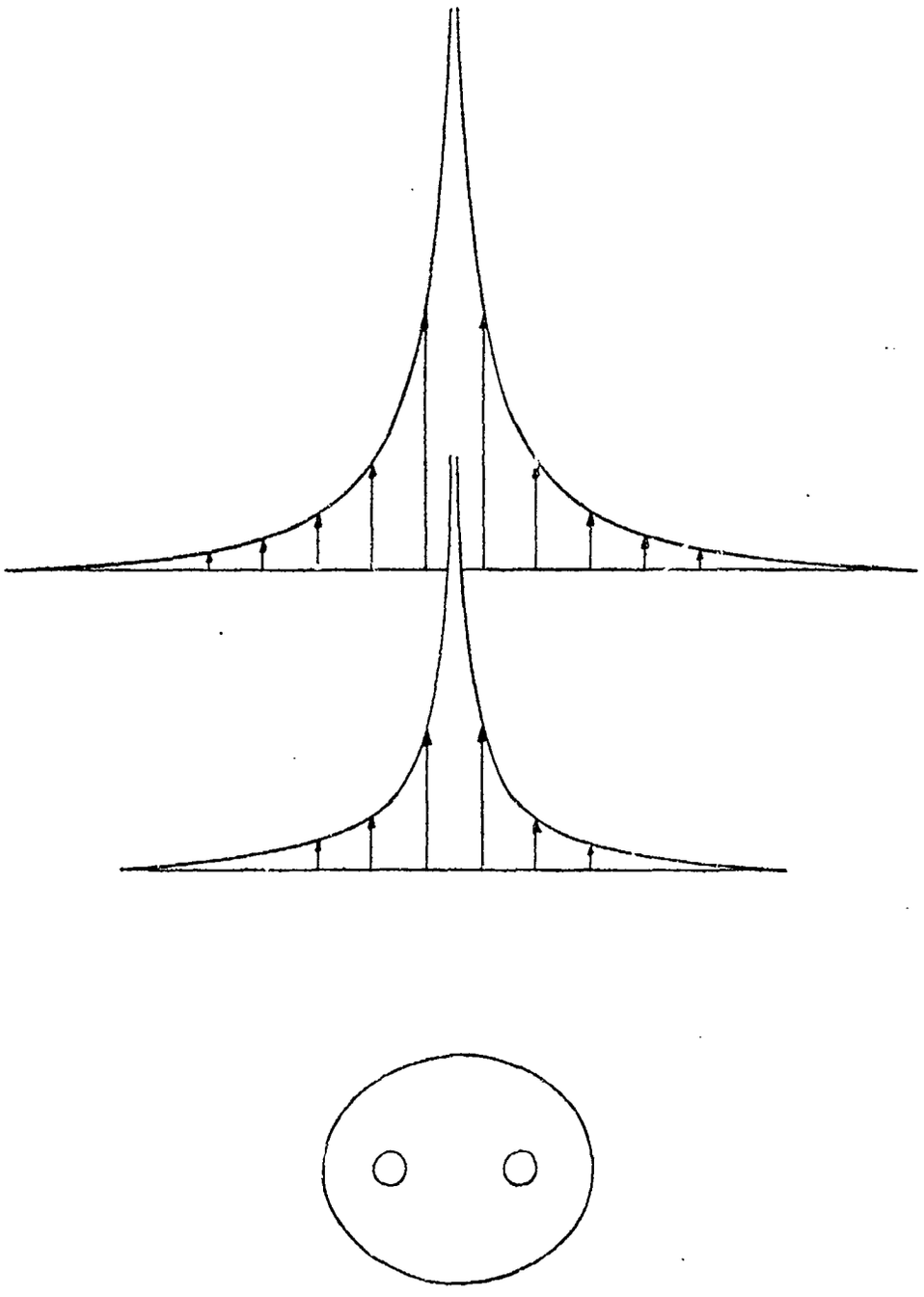

Figure 4-15. Profiles of the Buoyant Upwash.

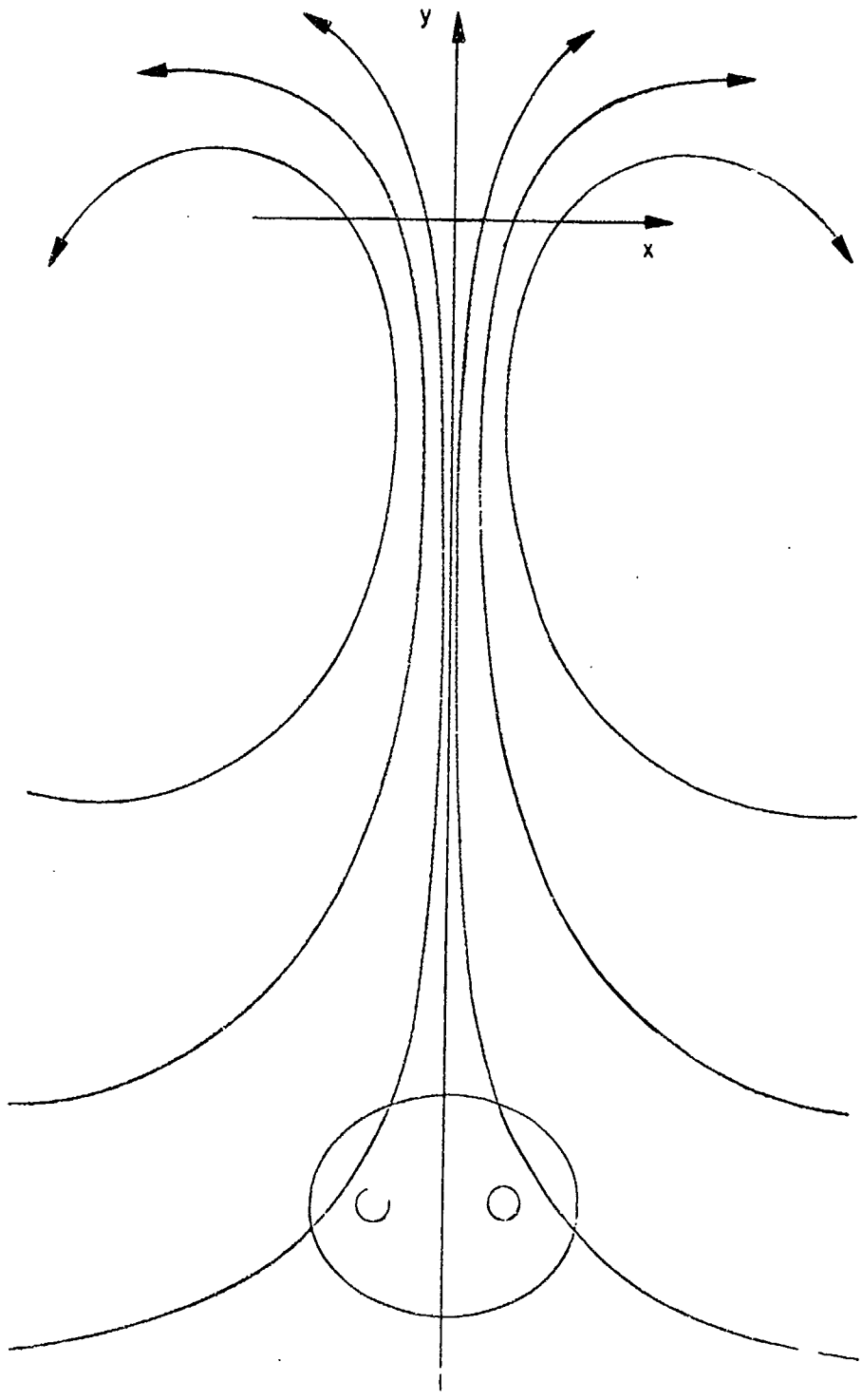


Figure 4-16. Induced Field of the Buoyant Upwash.

The vorticity distribution $\zeta$ determines u and v according to the construction shown in Figure 4-17 An area element dA is located at x , $y(\tau)$ a distance

$$r = \sqrt{[s(t)-x]^2 + [y(\tau) - y(t)]^2} \qquad (4\text{-}14)$$

away from the trailing vortex. A vorticity element $\zeta dA$ has evolved since time $\tau$ and currently induces a velocity

$$du = \zeta dA \frac{[y(\tau) - y(t)]}{2\pi r^2} \quad . \qquad (4\text{-}15a)$$

$$dv = \zeta dA \frac{[s(t) - x]}{2\pi r^2} \qquad (4\text{-}15b)$$

The induced velocity u, v follows by integrating Eqns. (4-15) over the x-y plane. It is convenient to introduce the transformation

$$dA = dx\, dy(\tau) = dx \left|\frac{dy}{d\tau}\right| d\tau \quad .$$

If $N(t-\tau)$ is everywhere small, the vorticity field (4-12) can be combined with Eqns. (4-15) to produce the following results:

$$u = \int_0^t d\tau \int_{-\infty}^{\infty} dx\, N^2(t-\tau)\, \eta' \left[\frac{x}{s(\tau)}\right] \left|\frac{dy}{d\tau}\right| \frac{[y(\tau) - y(t)]}{2\pi r^2} \quad ,$$

$$v = \int_0^t d\tau \int_{-\infty}^{\infty} dx\, N^2(t-\tau)\, \eta' \left[\frac{x}{s(\tau)}\right] \left|\frac{dy}{d\tau}\right| \frac{[s(t) - x]}{2\pi r^2} \quad ,$$

where r is given by Eqn. (4-14) A partial integration over x removes the derivative on $\eta$, and finally

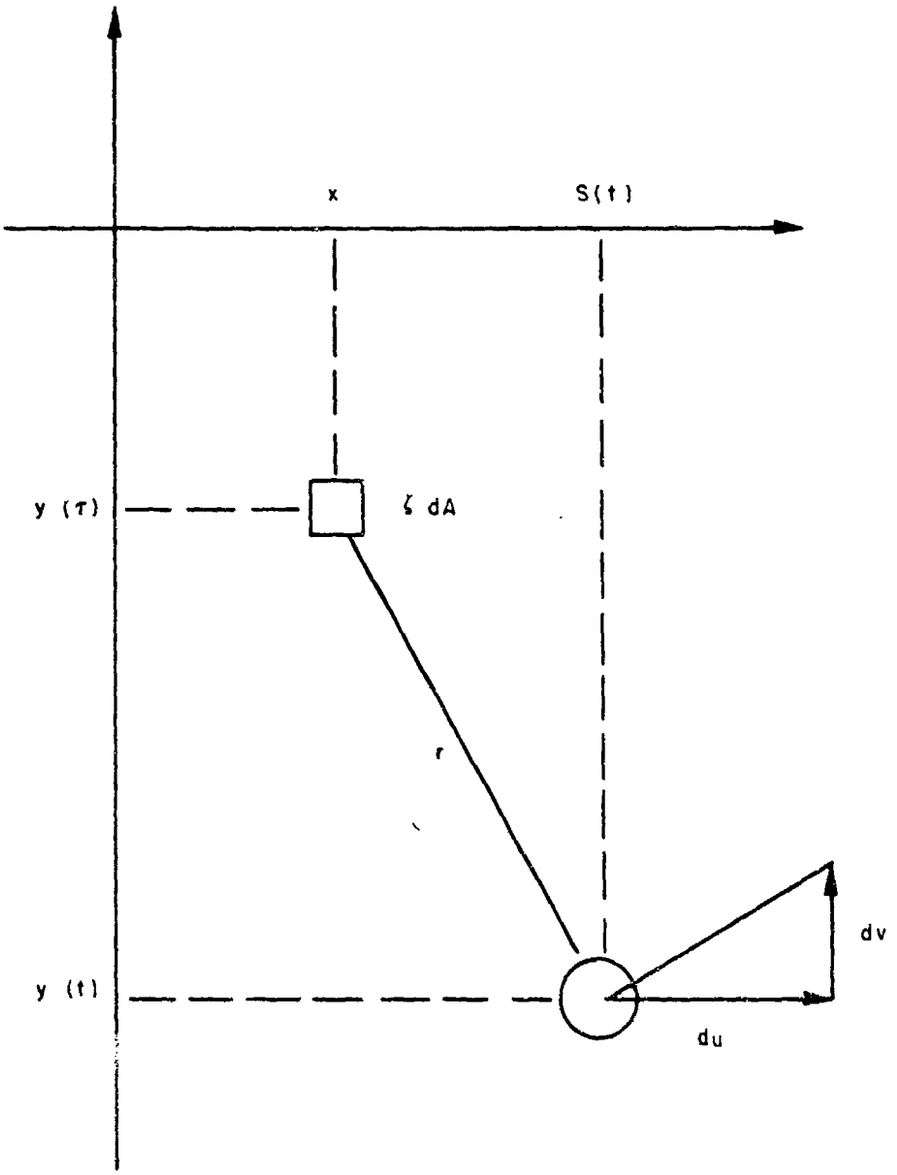


Figure 4-17. Framework for Calculating the Buoyancy-Induced Field at a Vortex Core.

$$u = \int_0^t d\tau \int_{-\infty}^{\infty} dx\, N^2(t-\tau)s(\tau)\eta\left[\frac{x}{s(\tau)}\right] \left|\frac{dy}{dt}\right| \frac{2[y(\tau)-y(t)][x-s(t)]}{2\pi r^4} \qquad (4\text{-}16a)$$

$$v = \int_0^t d\tau \int_{-\infty}^{\infty} dx N^2(t-\tau)s(\tau)\eta\left[\frac{x}{s(\tau)}\right] \left|\frac{dy}{dt}\right| \left\{\frac{[y(t)-y(\tau)]^2-[x-s(t)]^2}{2\pi r^4}\right\} \qquad (4\text{-}16b)$$

Now consider the structure of Eqns. (4-13) and (4-16). The integrations over x in Eqns. (4-16) could be carried out numerically if the current value s(t) and its previous values $s(\tau)$ were known. The remaining integrals over $\tau$ involve the prior history of the vortex trajectory $s(\tau)$, $y(\tau)$ weighted by the memory function $N^2(t-\tau)$. Equations (4-13) and (4-16) are thus a set of integro-differential equations for the trajectory s(t), y(t). They could be solved step-by-step numerically up to a time when Nt ceases to be small. Beyond that time the memory function $N^2(t-\tau)$ becomes suspect over earlier times $\tau$. We should expect the memory function to become oscillatory in the manner of an atmospheric gravity wave.

To pose the correct gravity-wave problem, we must examine the integrand of Eqn. (4-16b) under the simultaneous conditions

$$N(t-\tau) << 1 \ , \qquad (4\text{-}17a)$$

$$\Delta y = y(\tau) - y(t) >> s(\tau) \qquad (4\text{-}17b)$$

Both inequalities can be satisfied if the parameter NT is sufficiently small, because

$$\Delta y \sim \frac{(t-\tau)}{T} s \quad .$$

Inequality Eqn. (4-17a) means that we are dealing with a time lapse $(t-\tau)$ such that the simple vorticity formula Eqn. (4-12) is still valid, and Eqn. (4-17b) means that

$$\frac{(\Delta y)^2 - [x-s(t)]^2}{2\pi r^4} \approx \frac{1}{2\pi(\Delta y)^2}$$

for any x such that $\eta[x/s(\tau)]$ is appreciable. Then the integrand of the integral over $\tau$ is approximately

$$\frac{N^2(t-\tau)}{2\pi(\Delta y)^2}\left[\left|\frac{dy}{d\tau}\right| s^2(\tau) \int_{-\infty}^{\infty} \eta(\xi)\, d\xi\right] \qquad (4-18)$$

where the term in square brackets is the total rate of volumetric displacement per unit time. The exact shape of the drift $\eta(\xi)$ is immaterial at large $\Delta y$, which suggests that we look for gravity waves generated by a concentrated impulsive displacement of fluid.

## Boussinesq Far Field

A concentrated impulsive displacement can be represented as a product of delta functions:

$$\tilde{v}(x, y, t) = -Q\,\delta(x)\,\delta(y)\,\delta(t) \qquad (4-19)$$

The meaning of Eqn. (4-19) is that an element of fluid of vanishing area A is impelled downward an arbitrarily large distance D in such a way that the product AD equals a finite volume Q . The concentrated displacement imparts an infinite potential energy to the fluid, which serves as an infinite reservoir for the growth of kinetic energy later on. The problem is similar to the impulsive displacement of a free water surface, as treated at length by Lamb (1932).

Equation (4-19) is valid only near $t = 0$ . Throughout the course of its evolution, the vertical component of velocity $\tilde{v}$ satisfies the Boussinesq wave equation

$$\frac{\partial^2}{\partial t^2} \nabla^2 \tilde{v} + N^2 \frac{\partial^2 \tilde{v}}{\partial x^2} = \frac{\partial^2}{\partial t^2} \nabla^2 [Q\delta(x)\delta(y)\delta(t)] \qquad (4-20)$$

where the inhomogeneous forcing function on the right-hand side insures that Eqn. (4-19) is satisfied near $t = 0$ . The wave Eqn. (4-20) is based on the assumption that $\tilde{v}$ is small enough to render nonlinear convection unimportant (cf. Yih 1969). We are interested in the response of the stratified atmosphere to drift imposed many vortex spacings away (inequality Eqn. (4-17b), so the linearization implicit in Eqn. (4-20) should be all right. Once Eqn. (4-20) is solved in the form

$$\tilde{v}(x, y, t) = Qf(x, y, t)$$

for quiescent conditions prior to time zero, then the solution for a displacement source moving down the y-axis can be written as a Duhamel's integral:

$$v(x, y, t) = \int_0^t f[x, y-y(\tau), t-\tau] \frac{d\Omega}{d\tau} d\tau \qquad (4-21)$$

If the theory is correctly formulated, then the integrand of Eqn. (4-21) at $x = 0$ should match Eqn. (4-18) in the limit $N(t-\tau) \ll 1$. A condition for matching ought to be that

$$\frac{d\Omega}{d\tau} = \left|\frac{dy}{d\tau}\right| s^2(\tau) \int_{-\infty}^{\infty} \eta(\xi) d\xi \quad , \tag{4-22}$$

whereby $d\Omega/d\tau$ can be identified as the rate of creation of drift. The temporal behavior of $f(0, \Delta y, t-\tau)$ should yield a uniformly valid memory function, matching the function $N^2(t-\tau)$ of Eqn. (4-18) for small values of $N(t-\tau)$, and displaying oscillations for large $N(t-\tau)$. The approach resembles a singular-perturbation theory, with the vorticity distribution (4-12) as the inner solution, and the Boussinesq wave field as the outer solution.

The method for solving dispersive wave equations like (4-20) was developed in full generality by Lighthill (1965). The solution is assumed to have the form of a double Fourier integral,

$$\tilde{v} = \int_{-\infty}^{\infty} dk \int_{-\infty}^{\infty} d\ell \; e^{i(kx+\ell y)} \left[ F_1(k, \ell)\, e^{i\omega t} + F_2(k, \ell)\, e^{-i\omega t} \right] \tag{4-23}$$

in which $\omega(k, \ell)$ is chosen to satisfy the homogeneous wave equations for $t > 0$, and $F_1$ and $F_2$ are chosen to model the particular excitation that takes place at $t = 0$. In the case of Eqn. (4-20)

$$\omega = \frac{Nk}{K} \quad ,$$

where

$$K = \sqrt{k^2 + \ell^2}$$

The phase velocity $\underset{\sim}{c}_p$ of the waves and their group velocity $\underset{\sim}{c}_g$ play an important role in evaluating Eqn. (4-23) in the limit of large Nt:

$$\underset{\sim}{c}_p = \frac{\omega}{K}\left(\frac{k}{K}\underset{\sim}{e}_x + \frac{\ell}{K}\underset{\sim}{e}_y\right) = \frac{Nk}{K^3}\left(k\,\underset{\sim}{e}_x + \ell\,\underset{\sim}{e}_y\right) ,$$

and

$$\underset{\sim}{c}_g = \frac{\partial\omega}{\partial k}\underset{\sim}{e}_x + \frac{\partial\omega}{\partial \ell}\underset{\sim}{e}_y = \frac{N\ell}{K^3}\left(\ell\underset{\sim}{e}_x - k\underset{\sim}{e}_y\right) \qquad (4\text{-}24)$$

where $\underset{\sim}{e}_x$ and $\underset{\sim}{e}_y$ are unit vectors in the x and y directions. The phase velocity and group velocity are perpendicular to each other,

$$\underset{\sim}{c}_p \cdot \underset{\sim}{c}_g = 0 ,$$

which means the disturbance radiates outward as a fan, with radii of constant angle $\theta = \tan^{-1}(x/y)$ being lines of constant phase. Mowbray and Rarity (1967) evaluated Eqn. (4-23) in the limit of large Nt by the method of stationary phase and presented some beautiful photographs of the Boussinesq wave field around a point disturbance.

The method of stationary phase, however, is not applicable to the present analysis. In the first place, we need the behavior of Eqn. (4-23) in the limit of small Nt in order to match the inner solution (4-18) and secondly, we must fine $\tilde{v}$ on the y-axis, where the method of stationary phase happens to break down. The origin of the breakdown is evident in Eqn. (4-24); waves propagating directly down the y-axis must have $\ell = 0$, in which case $\underset{\sim}{c}_g = 0$. We must turn to the full solution (4-23), which takes the form

$$\tilde{v} = \frac{\partial^2}{\partial t^2}\left[-H(t)\,\frac{Q}{\pi^2 N}\int_0^\infty dk \int_0^\infty d\ell\,\frac{K}{k}\sin\frac{kNt}{K}\cos kx\,\cos \ell y\right] \qquad (4\text{-}25)$$

for the problem posed in Eqn. (4-20). H(+) is the Heaviside unit step function, and Eqn. (4-25) is valid throughout all time $-\infty < t < \infty$. For $t > 0$, the time derivatives can be carried through the integrations

$$\tilde{v} = \frac{QN}{\pi^2} \int_0^\infty dk \int_0^\infty d\ell \, \frac{k}{K} \sin \frac{kNt}{K} \cos kx \cos \ell y \ ,$$

$$t > 0 \ .$$

In particular

$$f(0, y, t) = \frac{N}{\pi^2} \int_0^\infty dk \int_0^\infty d\ell \, \frac{k}{K} \sin \frac{kNt}{K} \cos \ell y \ . \qquad (4\text{-}26)$$

which gives the response along the y-axis to a unit volumetric displacement at the origin.

Expression (4-26) can be evaluated by transforming the variables of integration from $k, \ell$ to $K, \ell$. Thus

$$f(0, y, t) = \frac{N}{\pi^2} \int_0^\infty dK \int_0^K d\ell \, \sin \left( \frac{Nt}{K} \sqrt{K^2 - \ell^2} \right) \cos \ell y \ .$$

According to entry 3.876.7 in the tables of Gradshteyn and Ryzhik (1965),

$$\int_0^K \sin \left( p \sqrt{K^2 - \ell^2} \right) \cos \ell y \, d\ell = - \frac{\pi}{2} \frac{\partial}{\partial p} J_0 \left( K \sqrt{y^2 + p^2} \right) \ .$$

Thus

$$f(0, y, t) = - \frac{N}{2\pi} \int_0^\infty \frac{J_0' \left[ \sqrt{(Ky)^2 + (Nt)^2} \right]}{\sqrt{(Ky)^2 + (Nt)^2}} \, Nt \, K \, dK \ .$$

Substitute

$$\kappa = \sqrt{(Ky)^2 + (Nt)^2} \quad ,$$

with the result that

$$f(0, y, t) = -\frac{N^2 t}{2\pi y^2} \int_{Nt}^{\infty} J_o'(\kappa) d\kappa$$

$$= \frac{N^2 t \, J_o(Nt)}{2\pi y^2} \quad . \qquad (4\text{-}27)$$

Equation (4-27) meets the objective of the Boussinesq-wave analysis. $J_o(Nt)$ is a Bessel function of the first kind, with asymptotic behavior such that

$$f(0, y, t) \rightarrow \sqrt{\frac{N^3 t}{2\pi^3}} \; \frac{\cos(Nt - \pi/4)}{y^2}$$

as $Nt \rightarrow \infty$ .

The impulse response $f(o, y, t)$ oscillates in time but not in space, in accord with the disappearance of group velocity in the y-direction. The amplitude of the oscillation grows parabolically with time, but an infinite reservoir of potential energy is available to feed the disturbance as in the case of the analogous water-wave problem (Lamb 1932).

Combining equations (4-27) and (4-21), we find the Duhamel's-integral representation for the vertical component of velocity beneath a moving source of displacement:

$$v(0, y, t) = \int_0^t \frac{N^2(t-\tau) J_o[N(t-\tau)]}{2\pi(\Delta y)^2} \frac{d\Omega}{d\tau} d\tau \qquad (4\text{-}28)$$

where

$$\Delta y = y - y(\tau) \ .$$

Since

$$J_o(o) = 1 \ ,$$

the integrand of (4-28) does indeed approach (4-18) in the limit of small $N(t-\tau)$, provided $d\Omega/d$ is chosen to satisfy (4-22). Equation (4-16b), moreover, preserves its character in the limit (4-17a) and approaches (4-28) in the limit (4-17b), if the approximate memory function $N^2(t-\tau)$ is replaced with

$$N^2(t-\tau)\ J_o[N(t-\tau)] \ . \qquad (4\text{-}29)$$

## Wake Trajectory

The trailing vortices move according to Eqn. (4-13), in which u and v represent the indication of the buoyant upwash. Equations (4-16) specify u and v for small values of $N(t-\tau)$, and the equations can be generalized for arbitrary times by replacing $N^3(t-\tau)$ with the more general memory function (4-29). The result is a uniformly valid set of integro-differential equations for the wake trajectory:

$$\frac{dy}{dt} = -\frac{\Gamma}{4\pi s(t)} + \int_0^t d\tau \int_{-\infty}^{\infty} dx \left\{ N^2(t-\tau)\, J_o[N(t-\tau)] \right.$$

(4-30a)

$$\left. s(\tau)\, \eta\left[\frac{x}{s(\tau)}\right] \left|\frac{dy}{d\tau}\right| \frac{[y(\tau)-y(t)]^2 - [x-s(t)]^2}{2\pi r^4} \right\}$$

$$\frac{ds}{dt} = \int_0^t d\tau \int_{-\infty}^{\infty} dx \left\{ N^2(t-\tau)\, J_o[N(t-\tau)]\; s(\tau)\, \eta\left[\frac{x}{s(\tau)}\right] \right.$$

(4-30b)

$$\left. \left|\frac{dy}{d\tau}\right| \frac{2[y(\tau)-y(t)]\,[x-s(t)]}{2\pi r^4} \right\} \quad ,$$

with r still given by Eqn. (4-14). The equations could be solved on a computer for given values of $\Gamma$, N, and the initial conditions

$$y(o) = 0 \; , \quad s(o) = s_o \; ,$$

and the exercise might produce some interesting results. Implicit in Eqns. (4-30), however, is the assumption that

$$\delta = NT << 1 \; ,$$

where T is the inner time scale $4\pi s_o^2/\Gamma$ discussed on page 4-51 otherwise the buoyant upwash would commence before the drift had approached its asymptotic value. So far the full power of the assumption $\delta << 1$ has not been exploited.

To appreciate the simplification that takes place for very small values of $\delta$, we should scale the variables appearing in Eqns. (4-30) as follows:

$$t = \frac{t^*}{N} \quad ,$$

$$x = s_o x^* \quad ,$$

$$s = s_o s^* \quad ,$$

$$y = \frac{\Gamma}{4\pi N s_o} y^*$$

$$r = \frac{\Gamma}{4\pi N s_o} r^* \quad .$$

The asterisk denotes a dimensionless quantity. To avoid a proliferation of asterises, they will be omitted from the trajectory equations in favor of a single asterisk beside the equation number. Thus

$$\frac{dy}{dt} = -\frac{1}{s(t)} + \frac{\delta^2}{2\pi}\int_o^t d\tau \int_{-\infty}^{\infty} d\xi \left\{(t-\tau)J_o(t-\tau)\, s^2(\tau)\eta(\xi) \right.$$

$$\left. \left|\frac{dy}{d\tau}\right| \frac{[y(\tau)-y(t)]^2 - \delta^2[\xi s(\tau)-s(t)]^2}{r^4}\right\} \quad , \qquad (4\text{-}31^*a)$$

$$\frac{ds}{dt} = \frac{\delta^2}{\pi}\int_o^t d\tau \int_{-\infty}^{\infty} d\xi \left\{(t-\tau)J_o(t-\tau)s(\tau)\eta(\xi)\left|\frac{dy}{d\tau}\right| \right.$$

$$\left. \frac{[y(\tau)-y(t)][\xi s(\tau)-s(t)]}{r^4}\right\} , \qquad (4\text{-}31^*b)$$

where

$$r^2 = [y(\tau)-y(t)]^2 + \delta^2[\xi s(\tau)-s(t)]^2 \qquad (4\text{-}32^*)$$

and the integration over $x$ has been transformed into an integration over $\xi$. An examination of the order of magnitude of the various terms in Eqns. (IV-31) reveals that

$$\frac{dy}{dt} \to -\frac{1}{s(t)} + O(\delta^2 \ln \delta) ,$$

$$\frac{ds}{dt} \to O(\delta) ,$$

as $\delta \to 0$. The quantity $\delta^2 \ln \delta$ is very much smaller than $\delta$, so the buoyant upwash moves the vortices horizontally much more effectively than it retards their descent vertically. For the purpose of calculating the trajectory for very small $\delta$, it is sufficient to retain the right-hand side of (4-31*b) as the only buoyant effect.

If $\delta$ were set equal to zero in the integrand of (4-31*b), then the integral would diverge near $(t-\tau) = 0$. The effect of finite $\delta$ is to prevent the denominator $r^4$ from going to zero at $(t-\tau) = 0$. The functions $s(\tau)$ and $y(\tau)$ influence the value of the integral only near $\tau = t$. With sufficient accuracy for the purpose of integrating in the limit of small $\delta$,

$$y(t) - y(\tau) \approx (t-\tau)\frac{dy}{dt} ,$$

$$r^4 \approx \left(\frac{dy}{dt}\right)^4 \left[(t-\tau)^2 + \frac{\delta^2 s^2(t)}{(dy/dt)^2}(1-\xi)^2\right]^2 ,$$

and so forth. The outcome of such approximations is that

$$\frac{ds}{dt} = \frac{\delta^2}{\pi} s^3(t) \frac{|dy/dt|}{(dy/dt)^3} \int_{-\infty}^{\infty} d\xi \int_0^t d\tau$$

$$\frac{(t-\tau)^2 \eta(\xi)(1-\xi)}{\left\{(t-\tau)^2 + \left[\frac{\delta s(1-\xi)}{dy/dt}\right]^2\right\}^2} ,$$

where the order of integration has been reversed. The integration over $\tau$ can be performed explicitly. Set

$$a = \frac{s(1-\xi)}{dy/dt}$$

Then

$$\int_0^t \frac{(t-\tau)^2 d\tau}{[(t-\tau)^2 + \delta^2 a^2]^2} = \frac{1}{2\delta a} \tan^{-1}\left(\frac{t}{\delta a}\right) - \frac{t}{2(t^2+\delta^2 a^2)} ,$$

which approaches

$$\frac{\pi}{4\delta |a|} = \frac{\pi}{4\delta s} \frac{\left|\frac{dy}{dt}\right|}{|1-\xi|}$$

in the limit of small $\delta$ . Thus

$$\frac{ds}{dt} = \frac{\delta}{4} s^2(t) \frac{|dy/dt|^2}{(dy/dt)^3} \int_{-\infty}^{\infty} \eta(\xi) \frac{(1-\xi)}{|1-\xi|} d\xi$$

$$= \frac{\delta}{4} \frac{s^2(t)}{(dy/dt)} \int_{-\infty}^{\infty} \eta(\xi) \operatorname{sgn}(1-\xi)\, d\xi .$$

Since $\eta(\xi)$ is a symmetric function, the factor $\text{sgn}(1-\xi)$ causes contributions to the integral from the region $\xi > 1$ to cancel those from $\xi < 1$. Thus

$$\int_{-\infty}^{\infty} \eta(\xi)\, \text{sgn}\,(1-\xi)d\xi = \int_{-1}^{1} \eta(\xi)d\xi = D \ ,$$

where D is the constant evaluated in Eqn. (4-9). Evidently the buoyant upwash outside the span of the two vortices contributes nothing to their rate of separation. The phenomenon is analogous to a spherical gravitating shell, which exerts no force on a particle inside.

The trajectory equations have reduced to a very simple form in the limit of small $\delta$ :

$$\frac{dy}{dt} = -\frac{1}{s} \ , \qquad (4\text{-}33^*a)$$

$$\frac{ds}{dt} = \frac{\delta D}{4} \frac{s^2}{dy/dt} \ , \qquad (4\text{-}33^*b)$$

to be solved in conjunction with the initial conditions

$$y(o) = 0, \quad s(o) = 1 \ . \qquad (4\text{-}34^*)$$

The solution is also simple. Take

$$\frac{d^2y}{dt^2} = \frac{1}{s^2}\frac{ds}{dt} = \frac{\delta D}{4\, dy/dt} \ ,$$

or

$$\frac{dy}{dt}\frac{d^2y}{dt^2} = \frac{1}{2}\frac{d}{dt}\left(\frac{dy}{dt}\right)^2 = \frac{\delta D}{4} \ .$$

Integrate from 0 to t , with dy(o)/dt = -1 according to (4-33*a) and (4-34*):

$$\left(\frac{dy}{dt}\right)^2 - 1 = \frac{\delta Dt}{2} \quad ,$$

or

$$\frac{dy}{dt} = -\left(1 + \frac{\delta Dt}{2}\right)^{\frac{1}{2}} \quad .$$

The vortex spacing follows at once from (4-33*a),

$$s(t) = \left(1 + \frac{\delta Dt}{2}\right)^{-\frac{1}{2}} \qquad (4\text{-}35^*)$$

and after a further integration with respect to time,

$$y(t) = -\frac{4}{3\delta D}\left(1 + \frac{\delta Dt}{2}\right)^{3/2} - 1 \qquad (4\text{-}36^*)$$

The trailing vortices gradually draw together under the induction of the buoyant upwash, and they travel downward under their own induction at an ever increasing speed.

## Concluding Remarks

Solutions (4-35*) and (4-36*) of the trajectory equations can be written in terms of dimensional quantities as follows:

$$s(t) = s_o \left(1 + \frac{D}{2} N^2 T t\right)^{-\frac{1}{2}} \quad , \qquad (4\text{-}37a)$$

$$y(t) = -\frac{4 s_o}{3D(NT)^2}\left[\left(1 + \frac{D}{2} N^2 T t\right)^{3/2} - 1\right] \qquad (4\text{-}37b)$$

where

$$T = \frac{4\pi s_o^2}{\Gamma} \quad \text{and} \quad D = 8.184 \ .$$

Figure IV-18 is a plot of the vortex separation $2s(t)$ and displacement $y(t)$ for the example mentioned on page IV-52, a Boeing 747 during approach to landing in an isothermal atmosphere. The effect of stratification is not very strong under such conditions. The vortex separation is halved, for example, only after 140 sec, by which time the mutual-induction instability (Crow 1970) would probably have destroyed the vortices anyway. The leveling of trailing vortices observed by Condit and Tracy (1971) should probably be attributed to instability rather than buoyancy.

The really interesting consequence of the solution (4-37) is qualitative. Intuitively it would seem that stable stratification ought to have somewhat the same effect as a rigid barrier, which would cause the vortices to decelerate and spread apart. The simplest derivation of the Brunt-Vaisala frequency, moreover, involves the idea of a blob of fluid bouncing under the action of buoyancy. It is hard to abandon the rigid barrier and bouncing blob as intuitive models, but that is what Eqn (4-37) ask us to do. Throughout the development we have assumed that $\delta = NT$ is small, in other words, that stratification exerts a weak (but sustained) influence on the local dynamics of the vortex pair. The rigid-barrier analogy might work for $NT >> 1$, and the textbook bouncing-blob argument is tailored for Boussinesq waves having $NT \sim 1$ by definition. Perhaps it should not be too surprising that the flow is qualitatively different when $NT << 1$.

The physical model implied by the theory can be appealing, once one accommodates the idea that the vortices contract together.

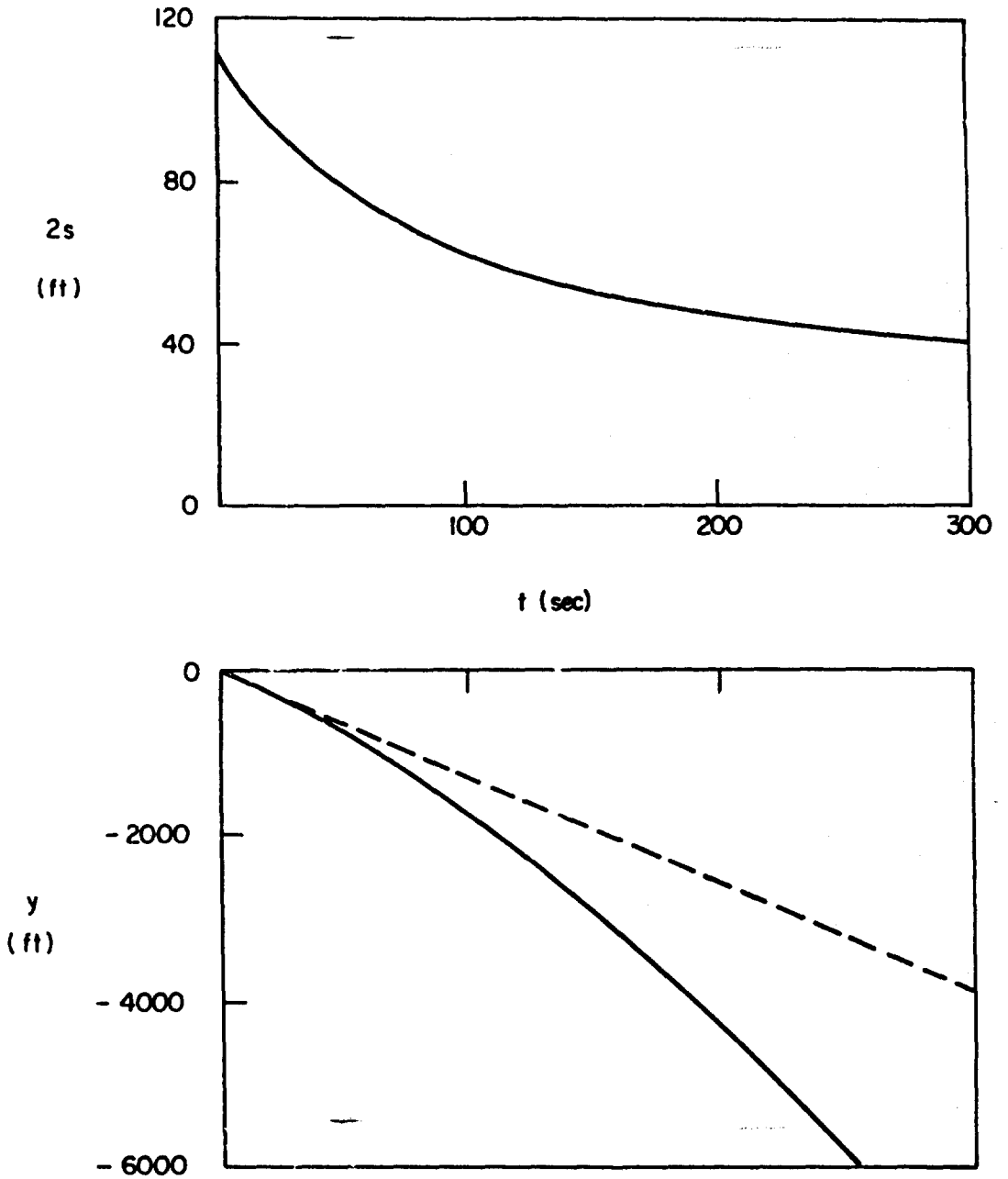


Figure 4-18. Wake Trajectory for the Case $\Gamma = 9000$ ft.$^2$/sec., $2s_o = 110$ ft., $N = 0.035$ sec$^{-1}$. The dashed line applies for zero stratification.

Figure 4-19 illustrates the density field and streamlines near the contracting recirculation cell. The white area represents fluid captured at the instant of wake formation, and the shaded area represents the denser fluid at the present wake location $y(t)$. The buoyant upwash is not represented (cf. Figs. 4-14 through -16) but is squeezing the recirculation cell, forcing light fluid to drain upward near the rear stagnation point. Vorticity arises at the interface between light and heavy fluid, but the trailing vortices sweep the vorticity back toward the rear stagnation point. The interfacial vorticity becomes the boundaries of the drainage filament, as described by Scorer and Davenport (1970). As far as the present theory is concerned, the drainage filament is an interior detail of the buoyant upwash that eliminates the integrable singularity $\eta(o) = \infty$ of the drift. The wake accelerates downward but loses captured fluid and impulse to the buoyant upwash. Ultimately the impulse due to the aircraft radiates away as gravity waves, while the trailing vortex cores overlap and annihilate each other.

A preliminary study suggests that the interfacial vorticity may contribute significantly to the induced velocity at the trailing vortex cores. If so, the contribution should be added to the induced field of the buoyant upwash treated in this report. The quantitative predictions of Figure 4-18 may change, but the qualitative conclusion that the vortices draw together and accelerate downward will be reinforced. The effect of interfacial vorticity will be incorporated in a further report.

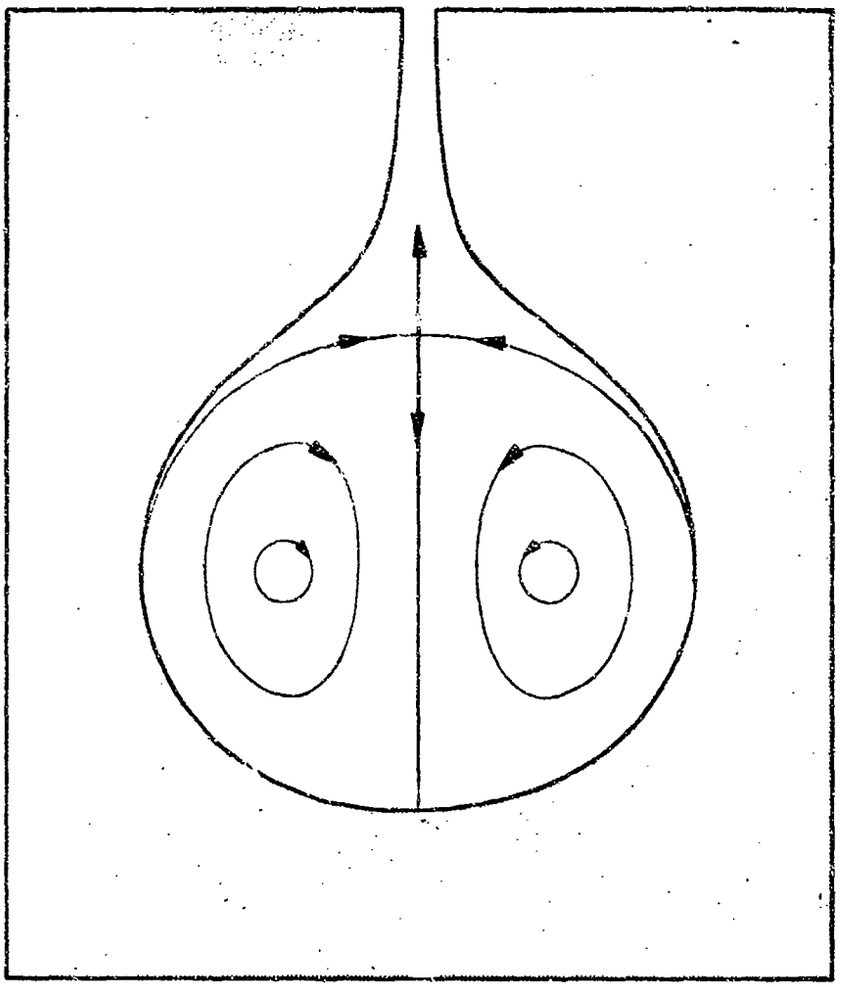

Figure 4-19. Flow Within the Contracting Recirculation Cell.

# 5. VORTEX DECAY

## 5.1 GENERAL

It appears that there are in general two major types of vortex decay, (1) the catastropic instabilities associated with Crow linking and vortex breakdown, and (2) the regular dissipative decays. It is believed that in most cases the instabilities terminate the vortex life. These are discussed in detail in Sections 5.2, 5.3. For completeness we discuss here the general dissipative modes although (except in special circumstances) they are probably less important than the instabilities.

Calculations for the regular laminar dissipation of a single viscous vortex show that the rate of decay is more gradual than any decay observed in flight tests. This causes one to expect that turbulent processes must come into play, although, as pointed out by Chigier (1972) and Owen (1970), there are grounds to expect that the core flow field will tend to suppress turbulence and even to relaminarize the flow. We see that there are three mechanisms which can introduce turbulence into the vortex core dynamics; the first is the turbulence of the ambient field it is immersed in, the second is the turbulence generated by other elements of the aircraft -- for example, the propulsion system -- and the third is the mechanically generated turbulence by motions in the vortex cell. The aircraft turbulence can, for these purposes, be regarded simply as increasing the ambient turbulent field in which the vortex is immersed, so we confine our attention to ambient and mechanical turbulence. The general effect of these is presumably to increase dissipation rates resulting in increase in core and cell size and reduction in descent velocity. These effects have been fully discussed in the section on vortex transport.

We now discuss the other factor which may be expected to affect the general core dissipation -- this is the presence of organized vorticity in the external field. Such a situation occurs in a uniformly sheared crosswind. It would be expected that the presence of this ambient vorticity (of one sign) would have opposite effects on the two core vorticity distribution; causing the cores to develop differently, and possibly causing the pair to tilt. This phenomenon has been fully discussed in the section on vortex transport. It is believed that this is the effect causing the appearance of the solitary vortex which is frequently exceptionally long lived.

The other process by which organized vorticity is developed in the ambient fluid is buoyancy. Although the effects of buoyancy are highly controversial, it is clear that the buoyancy field will generate vorticity both in the outer flow due to non-uniform vertical displacements of the stratified density layers, and on the cell boundary itself due to the density discontinuities between the cell flow and the external flow. A new approach to this problem has been described and analyzed in Section 4.4.

As postulated in the encounter hazard section, it is believed that, with the exception of the solitary vortex, the regular vortex dissipation, by whatever process, is sufficiently gradual that its effects on alleviating the encounter hazard are not important. In most cases the vortex pair retains its danger potential until it is destroyed by one of the two major instabilities. These instabilities are discussed in detail in the following sections.

## 5.2 LINKING INSTABILITY

### Introduction

A theory for the stability of a pair of trailing vortices has been developed by Crow (1970). This theory examines the time dependent displacements of vortex lines under an initial hypothetical perturbation in the wake of an aircraft. Under the mutual influence of the velocity fields associated with the perturbed vortex lines, the displacements become unstable and grow with time. Sinuous oscillations develop on the vortex lines, which, due to the instability, can grow sufficiently large to cause the two vortex lines to touch and subsequently link together. This linking occurs periodically in the downstream direction, $z$, at distances corresponding to the wavelength of the sinuous oscillation of the vortex pair. At each link point, each original vortex line is severed, the two originally parallel vortices join together, and a closed vortex loop or ring is formed. Such a vortex ring is formed between each link point, resulting in a train of vortex rings as the wake of the aircraft continues to develop. The coherent flow in the wake, characteristic of the energetic flow around the original organized trailing vortices, abruptly changes in character once the vortex rings have formed.

It is shown by Crow that several modes of instabilities can occur, although it is argued that the structure of atmospheric turbulence, acting in the capacity of providing forced turbulent excitation of the instability, imposes an overwhelming bias in favor of long waves, which are unstable only in the symmetric mode. Actual observations have confirmed this long wave interaction behavior, where, from the Crow theory, the wavelength is approximately 8.6 times the original, undisturbed vortex spacing (Smith and Beesmer, 1959; Chevalier, 1973).

Vortex lines move in accordance with the velocity field of the surrounding fluid. Atmospheric turbulence provides a continuous disturbance of the vortex lines and convective turbulent excitation of the resultant instability. Once initially distorted, the vortex lines also move in accordance to their own mutual and self-induced velocity fields, which was the condition originally treated by Crow in the analysis of the instability. No attempt was made to account in detail for the effects of atmospheric turbulent excitation, except to state that such turbulence is the probable factor which excites the long wave instability.

The present analysis examines the effects of atmospheric turbulence as an input forcing function for the instability. The time for the instability to grow to the point at which vortex linking occurs is found as a function of the vortex strength, $\Gamma_o$, and spacing, $b$, and the atmospheric turbulence dissipation rate, $\varepsilon$.

## Structure of the Atmospheric Turbulence

The vortices from the generating aircraft are originally undisturbed, but under the influence of atmospheric turbulence they are continuously deformed. The instability is thus initiated by turbulent convection, and further, the turbulence acts continuously as a source of input energy to drive the instability.

The structure of the atmospheric turbulence is assumed to be stationary with respect to the coordinates of the downward moving vortex pair. That is, the turbulent eddies are assumed large enough that any time variation of turbulence is small as the vortices move downward a distance $\ell = vT_\ell$ where $v = \Gamma/2\pi b$, and $T_\ell$ equals the time to linking. Typically, $v = .5\text{-}3\text{m/sec}$, and $T_\ell$ is of the order 50 sec for light to moderate turbulence. This requires a turbulent "cell" (in which the time variation of turbulence is small) of dimensions on the

order of 25-150m. It is also assumed that within this cell the turbulence is isotropic. The turbulent input to the instability is thus only a function of the energy spectrum, $E(k, \epsilon)$, where $k$ is the wave number.

The resulting behavior of the vortex motion under the influence of the turbulent field can be analyzed as a time-invariant linear filter interacting with the turbulent energy input spectrum integrated over all wave numbers, with $\epsilon$ constant. The frequency response function of the filter is obtained from the dynamics of the vortex instability, with a peak at $k_o$, the wave number associated with the maximum amplification rate of the instability.

From Crow, $k_o = \beta_{max}/b$, where $b$ is the undisturbed vortex-pair spacing, and $\beta$ is the dimensionless wave number. $\beta_{max}$ is of the order one so that $.02 \leq k \leq .10$ radians/meter, which is within the inertial subrange commonly encountered in geophysical flows (MacCready, 1962). Although turbulence supplies energy to the instability at all wave numbers, the filter action of the dynamics of the vortex instability responds only to the energy contained in the spectrum at or near $k_o$. Wave numbers not in the inertial subrange will be sufficiently far to either side of $k_o$ that the effects of the filter function will have attenuated their contribution. Their exact analytical form is thus not critical, and the assumption of an energy spectrum described by that of the inertial subrange will be adequate over all wave space.

With these assumptions, the input turbulent forcing function for the instability is taken as the one-dimensional, transverse energy spectrum in the Komolgorov inertial subrange. This energy spectrum is given (page 273, Tennekes and Lumley, 1972) as:

$$F_{22}(k) = \frac{12}{55}\,\bar{\alpha}\,\epsilon^{2/3}k^{-5/3} \qquad (5\text{-}1)$$

with $\bar{\alpha} = 1.5$ . The actual turbulent forcing function that drives the instability, $F(k)$ , will be some percentage of $F_{22}(k)$ , given by:

$$F(k) = \gamma F_{22}(k) \quad . \tag{5-2}$$

$\gamma$ will be determined by the geometrical relationship which couples $F_{22}(k)$ with the dynamics of the instability.

## Geometry of Vortex Interaction with the Turbulent Field

In order to determine the ratio, $\gamma$ , between the total available one-dimensional, transverse energy, $F_{22}(k)$ , and that which actually couples with the instability, $F(k)$ , the relationship of the available turbulent energy to that contained in the oscillating vortices must be established with respect to the interaction between the geometrics of these two flows.

With reference to Figure 5-1, the instability for the symmetrical mode develops at each vortex in a plane inclined at $\theta_s = 48°$ to the horizontal. At any downstream position, $z$ , the perturbation velocities develop in the x-y plane with velocity components $u$ , and $v$ respectively.

Let:

$$U_1(x, y, z, t) = U_1(x, y, z, 0) = \tilde{e}_x u_1(z, 0) + \tilde{e}_y v_1(z, 0) \tag{5-3}$$

$$U_2(x, y, z, t) = U_2(x, y, z, 0) = \tilde{e}_x u_2(z, 0) + \tilde{e}_y v_2(z, 0) \tag{5-4}$$

be the turbulent velocities at the positions of vortices 1 and 2, respectively. The velocities at these two positions have the same direction in the x-y plane, so that $u_1/v_1 = u_2/v_2$ , although they may have a different magnitude.

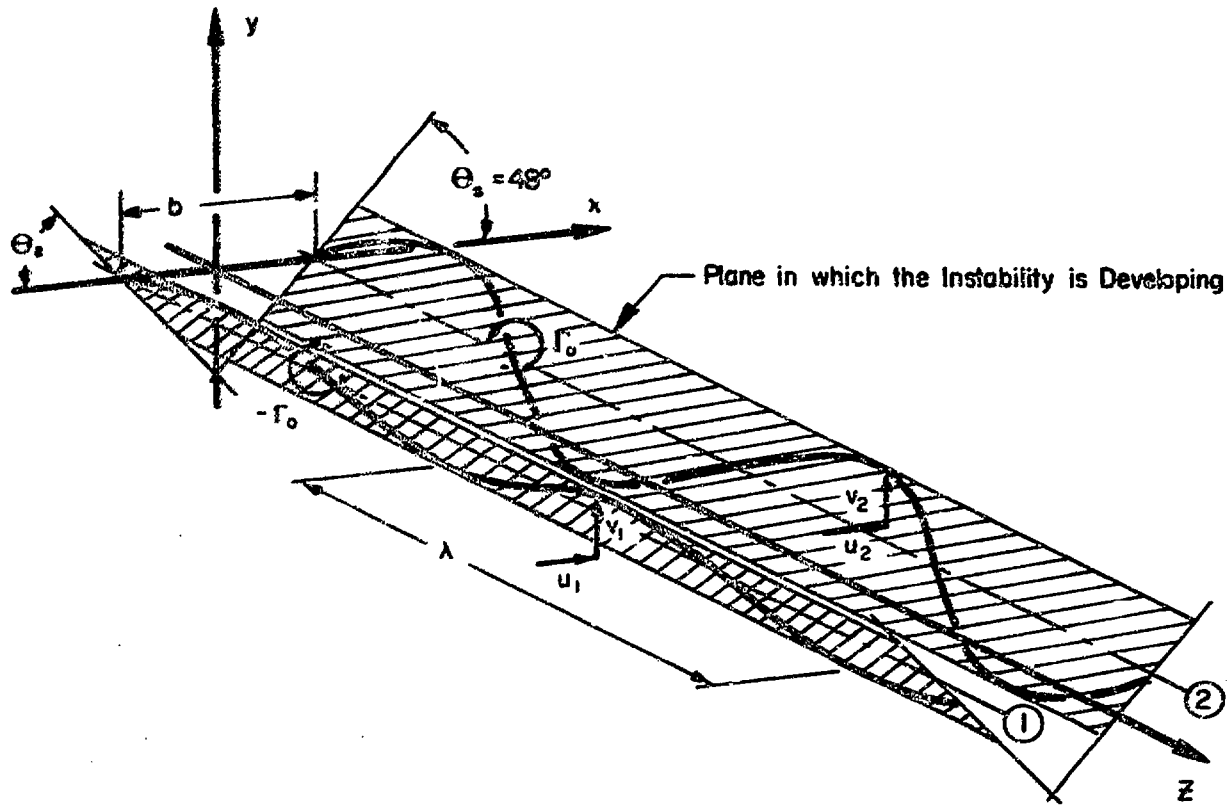


Figure 5-1. Geometry of the Oscillating Vortex Pair. The Vortices are Viewed from Above, and the Generating Aircraft Lies Beyond the Upper Left Hand Corner of the Figure.

If a velocity in wave space is defined as:

$$\int_{-\infty}^{\infty} \hat{v}_n(k, x, y, 0)\, e^{ikz}\, dk = V_n(x, y, z, 0) \qquad (5\text{-}5)$$

(n equals 1 and 2), then, from Eqns. (5-3 and (5-4) follows the definition of $\hat{v}_n(k, o)$ and $\hat{u}_n(k, o)$ in a like manner.

Since the ratios $\hat{v}_n/v_n$ and $\hat{u}_n/u_n$ for any constant, arbitrary wave number, $k$, and at the same distance, $z$, remain constant for $n = 1$ and $n = 2$, it is possible to use these transformed velocities as forcing functions to obtain the relative geometrical response of the two vortices in the x and y-directions. Differentiating Eqns. (9) of Crow for the symmetrical instability, and substituting Eqns. (8), with the transformed velocities added as forcing functions, the relationships between the components of velocity resulting from the turbulence, and the velocity components associated with the symmetrical instability mode are established:

$$\frac{\partial \hat{x}_s}{\partial t} = \frac{\Gamma_o}{2\pi b^2}(1 - \psi + \beta^2\omega)\,\hat{y}_s + (\hat{u}_2 - \hat{u}_1) \qquad (5\text{-}6)$$

$$\frac{\partial \hat{y}_s}{\partial t} = \frac{\Gamma_o}{2\pi b^2}(1 + \chi - \beta^2\omega)\,\hat{x}_s + (\hat{v}_1 + \hat{v}_2) \qquad (5\text{-}7)$$

where the dimensionless interaction functions $\psi(\beta)$, $\chi(\beta)$, and $\omega(\beta)$ are defined by Crow.

The instability develops in a plane inclined at an angle $\theta_s$ to the horizontal, and the vertical and horizontal velocities of the developing instability, $v_s$ and $u_s$, are coupled by $v_s/u_s = \tan\theta_s$. Therefore, the equation of motion of the system is a linear combination of Eqns. (5-6 and (5-7) differentiated with respect to time. Because of the linear relationship, it is sufficient to deal with only a single component

of the equation of motion for the purposes of establishing geometrical relationships between velocity components.

Differentiating Eqn. (5-6) and substituting Eqn. (5-7) results in the x-component of the equation of motion:

$$\frac{\partial^2 \hat{x}_s}{\partial t^2} = \left(\frac{\Gamma_o}{2\pi b^2}\right)^2 (1-\psi+\beta^2\omega)(1+\chi-\beta^2\omega)\hat{x}_s + \frac{\Gamma_o}{2\pi b^2}(1-\psi+\beta^2\omega)(\hat{v}_1+\hat{v}_2) \quad (5\text{-}8)$$

with: $$\hat{x}_s(k,0) = 0, \quad \frac{\partial \hat{x}_s(k,0)}{\partial t} = (\hat{u}_2 - \hat{u}_1) \quad (5\text{-}9)$$

and $$a^2(k) \equiv \left(\frac{\Gamma_o}{2\pi b^2}\right)(1-\psi+\beta^2\omega)(1+\chi-\beta^2\omega) .$$

A solution exists of the form:

$$\hat{x}_s(k,t) = A + B\, e^{a(k)t} + C\, e^{-a(k)t} \quad (5\text{-}10)$$

Substitution of Eqn. (5-10) in Eqn. (5-8) with the initial conditions (5-9), and from Crow, Eqn. (12), the expression for $\theta_s$:

$$\tan\theta_s = \sqrt{\frac{1+\chi-\beta^2\omega}{1-\psi+\beta^2\omega}} ,$$

results in the determination of the coefficients A, B, and C.

$$A = -\frac{(\hat{v}_1+\hat{v}_2)}{\frac{\Gamma_o}{2\pi b^2}(1+\chi-\beta^2\omega)} .$$

$$B = \frac{(\hat{u}_2 - \hat{u}_1) + \frac{(\hat{v}_1 + \hat{v}_2)}{\tan\theta_s}}{2a(k)} ,$$

and

$$C = \frac{(\hat{v}_1 + \hat{v}_2)}{\frac{\Gamma_o}{2\pi b^2}(1 + \chi - \beta^2\omega)} - \frac{(\hat{u}_2 - \hat{u}_1) + \frac{(\hat{v}_1 + \hat{v}_2)}{\tan\theta_s}}{2a(k)} .$$

At large times Eqn. (5-10) becomes:

$$\hat{x}_s(k,t) - B\, e^{a(k)t} = \frac{\hat{u}_s(k,t)}{a(k)} e^{a(k)t} , \qquad (5-11)$$

from which $$B = \frac{\hat{u}_s(k,t)}{a(k)} , \qquad (5-12)$$

and

$$\hat{u}_s(k,t) = a(k)B = \frac{(\hat{u}_2 - \hat{u}_1) + \frac{(\hat{v}_1 + \hat{v}_2)}{\tan\theta_s}}{2} . \qquad (5-13)$$

If now the radial displacement of one of the vortices from its original, undisturbed position is given by $\hat{r}$, then by definition:

$$\hat{r}(k,t) = \frac{\hat{x}_s}{2\sin\theta_s} = \frac{\hat{v}_s}{a(k)} \frac{e^{a(k)t}}{2\sin\theta_s} .$$

Similarly to Eqn. (5-11), at large times:

$$\hat{r}(k,t) \to \frac{\hat{v}_r\, e^{a(k)t}}{a(k)} .$$

from which,

$$\hat{v}_r = \frac{\hat{u}_s}{2\sin\theta_s} = \frac{(\hat{u}_2-\hat{u}_1)+\dfrac{(\hat{v}_1+\hat{v}_2)}{\tan\theta_s}}{4\sin\theta_s} \quad ,$$

$\tan\theta_s = \tan 48^\circ = 1.11$ , so that:

$$\hat{v}_r = \frac{(\hat{u}_2-\hat{u}_1)+\dfrac{(\hat{v}_1+\hat{v}_2)}{1.11}}{4\sin\theta_s} \qquad (5\text{-}14)$$

If long waves are considered, that is, $\ell >> \gamma >> b$ , the turbulent velocity field within the "cell" of dimension $\ell$ would result in velocity components at each vortex position such that

$$\hat{u}_2-\hat{u}_1 << \hat{v}_1+\hat{v}_2$$

and, from Eqn. (5-14)

$$\hat{v}_r \approx \frac{\hat{v}_1+\hat{v}_2}{4.44\sin\theta_s} = \frac{2\hat{v}}{4.44\sin\theta_s} = \frac{\hat{v}}{2.22\sin\theta_s} \quad . \qquad (5\text{-}15)$$

Thus, a coupling between the vertical vortex motion and the atmospheric turbulence will produce maximum energy input to the developing instability. The ratio of the energy in the oscillating vortex to that available from the turbulent field is:

$$\gamma = \left(\frac{\hat{v}_r}{\hat{v}}\right)^2 = \frac{1}{4.92\sin^2\theta_s} \quad .$$

and, from Eqn. (5-1) and Eqn. (5-2):

$$F(k) = \gamma F_{22}(k) = \frac{2.43\,\bar{a}}{55 \sin^2\theta_s}\, \epsilon^{2/3}\, k^{-5/3} \quad . \tag{5-16}$$

Dynamics of the Vortex Motion

The radial displacement of a vortex line from its original, undisturbed position is given by $r(z,t)$. Let:

$$r(z,t) = \int_{-\infty}^{\infty} \hat{r}(k,t)\, e^{ikz}\, dk \quad .$$

An exponential solution in time for $\hat{r}(k,t)$, similar to that for Eqn. (5-10) exists:

$$\hat{r}(k,t) = A' + B'\, e^{a(k)t} + c'\, e^{-a(k)t} \quad , \tag{5-17}$$

which at large times becomes:

$$\hat{r}(k,t) \rightarrow B'\, e^{a(k)t} = \frac{e^{a(k)t}}{a(k)}\, \hat{V}_r(k) \quad . \tag{5-18}$$

The mean square displacement of a vortex element is defined by:

$$\langle r^2(z,t) \rangle = \langle r^2 \rangle = \int_{-\infty}^{\infty} \int_{-\infty}^{\infty} \langle \hat{r}(k,t)\, \hat{r}(k',t) \rangle e^{i(k+k')z}\, dk dk' \quad . \tag{5-19}$$

and

$$\langle \hat{r}(k,t)\, \hat{r}(k',t) \rangle = \left[\frac{e^{a(k)t}}{a(k)}\right]\left[\frac{e^{a(k')t}}{a(k')}\right] \langle \hat{V}_r(k)\, \hat{V}_r(k') \rangle \quad . \tag{5-20}$$

Define a function $R(k, t)$:

$$\langle r^2 \rangle = \int_{-\infty}^{\infty} \int_{-\infty}^{\infty} R(k, t)\delta(k+k')e^{i(k+k')z} dk dk' \qquad (5\text{-}21)$$

which has the property that:

$$\langle r^2 \rangle = \int_{-\infty}^{\infty} R(k, t) dk \quad , \quad \text{at } k' = k \quad . \qquad (5\text{-}21a)$$

Thus, from Eqns. (5-19) and (5-21)

$$R(k, t)\delta(k+k') = \langle \hat{r}(k, t)\, \hat{r}(k', t) \rangle \quad . \qquad (5\text{-}22)$$

Also define:

$$F(k)\, \delta(k+k') = \langle \hat{V}_r(k)\, \hat{V}_r(k') \rangle \quad . \qquad (5\text{-}23)$$

Combining Eqns. (5-20), (5-22), and (5-23) gives:

$$R(k, t) = \left[\frac{e^{a(k)t}}{a(k)}\right]\left[\frac{e^{a(k')t}}{a(k')}\right] F(k) \quad ,$$

and for $k' = -k$ :

$$R(k, t) = \left[\frac{e^{a(k)t}}{a(k)}\right] \left[\frac{e^{a(-k)t}}{a(-k)}\right] F(k) \quad . \qquad (5\text{-}24)$$

The wavelength, $\lambda$ , is related to the wave number, k , by:

$$\lambda = \frac{2\pi}{|k|} \quad .$$

Therefore, $a(k) = a(-k)$, and

$$R(k,t) = \left[\frac{e^{a(k)t}}{a(k)}\right]^2 F(k) \quad . \tag{5-25}$$

Substituting Eqn. (5-25) in Eqn. (5-21a) gives:

$$\langle r^2 \rangle = \int_{-\infty}^{\infty} \left[\frac{e^{a(k)t}}{a(k)}\right]^2 F(k)\, dk \quad . \tag{5-26}$$

This integral is significant only near the wave number of maximum amplification rate, $k_o$ , for the symmetrical mode of instability. The term in brackets represents the filter function of the forced oscillation, and F(k) represents the turbulent forcing function.

Equation (5-26) becomes, upon squaring the term in brackets:

$$\langle r^2 \rangle = \int_{-\infty}^{\infty} \frac{F(k)}{a^2(k)}\, e^{2a(k)t}\, dk \tag{5-27}$$

Expanding a(k) in the exponential term in a Taylor series and substituting in Eqn. (5-27),

$$a(k) = a(k_o) + (k-k_o)a'(k_o) + \frac{(k-k_o)^2}{2} a''(k_o) + \cdots ,$$

with:

$$a'(k_o) \equiv 0 \quad ,$$

so that:

$$\langle r^2 \rangle = \frac{2F(k_o)}{a^2(k_o)} e^{2ta(k_o)} \int_o^\infty e^{-t|a''(k_o)|(k-k_o)^2} dk \quad . \quad (5\text{-}28)$$

$a''(k_o)$ is negative so that $t\, a''(k_o)(k-k_o)^2 = -t\left|a''(k_o)\right|(k-k_o)^2$ .

Equation (5-28) has a solution of the form:

$$\langle r^2 \rangle = \frac{2F(k_o)}{a^2(k_o)} e^{2ta(k_o)} \sqrt{\frac{\pi}{t|a''(k_o)|}} \quad (5\text{-}29)$$

From the definition from Crow:

$$a(k) = \frac{\bar{o}}{2\pi b^2} \alpha(\beta) , \quad \beta = kb ,$$

and

$$a(k_o) = \frac{\Gamma_o}{2\pi b^2} \alpha(\beta_{max}) = \frac{\Gamma_o}{2\pi b^2} \alpha_{max}$$

$$a''(k_o) = \frac{\Gamma_o}{2\pi} \alpha''(\beta_{max}) = \frac{\Gamma_o}{2\pi} \alpha''_{max}$$

The "lifetime" of a vortex pair is that time $T_\ell$ at which $\langle r^2 \rangle = (b/2 \sin\theta)^2$. Substituting this condition in Eqn. (5-29), and recalling that:

$$F(k_o) = F(\frac{\beta_{max}}{b}) = \frac{2.43\,\bar{\alpha}}{55 \sin^2\theta_s} \varepsilon^{2/3} (\frac{\beta_{max}}{b})^{-5/3} ,$$

$$\frac{b^2}{4 \sin^2\theta_s} = \frac{4.86\bar{\alpha}\, \varepsilon^{2/3} (\frac{b}{\beta_{max}})^{5/3} e^{2T_\ell \frac{\Gamma_o}{2\pi b^2} \alpha_{max}}}{55 \sin^2\theta_s (\frac{\Gamma_o}{2\pi b^2})^2 \alpha^2_{max}} \sqrt{\frac{\pi}{T_\ell \frac{\Gamma_o}{2\pi} |\alpha''_{max}|}} \quad .$$

(5-30)

Introducing non-dimensional time and turbulence parameters as:

$$\tau = \frac{T_\ell \Gamma_o}{2\pi b^2} ,$$

and

$$\eta = \frac{\varepsilon b^4}{\Gamma_o^3} ,$$

Eqn. (5-30) reduces to:

$$\eta^{2/3} \frac{e^{2\tau \alpha_{max}}}{\sqrt{\tau}} = \frac{\alpha_{max}^2 (\beta_{max})^{5/3} \sqrt{|\alpha''_{max}|}}{32(\pi)^{5/2} \frac{2.43}{55} \bar{\alpha}} . \qquad (5-31)$$

Thus the condition of time to linking for the sinuous instability of a vortex pair has been stated in terms of the vortex parameters $\Gamma_o$ and b , and the turbulent dissipation rate, $\epsilon$. The relationship between these parameters involves the dimensionless amplification rate $\alpha(\beta_{max})$ and wave number $\beta_{max}$ . From Crow, for the symmetrical mode, $\beta_{max} = 0.73$ and $\alpha(\beta_{max}) = 0.83$ . A parabolic approximation of $\alpha$ vs $\beta$ gives $\alpha''(\beta_{max}) = -3.12$ . With $\bar{\alpha} = 1.5$, Eqn. (5-31) becomes:

$$\eta = 0.00271 \frac{(\tau)^{3/4}}{e^{2.49\tau}} , \qquad (5-32)$$

from which a "universal lifetime" plot may be constructed in terms of the dimensionless parameters $\eta$ and $\tau$ . Such a plot is shown in Fig. (5-2). Figure (5-3) shows in dimensional form the time to vortex linking, $T_\ell$, as a function of turbulence dissipation rate, $\epsilon^{1/3}$ for various aircraft.

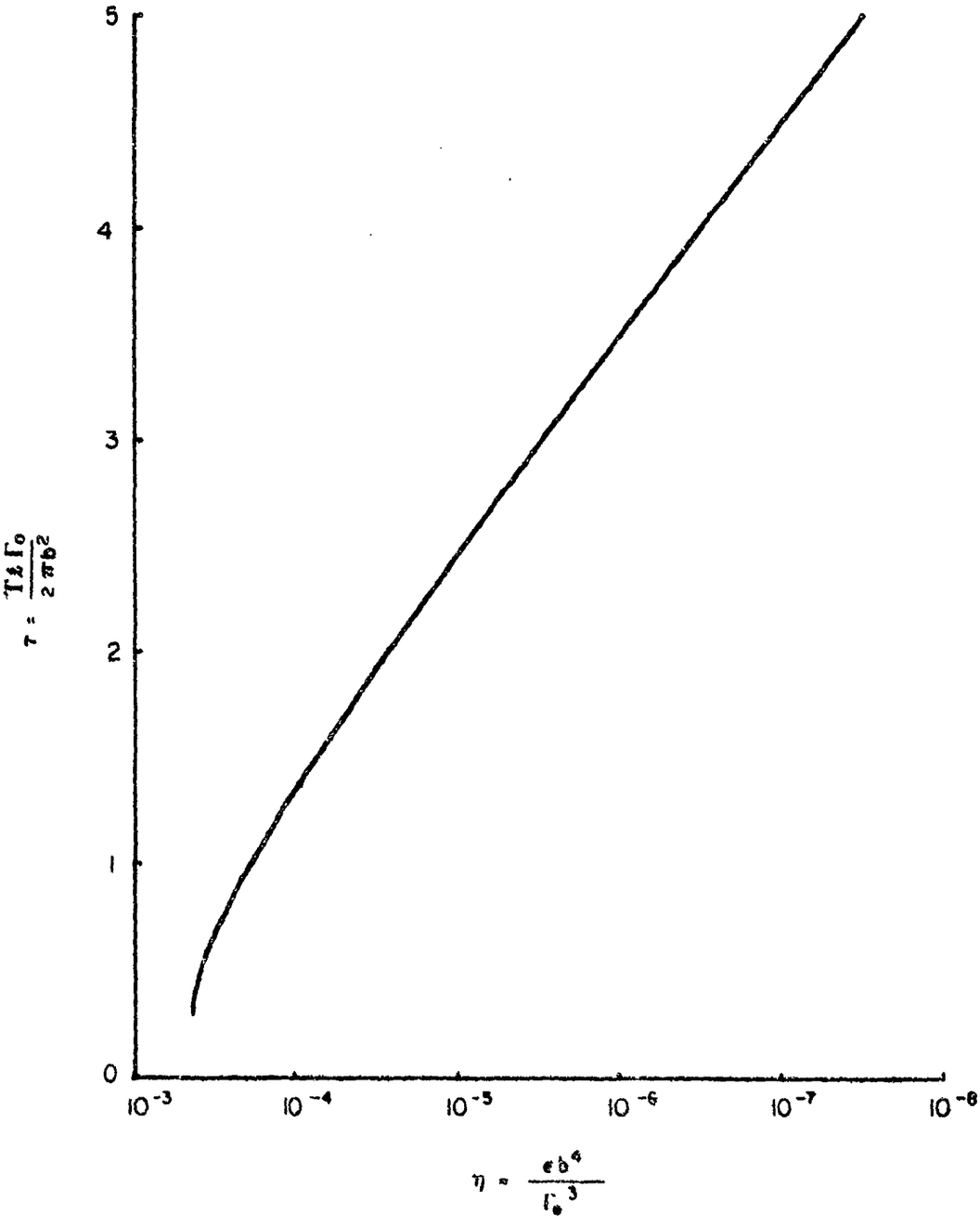


**Figure 5-2. Non Dimensional Vortex Pair "Lifetime" to Linking, Eqn. 5-32.**

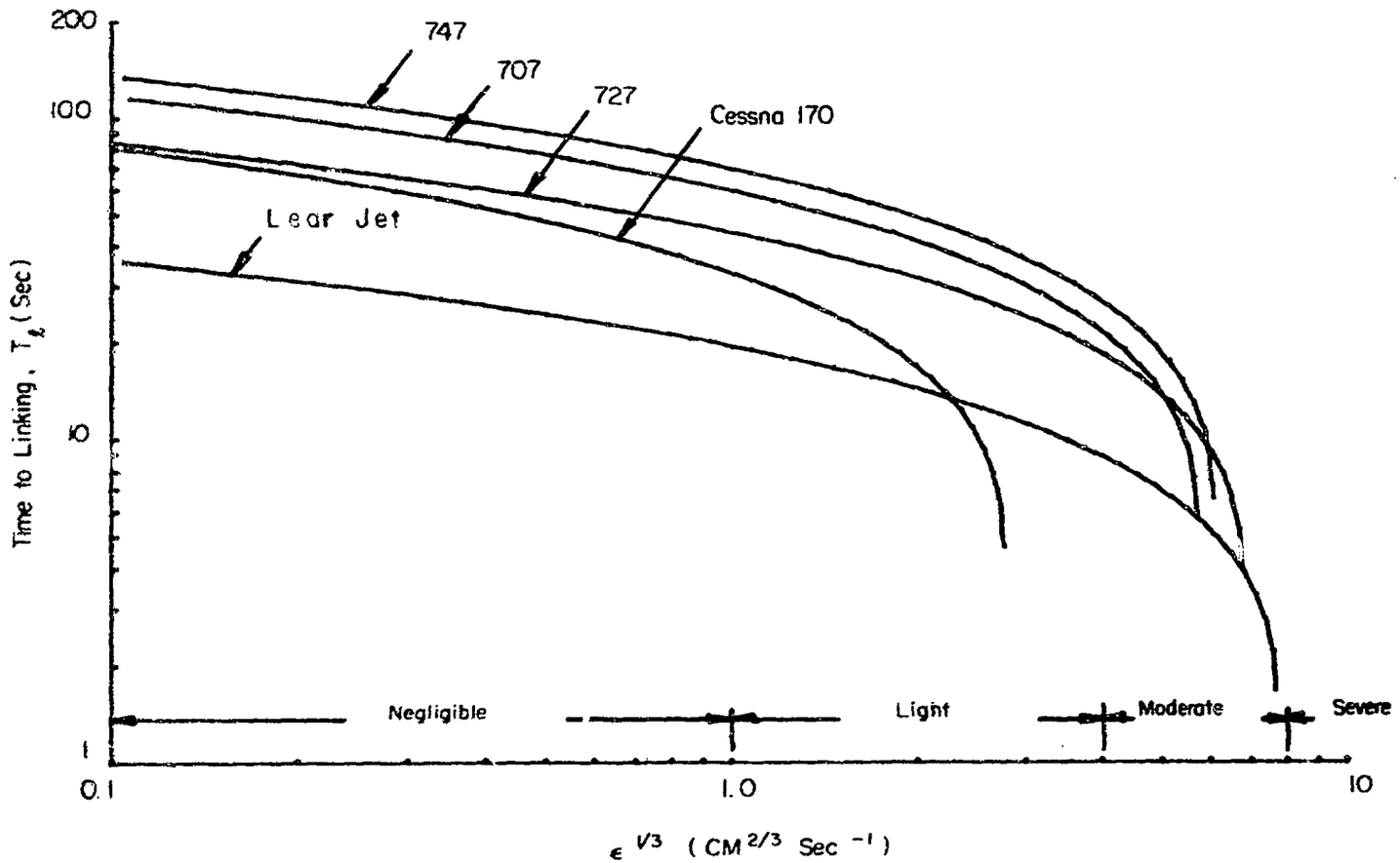


Figure 5-3. Time to Vortex Pair Linking as a Function of Atmospheric Turbulent Dissipation Rate, $\epsilon$, for take off.

## Correlation of Present Theory with Experiment

The predictions of time to linking for various turbulence levels follow straight from the theory, and involve no fitted constants. There is scant experimental information with which to compare the present theory. However, a series of experiments in which motion pictures were taken of the trailing vortices from a light plane were performed (Tombach, 1972). The linking phenomenon was observed in some of these experiments, and the time to linking was measured from the motion pictures for various levels of atmospheric turbulence. The results of these experiments are presented in Figure (5-4) along with the present theory in which the vortex parameters, $\Gamma_o$ and b , characteristic of the light plane used (Cessna 170) were included.

The agreement between experiment and the present theory is quite good. The scatter in the data are well within reason, considering that the experiments were performed under field conditions, with random effects undoubtedly influencing the limited amount of data obtained.

When future experimental data becomes available with respect to the vortex linking phenomena for different classes of aircraft subjected to varying degrees of atmospheric turbulence, the constants in Eqn. (5-32) can be modified (if required) in a rational and consistent manner to account for such effects as non-elliptical wing loading, flap deflections, wing/non-wing mounted engines, etc.

The present theory was developed for assumed "large" times. For this reason, the behavior of the predictions of the theory for small times, say less than 10-20 sec, is not as reliable as for larger times. Modifications to the theory can be performed that will extend the range of the theoretical predictions into the small time region. However, examination of Fig. 5-3 shows that for the class of large airplanes that

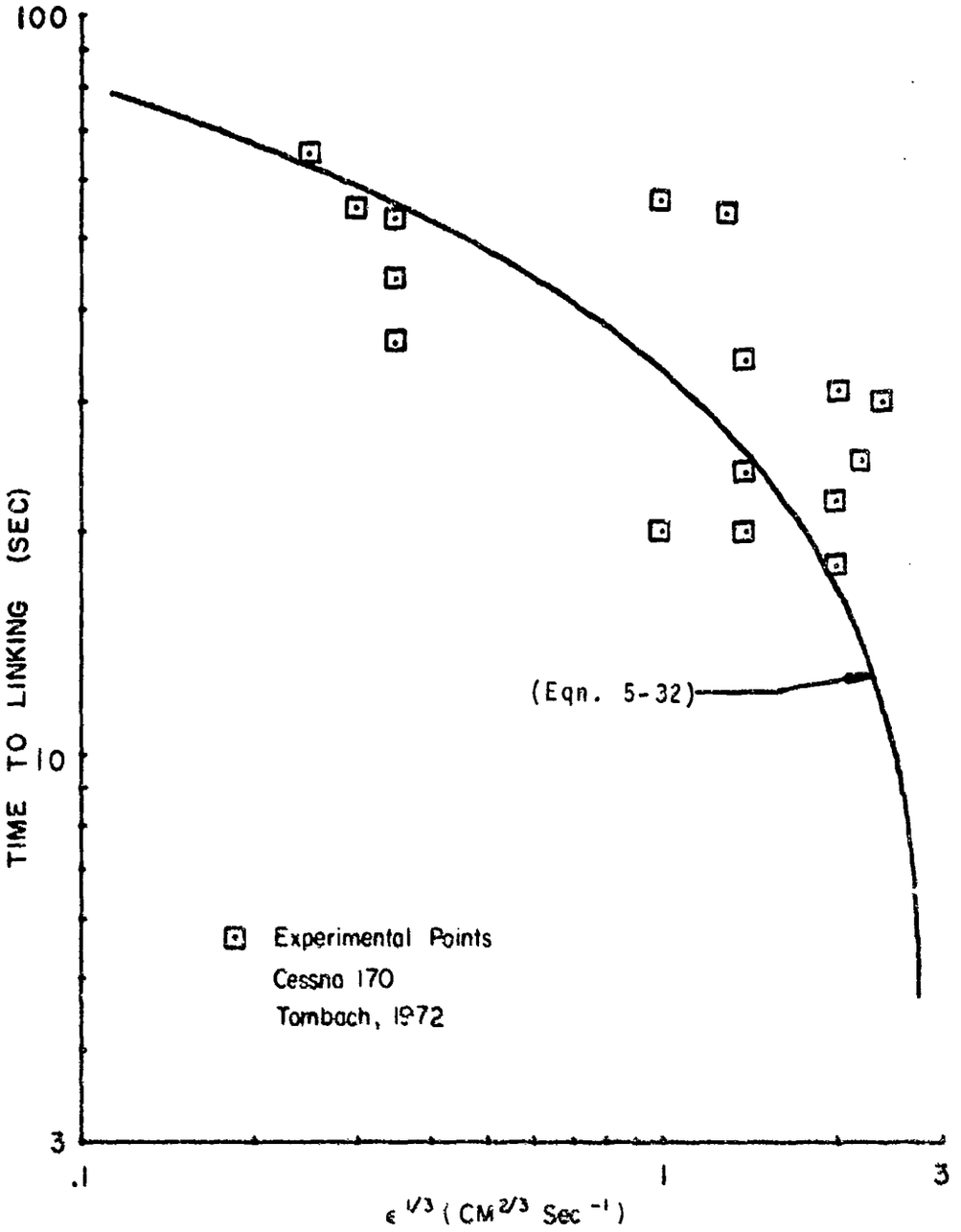


**Figure 5-4. Comparison of Theoretical Prediction of Time-to-Linking with Experiment.**

would present a wake hazard, this small time region occurs in the area of atmospheric turbulence that is described as moderate-to-severe. It is expected that for such levels of turbulence, other vortex transport and decay mechanisms may dominate the wake behavior. In any event extreme accuracy in predicting wake behavior at the short lifetime end is not required since, from an operational viewpoint, practical factors other than wake turbulence require aircraft spacings of greater than 10 to 20 seconds.

Range of Validity of Theory

Three assumptions were made in the development of the present theory which bear directly on the validity of the results. These assumptions were that the disturbance energy spectrum could be represented analytically as the two dimensional, transverse turbulent energy spectrum in the inertial subrange, that the turbulence is isotropic, and that vortex linking is a "long time" phenomenon.

The wave number of maximum amplification rate, $K_o$, is defined by $K_o = \beta_{max}/b$ where $\beta_{max}$ the dimensionless wave number, is of the order one, and b is the vortex spacing. For the class of airplanes that would present a wake hazard, $.02 \leq K_o \leq .10$ radians/meter. This range in wave number is within the atmospheric inertial subrange. Turbulent excitation of the instability at wave numbers outside of this range would be greatly attenuated due to the filtering effect of the vortex dynamics. Thus, the inertial subrange model of the turbulent energy spectrum over all wave numbers is valid since only those wave numbers at or near $K_o$ (which are actually within the inertial subrange) contribute significantly to the growth of the instability, and the model is accurate here.

The value of the turbulent dissipation rate, $\epsilon$, is only a scaling parameter and does not affect the analysis. The value of $\epsilon$ enters into the end result and in this respect it must be chosen properly. The figures

shown assume that $\epsilon$ has been chosen for the case of isotropic turbulence. This is realistic for situations where the aircraft wake exists in an unbounded medium (at altitude). Near the ground, the turbulence is not isotropic, and an effective $\epsilon$ should be used. The section on Meteorology gives guidelines for appropriate corrections for $\epsilon$ near the ground. However, near the ground, the vortices interact with the ground plane itself. This interaction produces velocity fields at the vortices which alters the nature of the dynamics assumed in the present analysis. Thus, near the ground the theory may not be directly applicable or at best the constants may differ from those quoted.

However, for the isotropic turbulence situation, the theory agrees very well with the limited amount of experimental data available. For the case of $\epsilon \to 0$, the theory predicts an infinite time to linking. The figures of link time vs. $\epsilon$ are drawn with logarithmic axes so that this limit is not immediately obvious from the graphs.

The theory was developed for assumed large times in which the first order exponential term in the expression for the radial displacement at the vortex lines dominates. Exactly what constitutes "long times" depends upon the type of airplane which is generating the wake. This is so because the amplification rate, a(k), contained in the exponential term depends upon the aircraft parameters $\Gamma_o$ and b. As an example, for a 727 aircraft, it is estimated that the error in the theory is less than 10% for a time greater than about 30 seconds. Thus, for this particular aircraft, the theory does not give realistic results for times less than 30 seconds.

The theory can and will be modified to account for the "small time" region. However, with respect to the encounter hazard, the small time region is of little practical significance because factors other than wake turbulence dictate aircraft spacings much greater than would exist at "small times."

## 5.3 CORE BURSTING

### General

One major form of vortex instability is core bursting or vortex breakdown. This mode consists of a sudden abrupt widening of the vortex core and in the case of a smoke-marked aircraft vortex, the disappearance of the tracer elements. This phenomenon has been observed in the laboratory (Sarpkaya 1970) and in flight tests (Tombach 1972).

The qualitative details of the breakdown are still quite obscure. In the experiments of Sarpkaya, the first effect seemed to be an axisymmetric disturbance under which the core expanded and contracted smoothly. Downstream of this was a distinct spiral disturbance which was then followed by a disorganized but roughly axisymmetric core widening, the final breakdown. In Tombach's experiments the same sequence of events seems to take place, although the initial smooth axisymmetric bulging is not as distinct.

Several explanations of vortex breakdown have been proposed and are listed by Bilanin and Widnall (1973). These are the stagnation of the axial velocity (Hall, 1966; Bossel, 1969), the conjugate jump theory (Benjamin 1962), and a stability approach (Ludwig, 1962). None of these is entirely satisfactory, yet all contain common elements and all seem partially supported by experiment. It appears agreed that the rapid enlargement of the vortex core is accompanied by axial pressure gradients, and that this breakdown can only occur when the flow approaches a certain critical combination of axial and tangential flow profiles. Apparently the magnitude of the triggering adverse pressure gradient required depends upon the proximity of the flow to its critical state. It is generally agreed that dissipation and core development will cause the core to approach the critical state so that in most cases the core will eventually develop to a state capable of breakdown.

It appears likely that this critical state can be described crudely as a function of the axial velocity on the center line and the swirl ratio. This swirl ratio is the ratio of the maximum tangential velocity to the freestream speed. A recent paper by Mager (1972) gives the critical conditions in fair agreement with Benjamin's results. Qualitatively, both of these papers claim that as the axial velocity reduces so does the critical swirl ratio.

If the critical axial/tangential flow combination could be determined, then the breakdown prediction problem would reduce to testing for the critical state after computing the core development.

It appears that the core bursting-phenomenon is not related to interaction between the left and right elements of the horseshoe vortex pair, but rather to the development of the core itself and this development is a function of the kinematic viscosity controlling the core development. Observations by Tombach (1973) have shown that, at the scale of his flight test, in which vortices were generated by a single engine light airplane (Cessna 170) core bursting occurred first in light atmospheric turbulence, while in high ambient turbulence the Crow Instability invariably terminated the vortex life.

Thus it is possible that, at the same turbulence level, the time scales for core bursting and Crow Instability are related to some function of the airplane Reynolds Number, which could be defined as $Ub/\nu$, where U, b are flight speed and span and $\nu$ the kinematic viscosity. On this basis the vortices due to small slow aircraft might be expected to dissipate principally due to core bursting while those due to large fast aircraft due to Crow Instability. Some supportive evidence for this is that most small scale lab type tests exhibit core bursting (although Crow Instability can certainly be excited), while very large scale flight tests usually show sinuous instability.

Thus it is possible (although not definitely substantiated) that Crow Instability is the most significant mode of decay for vortices characteristic of large transport aircraft. However under unusual, or artifically perturbed circumstances, core bursting may be important.

The development of the core is principally a function of time, vortex strength, ambient turbulence, viscosity and wing drag. Many attempts have been made to analytically determine axial and circumferential velocities in the core. The significance of such a calculation is that if core bursting is related only to local details of core velocity; then breakdown could be predicted if the criteria on velocity profiles were known and the profiles could be analytically determined. Consequently we discuss some of the global aspects of the core development problem, and specifically state the invariants involved.

Force and Moment In Global Terms

Considering the steady flow behind a lifting wing, it is clear that in any plane normal to the flight path that the total drag and lift must be conserved. For this analysis we will ignore the propulsive system, noting that usually this does not contribute to the lift and that its axial contribution will be a thrust associated with the slipstream due to the jet engines or propellors. Thus we will find that considering the wing only, application of the momentum theorem in an axial direction gives a drag on the wing associated with its profile and induced drag.

If we consider a large circuit, along the centerline and around one side of the flow system (Fig. 5-5) we see that on the outer boundaries there can be no viscous torque since the flow is that of a potential dipole having velocity gradients decaying like the inverse cube of the distance. On the center line, even if vorticity is present, the shear

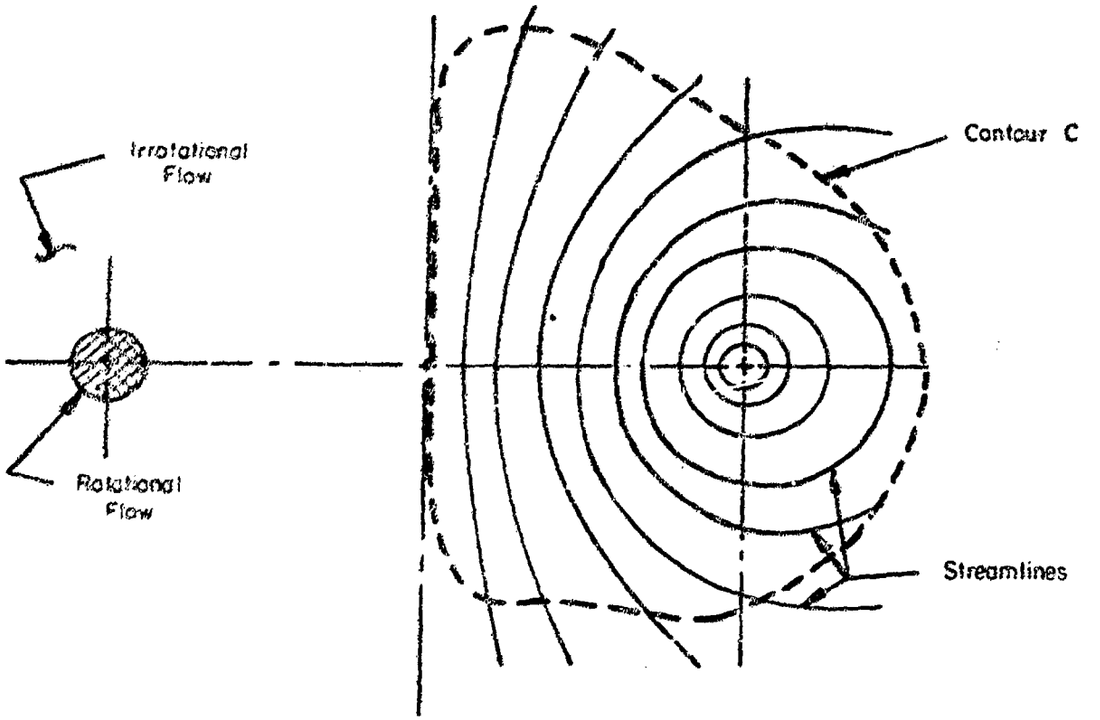


Figure 5-5. Vortex Wake Streamlines and Core Geometry

is zero by symmetry, so there can be no force due to laminar viscosity. Thus no torque can be applied to the circuit C , so the impulse moment (loosely called the "moment of momentum") is conserved, implying that the angular momentum on each side is conserved. This observation seems first to have been made by Betz (1933) by considering a set of free trailing vortices. We digress temporarily to show that the polar moment of vorticity referred to by Betz is directly related to the impulse moment.

## Relationship Between Impulse Moment and Polar Vorticity Moment

It is shown in Lamb's Hydrodynamics that all potential motions can be described by an impulsive wrench applied to the fluid. This wrench consists of both force and couple constituents. The force term is most familiar and is usually called the impulse. We note that the impulse is not strictly equal to the momentum of the system, which in many cases is mathematically indeterminate. However, the impulse is frequently loosely referred to as the "momentum." In our analysis we refer to the moment of the impulse as the "moment of momentum," recognizing again that this term is mathematically indeterminate, but that the impulse moment is a well-defined quantity. Here we show how this is connected to the polar vorticity moment developed by Betz (1933).

Take a two dimensional field, with a curved line of vorticity, representing the shed vortex wake. The wake vorticity, $\gamma$ , is given by $d\Gamma/ds$ where $\Gamma$ is the bound vorticity on the wing and ds the element of length in the wake plane. The potential $\phi$ in the wake plane is directly proportional to the circulation $\Gamma$ , with scale constants which do not concern us. We assume the wake is symmetrical about the vertical centerline and consider only one side as shown in Fig. 5-6.

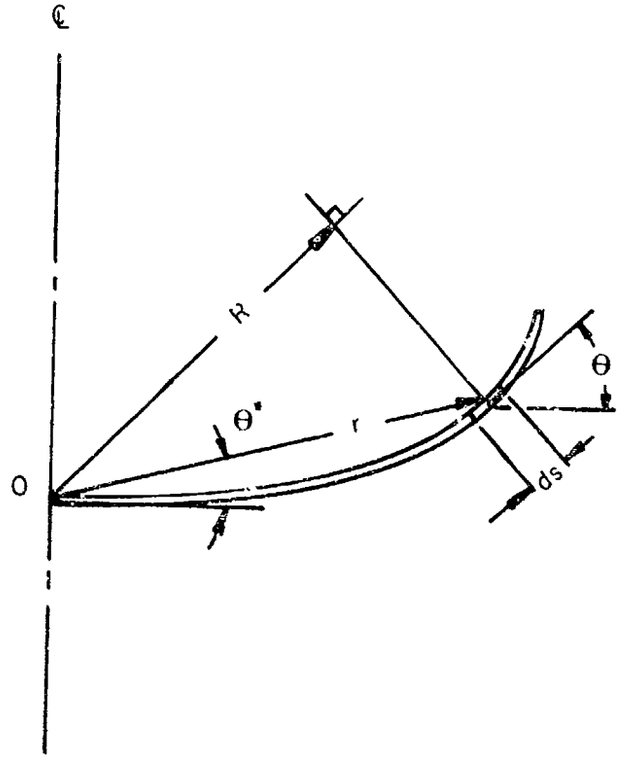


Figure 5-6. Shed Vorticity in Transverse Plane

Taking the impulsive moment about 0, $M_o$, and referring to the figure, we get

$$M_o = \int \phi R ds \ .$$

Now, according to Betz, the polar moment of the vorticity about 0, $M_p$, is given by

$$M_p = \int \gamma r^2 ds \ .$$

We note that $\gamma = d\Gamma/ds \sim d\phi/ds$ so get

$$M_p = \int \left(\frac{d\phi}{ds}\right) r^2 ds$$

Integrating by parts gives

$$M_p = \phi r^2 \Big] - 2 \int \phi r \frac{dr}{ds} ds \ .$$

The first term vanishes at the limits of integration since at the centerline $r = 0$ and at the tip $\phi = 0$ . Now we note that $dr/ds = \cos(\theta - \theta^*)$, so obtain

$$M_o = -2\ M_p$$

This shows that the Betz formulation, which is frequently simpler analytically, does in fact express the impulsive moment. The impulsive force and moment can be transferred to other centers. When taken about the centroid of shed vorticity the inpulsive moment corresponds to the angular "momentum" of the flow about that point and is a measure of the "swirl" in the vortex core and surrounding flow.

Global Invariants

We have discussed the determination of lift, drag, and moment of momentum for a viscous vortex system. These three quantities must be invariant. We note further, that if vorticity has not yet reached the centerline, as is the case during the early core development, then this total vorticity on each side is conserved even though it diffuses radially under viscous and turbulent influences.

If the total vorticity on one side is conserved, it can be shown by arguments in the Trefftz Plane (Munk, 1924) that the centroid of this vorticity (or the mean vortex span) must be fixed for the lift to remain constant. Thus, we can summarize the results to state that the following four properties must be conserved along the wake on each side of the centerline at least within a few hundred spans downstream of the wing:

a. the total vorticity,
b. the centroid of vorticity,
c. the moment of momentum,
d. the axial force.

As explained previously, after mixing or interaction between the vorticity generated on each side of the wing, then only conditions (c) and (d) will still hold as an expression of drag and moment invariance. Although the lift will still be conserved, it can no longer be expressed by the statements (a) and (b).

It is of interest to note that as vorticity diffuses through the cell, it is annihilated at the centerline. Then, for lift to be conserved, the centroid of the remaining vorticity must move outboard. We see that this is consistent with the requirement of conserving vorticity polar moment, since although the total vorticity is reduced, it occupies a larger area.

In general terms the drag (or axial force) can be determined by applying the momentum equation to a normal plane and the impulse moment calculated by taking the second moment of vorticity. To determine the axial force both pressure and velocity must be known. However, since the flow is in general not homoenergetic (because of viscous dissipation) the pressure cannot be inferred from the velocity. Thus both pressure and velocity must, in principle, be known for the momentum theorem to be applied.

This difficulty is avoided by a convenient approximation, valid when the core is still fairly compact and circular in shape.

Representation of the Drag and Moment Integrals for Vortex Cores

The standard technique of simplification is to assume the region to be divided into two portions, an outer portion where the flow is irrotational so that the total head is conserved and where the axial perturbation is negligible, and an inner core region where it is assumed that the flow field is axisymmetric, consisting of a tangential and an

axial component. In this core region there is appreciable dissipation due to viscosity and the Bernoulli equation cannot be used to determine pressure from velocity. Fortunately, the assumption of axisymmetric flow permits one to couple the tangential velocity at a given radius to the radial pressure gradient by use of the equation $dp/dr = v^2/r$, where $v$ is the tangential velocity at radius $r$.

It will be seen that the assumption of irrotationality in the outer flow, and of axisymmetry in the core flow, permits us to infer the pressure from the velocity in both regions. It is instructive to consider the consequence of this assumption, which clearly shows the coupling of the axial and tangential velocities due to viscous effects as analyzed by Batchelor (1964). Figure 5-7 shows the inviscid velocity distribution, $v$, due to a potential vortex with a linear core distribution. In the inviscid outer field we assume that the axial flow $W$ is at the free stream level, and the total head is conserved. Thus the static pressure can be calculated directly from the rotational velocity component. For the core region, we assume that the streamlines are circular; thus here the pressure can be determined (subject to a constant) by centrifugal equilibrium, depending only on the core tangential velocity. The constant is determined by matching with the outer flow. This is shown in Figure 5-7.

We now assume that the total head in the core is nearly the same as that in the outer flow, as might be the case during the early core rollup. We then find from Bernoulli's equation, that the axial velocity in the core must increase to conserve total head. This will create a jet-like axial wake, that is a velocity away from the wing if the wing were moving in still air. As the total head in the core is reduced due to dissipation, this jet-like flow will reduce and finally become a velocity deficit or wake-like flow.

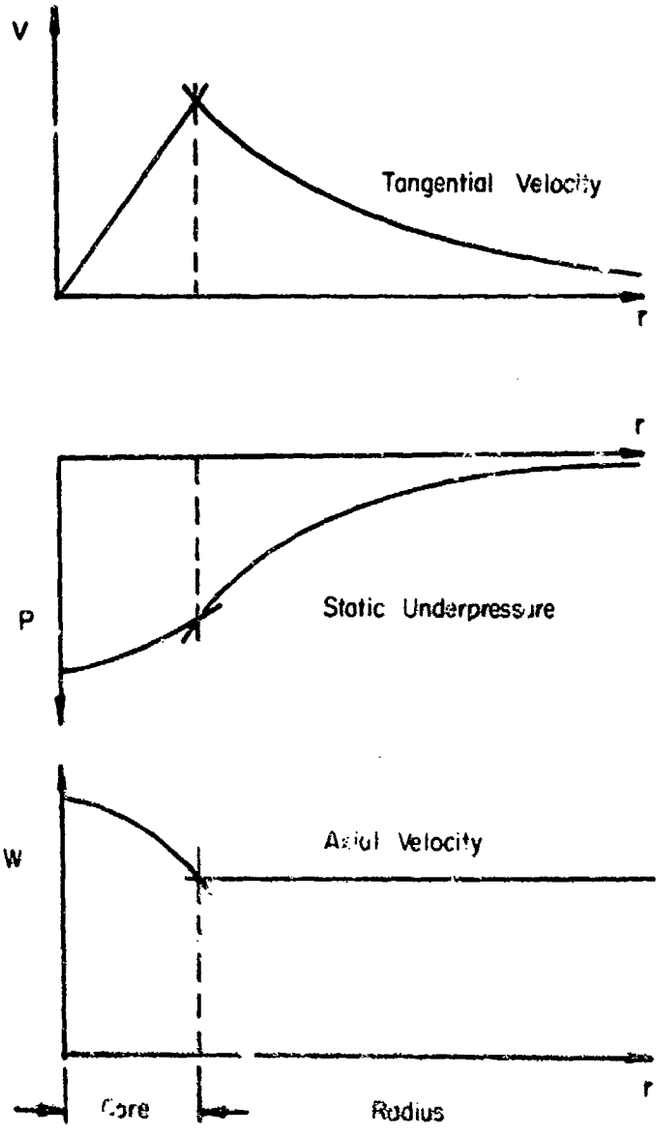


Figure 5-7. Pressure and Velocities Near Representative Vortex.

Superimposed on this flow is the wake-like flow associated with the profile drag of the wing, and represented by the boundary layer shed from the trailing edge. It is assumed that this spanwise vorticity and the streamwise lifting vorticity are "attached" to the same particles in the flow leaving the wing, and is thus swept into the core during the rollup process. Consequently, reduction in total head is present even before there is any dissipation due to motion in the core. Thus the profile drag of the wing (a wake-like component) will reduce or even eliminate the jet-like flow at the center of the vortex core.

In general terms, then, the swirling flow due to lift, and represented by induced drag, develops the initial jet-like flow; while the profile drag develops the wake-like flow. As the core develops, dissipation produces reductions in head, causing the axial flow to become more and more wake-like.

When the core becomes very large, the centrifugal pressure gradients reduce and the final flow state is one of a constant pressure wake, with both the profile and the induced drag appearing as a velocity defect wake.

Of course, the magnitude and rate of change of axial flows depends on the ratio of induced to profile drag and the dissipative process. It is not certain whether the latter is laminar or turbulent. However, we see that this can qualitatively account for the observations of a jet-like flow near the wing developing later into a normal wake-like axial flow.

This model so far conserves lift by conserving circulation and vortex span. We note now that if we assume vorticity and total head loss are uniform in the core, then the additional two global relations of impulse moment and drag are sufficient to determine the core radius and the head loss. Thus, in a crude fashion, one can obtain the major characteristics of the viscous vortex field, which are the swirl number

and scale of the axial flow. Unfortunately, such an analysis can not give any streamwise variation in the core parameters. To obtain an insight into the core development with time (or axial distance), more parameters must be introduced to relax the core assumptions of uniform vorticity and uniform head loss.

An interesting approach to this was made by Mager (1972). He considered a single vortex only, and ignored all but the core flow. Then he assumed a normalized distribution for the tangential velocity with no free parameters, and a normalized distribution for the axial velocity with one free parameter, $\alpha$ , scaling this velocity. In this model, of course, angular momentum of the core is not conserved, but is continuously reduced by viscous torques on the circumference, taken by the author to be laminar. Thus a core development with axial distance can be predicted.

Mager showed that, according to his assumptions, for given initial conditions of angular momentum and axial drag, there were in general two possible flow states, provided certain conditions were met. The one state was characterized by a larger core and lower axial flow speed than the other. Moving downstream, subject to viscous attenuation, these states converged to a single solution. Beyond this point no solution was possible. He defined the point at which no solutions (in his assumed similarity form) existed as the critical point, and derived a curve of critical axial velocity as a function of swirl number. This curve has a very similar character, and is also quite close numerically, to that given by Benjamin.

In order to continue the flow beyond this critical point (at which regular solutions vanished), Mager introduced a further parameter into the tangential velocity profile. With this parameter added, it was found that the flow beyond the critical point exhibited a very large increase in core size (about doubling) and a severe reduction in axial velocity, such that the flow near the centerline was close to stagnation.

Mager postulated that this model accounted for the observed vortex breakdown phenomena, the two solutions in the regular laminar state representing the bulging and contraction of the axisymetric bubble, the vanishing of the axisymmetric solution representing the spiral instability, and the final axisymmetric solution (with the large core and large axial flow deficit) representing the vortex breakdown.

It is clear that the actual critical values obtained by Mager are dictated by the form of the axial and tangential profiles assumed. However, the forms used are properly continuous and appear fairly reasonable, thus other selections would probably not greatly affect the numerical results. However, the vanishing of the solutions, a key element in hypothesizing the spiral instability followed by breakdown, apparently occur because of the limited number of parameters. Additional profile parameters could be introduced, which would continue the real solutions beyond Mager's critical value. It is believed that it would be valuable to make an extension of Mager's technique, extending the analysis from a single axisymmetric vortex core to the vortex pair associated with an aircraft vortex. Here one would take into account the force and moment contributions of the outer inviscid flow and investigate numerically the significance of further parameters on the disappearance of solutions. It should be noted, too, that Mager's solution does not consider unsteady flows so any wave-like instabilities are excluded.

In this light we refer to a new result by Bilanin and Widnall (1973) in which the unsteady core instability is treated. Here the authors state that the Crow instability induces unsteady axial pressure perturbations which in turn cause the vortex core to undergo breakdown. According to this theory the breakdown will occur where the two vortices are furthest apart.

This phenomenon has been observed in lab tests and also appears to occur in some of Tombach's flight tests. It is believed that this is another unsteady way of exciting vortex breakdown and is thus not inconsistent with the other theories quoted.

We note that this does not imply that sinuous instability is a necessary condition for core bursting. In fact, the movies of Tombach (1973) show many cases where core bursting is clearly occurring on a trailing vortex which is essentially rectilinear.

## Conclusion

The nature and precise mechanism of vortex breakdown is still controversial. It is generally agreed that the breakdown is always associated with adverse pressure gradients, apparently these may be either cause or effect. The conditions for breakdown to occur are related principally to the swirl ratio and the magnitude of the axial flow. No general agreement on this critical function has been reached but both Benjamin and Mager give similar results which can be expressed as Figure 5-8. Here we have expressed the axial velocity as the ratio of the mean core axial velocity to the freestream flow. We stress that although scales are given this is only a representative sketch.

It should be noted that both supercritical and subcritical states are driven by dissipation towards the critical condition so that in general most cores will approach the breakdown state. We note that Mager defines a further dividing line in the R, $\overline{W}_c/W$ diagram above which no breakdown is possible.

If proper conditions for breakdown were known, then it would still be necessary to be able to calculate core development to determine the core state.

One of the controversial factors of this calculation is the viscous transfer constant and whether it is turbulent or laminar. This is certainly extremely important in any prediction scheme since turbulent dissipation would cause breakdown an order of magnitude more rapidly than laminar flow.

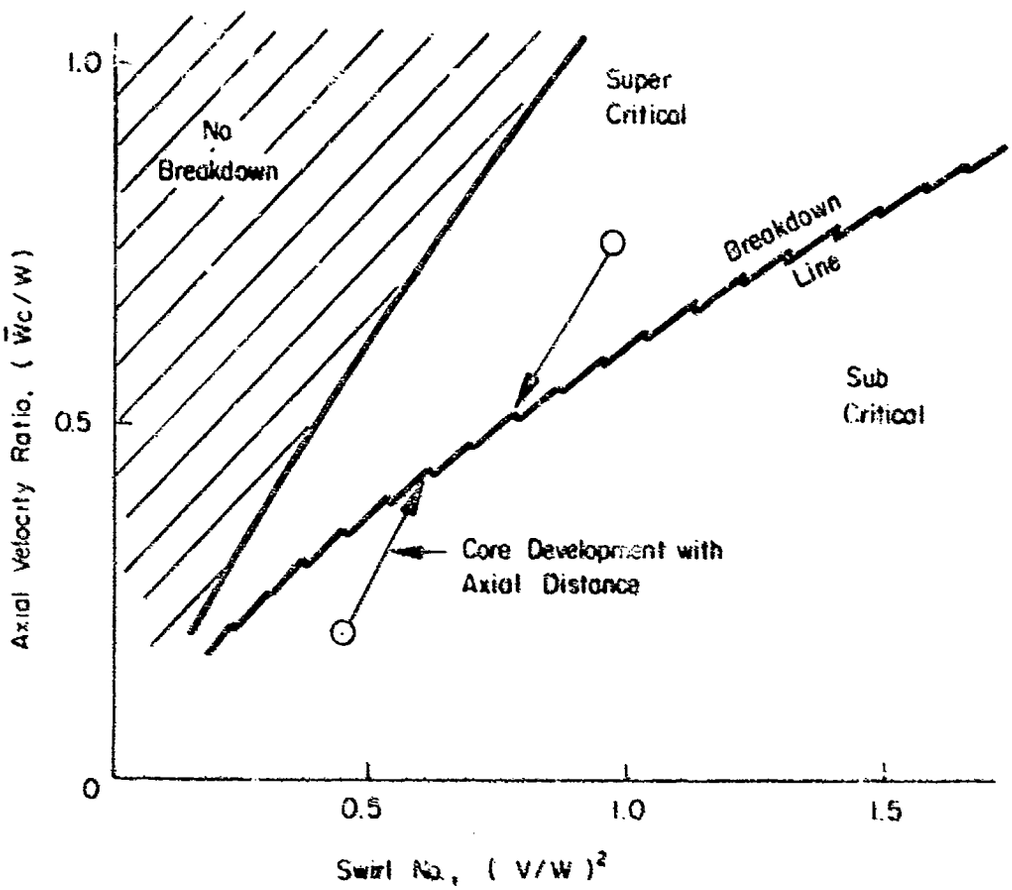


Figure 5-8. Estimated Vortex Breakdown Diagram.

# 6. METEOROLOGICAL ASPECTS

## 6.1 GENERAL

In this section of the report we describe flow, stability, and turbulence characteristics in the layer up to about 70m. Formulas interrelating factors in this layer are presented and discussed. Then a data system is presented which can be a starting point for the design of a system to monitor the atmosphere for the evaluation of techniques to monitor and forecast wake behavior. An eventual operational system will be simpler than the research/evaluation system.

The 70m height arises from considering that the greatest danger from vortex-wake encounters occurs at low altitudes where there is too little height (time) for the encountering aircraft to recover from an unusual attitude. For the standard medium and large jet transports, it is estimated that this critical height can reach up to about 70m, and of course the danger gets greater as the aircraft height above ground decreases. Any exact assessment of the hazard is complex and depends on many quantities. This height also coincides approximately with the height along the glide slope at the middle marker of an ILS system. Concentration on such an area as a test area is used because many vortex sources are available, and the area begins the hazardous region in the landing approach when the vortices from low-flying and slow-flying generating aircraft are strong and the hazard to subsequent slow-flying aircraft is high.

### The Atmospheric Environment

The lowest 1 km of the atmosphere, and especially the lowest 100m, have been intensively studied inasmuch as this covers the region where humans live, where pollutants are initially dispersed, and

where the vertical fluxes of momentum, heat, and moisture are strongest. Out of the studies there have evolved various formulas for the mean profiles and turbulent characteristics, formulas usually based on a theoretical treatment tailored by empirical results. To summarize the situation, the overall understanding of the characteristics of these lowest layers can be deemed "good". In the simplest situations of homogeneous terrain, and constant meteorological conditions, which do not have strongly stable lapse rates, there are satisfactory semi-empirical formulas available to represent conditions. In the more common complex conditions the application of the formulas is more difficult and the apparent success in applying the formulas probably relates more to the fact that great accuracy is not required by the problem nor are the data available to show what accuracy was attained.

## A General View

The planetary boundary layer is the layer near the surface where momentum and heat flux can be large, i.e., where there is a flux link between the upper flow and the earth's surface. The boundary layer height can be under 0.1 km or over 10 km, with 1 km being a common height in daytime. In most typical form, the boundary layer is divided into two parts: (1) the surface boundary layer, across which the vertical fluxes are constant (this constancy provides simplifications which yield rather simple equations for mean and turbulent properties), and (2) the total boundary layer, whose top is found where the fluxes become small.

The height (cm) of the surface boundary layer below which the stress magnitude varies by less than 20% is put by Lumley and Panofsky (1964) at 2000 $\tau$ (where $\tau$ is the surface stress in dynes/cm$^2$). Since $\tau$ is typically of the order 1-10 dynes/cm, h is typically between $2 \cdot 10^3$-$2 \cdot 10^4$ cm, or 20 and 200m.

In analogous fashion, the vertical heat flux, H , varies little with height near the ground. Above the first meter radiation can be neglected. Then with typical values of heat flux on a clear day the height h' of the surface layer comes out at about 50m. However, on nights with little wind, h' will be much lower. The top of the total boundary layer is where the link between upper flow and ground becomes small -- say the momentum flux (shearing stress) drops to 1% of its surface value.

Turbulence is an inherent characteristic of the boundary layer, since it is turbulence (or convection, where the turbulence is organized) which carries the fluxes. The difficult cases to handle are those where the lapse rate is strongly stable and the wind is light -- a common situation at night. Then the layers with appreciable vertical fluxes may be quite low -- a few tens of meters or less -- and there is no way to infer characteristics aloft from direct measurements near the ground.

## 6.2 THE QUANTITIES OF INTEREST

### The Various Quantities

Present thinking suggests that the primary meteorological variables of importance in the transport and decay of a vortex-wake system are: the mean horizontal wind field which causes horizontal drift, and the turbulence and stability fields which play a role in determining descent and decay of the vortex-wake. These wind, turbulence, and stability conditions need to be known throughout the region occupied by the wake during its whole life until it has decayed to the point where it cannot constitute a hazard. Another meteorological quantity will in some cases also prove to be of primary importance -- the mean vertical motion of the local atmosphere. One final property, the vertical shear of the horizontal wind, across the aircraft flight path, may be of importance.

Evidence is accumulating that stability of the atmosphere may have only secondary importance in either vortex decay or vertical descent. Thus we do not consider stability a primary variable, but measure it because of its effect on determining turbulence, drift, or the location of vertical shears.

When we talk about the mean wind, horizontal or vertical, we are thinking of "mean" as referring to events taking place for a minute or two, the lifetime of the wake. Viewed on a longer scale, the same motion might well be considered as turbulence. Such considerations of scale and averaging are important in the design of an operational system.

## Turbulence

Turbulence covers all wavelengths, and multiple correlations, in the three directional components, so one major problem here is to decide what wavelength range and component is most appropriate for the problem of vortex-wake decay. One powerful simplifying assumption which has been used by AeroVironment Inc. is that the turbulence of significance is in the inertial subrange of eddy sizes. Kolmogorov's similarity hypothesis results in the conclusion that all statistical properties of turbulence within the inertial subrange relate only to $\epsilon$, the equilibrium rate of turbulent eddy dissipation. This picture of turbulence is so simple it permits many important formulas to be derived easily by dimensional analysis and it also permits useful empirical relations to be made even when all the physical connecting links may not be understood. Kolmogorov's similarity hypothesis starts from a very simple picture of turbulence mechanisms. It pictures that turbulence enters a system continually, primarily at large wavelengths. The large eddies break down to smaller eddies, which eventually break down to molecular motions through viscosity effects. The smaller eddies are so decayed from the large "input" eddies that the smaller eddies have "forgotten" their ancestry and so cannot be aware of direction -- statistically their energy must be isotropic. There is an "inertial subrange" within the range of eddies which exhibit isotropy; the inertial subrange covers all those except the tiny ones which are strongly affected by viscosity. In the inertial subrange the only quantity to which any statistical property of the flow can be related is $\epsilon$, the equilibrium rate at which energy enters the system, cascades through the inertial subrange of eddy sizes, and is removed (as heat) by viscous effects. In the atmosphere well above the ground the inertial subrange of eddy sizes extends typically from a few centimeters to many hundreds of meters. Even though it is an idealized concept, the relations derived using it are found to be surprisingly good representations of the atmosphere.

The atmospheric wavelengths under discussion for vortex-wake breakup are probably no larger than the primary wavelength for the Crow looping instability (300m for a large jet), and may even be considerably smaller. Thus they fit into the inertial subrange and $\epsilon$ is the appropriate turbulent quantity to use. The Crow-Kolmogorov quantitative instability theory considers that vortex motions in a V-shaped (approximately 90°) trough along the line of flight are the primary instability initiators, and assumes the strength of such motions to be related to $\epsilon$. The theory assumes that symmetrical perturbations along this specific trough surface are as likely as motion of a single line in any single plane. It is certainly possible that other modes of motion, including correlations between vortex lines, are fundamental to the initiation of Crow instability. However, all modes are within the inertial subrange, and so $\epsilon$ is the turbulent quantity to observe and to fit into theories about vortex lifespan as related to atmospheric turbulence.

If we were concerned with wakes only at altitudes of, say 300m or more, thus we could probably comfortably use $\epsilon$ as the most appropriate turbulent quantity and avail ourselves of the simplicity inherent in inertial subrange concepts. However, we are actually interested in wakes at 70m, 50m, and often even lower. Studies have shown (MacCready, 1962, and the discussion by Lumley and Panofsky, 1964, pg. 166-167) that near the ground the spectrum laws seem reasonably valid even at wavelengths about twice the height of observation (and still longer in unstable cases). It may seem surprising that wavelengths greater than z can actually show statistical energy isotropy and agree with the simplified spectrum laws, but it should be remembered that in our turbulence formulas we are dealing with energies and velocities, not final displacements, and so isotropy of energy for the three directional components for 100m horizontal wavelengths may be reasonable at a height of only 30m.

In summary, the strength of the inertial subrange concept is so great in the wake area that the monitoring or predicting of its sole variable, $\epsilon$, may be quite useful for any evaluation program of monitoring/predicting systems. However, we must realize the possible increasing inadequacy of the inertial subrange concept for wake decay predictions as we approach the ground, and therefore also consider other formulations for turbulence there, especially the vertical turbulence component at wavelengths near the Crow looping stability.

## 6.3 BOUNDARY LAYER RELATIONSHIPS

### The Monin-Obukhov Similarity Theory

The Monin-Obukhov similarity theory develops useful relationships in the surface boundary layer based on certain quantities which are constant. Lumley and Panofsky (1964) provides a critical review of the concepts.

Throughout the surface boundary layer the momentum flux (and hence the shearing stress $\tau$ ) is constant, and the heat flux (H) is constant. Using these, together with $\frac{g}{T}$ (where g is gravity and T is temperature) which is another dimensional "constant", it is possible to develop a velocity (u*), a length (L), and a temperature (T*) which are also constant and are three convenient dimensions for scaling. When the principal variables, such as temperature, wind, and height, are expressed non-dimensionally as fractions of these quantitites, a series of non-dimensional equations results that are of general validity in the surface boundary layer for conditions not too far from neutral. For simplicity, we neglect humidity in this discussion since its effects are ordinarily small.

The equations reduce to simple laws for the neutral stability case ($H = 0$), but turn out to be rather complex and awkward to apply when $H \neq 0$. Much attention has been paid to empirical approximations to the basic equations, with the final equations having a general form which relates well to the fundamental theory.

The friction velocity, $u^*$ , is related to the shearing stress $\tau$ and density $\rho$ by

$$u^* = (\tau/\rho)^{\frac{1}{2}} \tag{6-1}$$

Since we are in the "constant" stress region, $\tau$ is the same as $\tau_o$ , the surface stress. The wind direction is constant in the surface boundary layer.

The scaling length L is given by

$$L = u^{*3} C_p \rho T/(kgH) \qquad (6\text{-}2)$$

where $C_p$ is the specific heat at constant pressure, and k is a dimensionless coefficient (the von Karman constant, K= 0.4). The dimensionless height $\frac{z}{L}$ turns out to be especially useful for quantifying the effects of non-neutral lapse rates. L , a length which can be negative as well as positive, is basically a convenient lapse rate parameter. $\left|\frac{L}{30}\right|$ defines the height below which mechanical turbulence is dominant.

$$\frac{z}{L} = \frac{\text{-production rate of convective energy}}{\text{production rate of mechanical energy}} = \frac{zkgH}{u^* C_p \rho T} \qquad (6\text{-}3)$$

Because H is usually not measured, another quantity L' is often used rather than L .

$$L' = L\, K_h/K_m \qquad (6\text{-}4)$$

where $K_m$ is the eddy viscosity (exchange coefficient for momentum) and $K_h$ that for heat flux. $K_h/K_m$ is near unity, being larger in unstable conditions and smaller in stable conditions.

$$L' = \frac{u^* T \frac{\partial v}{\partial z}}{kg \frac{\partial \theta'}{\partial z}} \qquad (6\text{-}5)$$

where $\theta'$ is potential temperature. All the quantities in Eqn. (6-5) are fairly readily measurable.

Another measure of "non-neutralness" is $R_f$ , the flux Richardson Number, which is sometimes involved in derivations. It is defined

as the ratio of the production of turbulent energy due to buoyancy forces to that due to Reynolds stresses (mechanical forces).

A gradient Richardson Number $R_i$ is defined by

$$R_i = R_g K_m / K_n \tag{6-6}$$

$R_i$ is the ratio of buoyancy to inertia forces.

$$R_i = \frac{g}{T} \frac{\frac{\partial \theta'}{\partial z}}{(\frac{\partial u}{\partial z})^2} \tag{6-7}$$

$R_i$ can be ascertained from mean wind and temperature measurements at two levels of a tower.

By various derivations, the logarithmic wind profile is found for neutral conditions:

$$\frac{\partial u}{\partial z} = \frac{u^*}{k(z+z_o)} \tag{6-8}$$

where $z_o$ is the roughness height. For $z >> z_o$, substituting Eqn. (6-8) in (6-7) and comparing with Eqn. (6-5) shows us

$$z/L' = R_i \tag{6-9}$$

for cases very close to neutral. The relation is more complex as we move away from neutral. The more complete relations are shown in Table 6-1. For $R_i$ greater than (more stable than) about 0.1 the ex-

change between layers diminishes so much that similarity laws are not applicable. For $R_i$ less than (more unstable than) about -1 the region of free convection is reached and $L'$ no longer is a useful scaling parameter.

TABLE 6-1. $R_i$ - $z/L'$ RELATIONSHIP

| $z/L'$ | | $R_i$ | $\frac{z}{L'}$ |
|---|---|---|---|
| $R_i/(1-7R_i)$ | Stable | 0.1 | 0.3 |
| | | 0.01 | 0.01 |
| $R_i$ | Neutral | 0.00 | 0.00 |
| | | -0.01 | -0.01 |
| $R_i/(1-18R_i)^{1/4}$ | Unstable | -0.1 | -0.07 |
| | | -0.3 | -0.2 |
| | | -1.0 | -0.4 |

The Wind Profile

The gradient form of the wind profile valid for neutral conditions has already been given in Eqn. (6-8). Integrated, this becomes

$$U = \frac{u^*}{k} \ln \left(\frac{z+z_o}{z_o}\right) \qquad (6\text{-}10)$$

which is usually compromised to

$$U = \frac{u^*}{k} \ln \frac{z}{z_o} \qquad (6\text{-}11)$$

since $z >> z_o$ where the formula is usually applied.

Fiedler and Panofsky (1972) summarize information on the validity of the logarithmic wind profile. They point out that Eqn. (6-11) may be valid only up to 30m or so, and offer a more accurate form which should serve up to 100m:

$$U = \frac{u^*}{k} \ln \frac{z}{z_o} + 144\, f z \qquad (6\text{-}11a)$$

where $f$ is the Coriolis parameter ($f = 2X$ radians per second rotation of earth X sine of latitude). New evidence suggests the constant 144 may be large. In any case, in the present review, for simplicity we will use Eqn. (6-11) rather than (6-11a).

The surface from which $z$ is measured is the ground, for $z_o$ small, but should be elevated when $z_o$ is large. For example, in a forest the "surface" may be set at about 2/3 the height of the trees -- about where obstruction density is maximum.

If U vs $z$ is known at two heights, $u^*$ and $z_o$ can both be found from Eqn. (6-11). For accuracy, the calculation is often made from a more complete wind profile. $z_o$ is a property of the local surface -- a constant for all conditions (although at a given point it will vary with wind direction since it relates to upwind conditions). With $z_o$ known, Eqn. (6-11) gives the whole U vs $z$ profile throughout the layer corresponding to one velocity U at a particular measurement height $z$.

For non-neutral conditions there are various approaches to modifications to Eqn. (6-11) based on the Monin-Obukhov concepts, yielding a log-linear curve. The most complete form of the equation is

$$U = \frac{u^*}{k}\left[\ln\frac{z}{z_o} - \psi\left(\frac{z}{L'}\right)\right] \qquad (6\text{-}12)$$

where the universal function $\Psi(\frac{z}{L'})$ is presented graphically by Lumley and Panofsky (1964) in Figure 6-1 reproduced on the following page.

Equation (6-12) covers adequately from the most stable conditions for which the Monin-Obukhov theory can hold (about $R_i = 0.1$) to strongly unstable cases, say $R_i < -5$.

Note that for conditions very close to neutral ( $R_i < 0.01$) $\Psi$ is given explicitly in the legend of Fig. 6-1. For greater stability, up to $R_i = 0.1$, the explicit equation for $\Psi(\frac{z}{L'})$ is still $4.5\frac{z}{L'}$, although there is some controversy about the coefficient which may be as large as 7.0 instead of 4.5.

The above relations are derived for forced convection, where the vertical transfer of heat and momentum is more from mechanical turbulence than by heat convection. Other results are obtained for free convection, when the relative effect of heat convection is larger, say $R_i \sim -1$, when mechanical and heat energy are produced at about the same rate. Eqn. (6-12) is still a fair interpolation formula for this condition. Heat energy results in much more efficient vertical transfer of properties than is the case for mechanical energy; the convective eddies are larger, with more vertical continuity. For free convection the Monin-Obukhov approach is not used but a different dimensional argument (mixing length theory) gives:

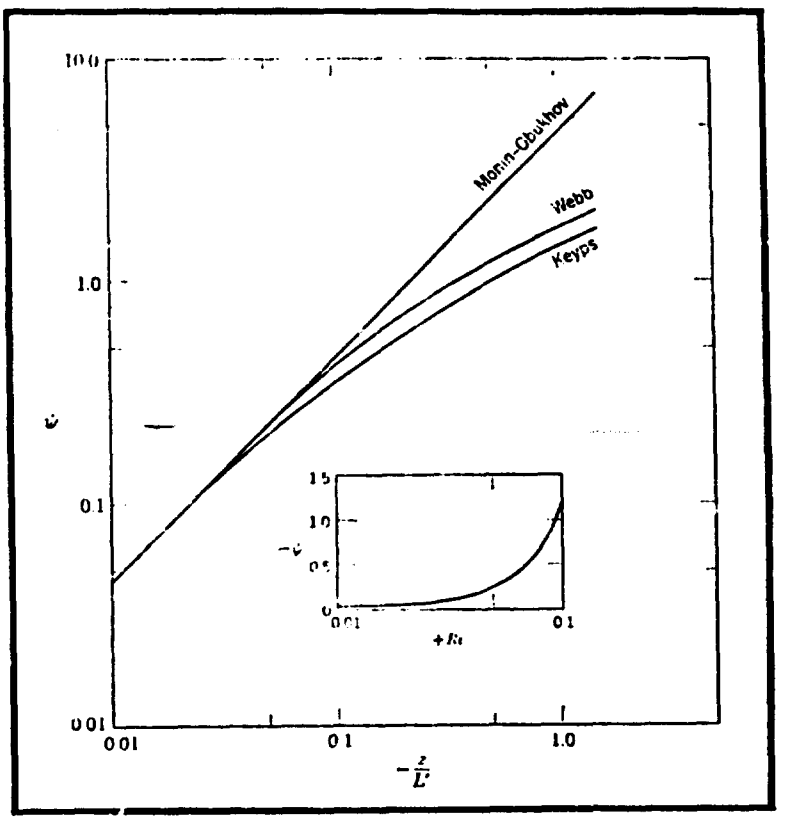


Figure 6-1. Universal Function $\Psi$ for the Integrated Wind Profile. Main Graph for Unstable Stratification; Insert, for Stable Conditions. For $|z/L'|$ or $|R_i| \leq 0.01$, $\Psi = 4.5\ z/L' = 4.5\ R_i$.

$$\frac{\partial U}{\partial z} = \frac{K_h}{K_m} u_*^2 \left(\frac{gH}{C_p \rho T}\right)^{-1/3} z^{-4/3} \qquad (6\text{-}13)$$

If $K_h/K_m$ is constant with height, Eqn. (6-13) shows and $U \sim z^{-1/3}$, predictions which are reported to fit wind observations on convective days with moderate wind speeds quite well. In strong convection with little wind, the U profile is rather indeterminant.

Another approach, the power law method, has been found convenient for describing wind profiles, especially for stable conditions. It has no theoretical basis, but has a flexibility and simplicity which makes it useful for tailoring to empirical data.

$$\frac{U}{U_1} = \left(\frac{z}{z_1}\right)^p \qquad (6\text{-}14)$$

where the subscript (1) refers to the conditions at a reference level and p is an exponent varying between 0 and 1. Panofsky, Blackadar, and McVehil (1960) showed p could be derived from z, L', and $z_o$, and that the resulting values of p were consistent with numerous observed values. p is not a constant with height of the layer concerned; it increases with height in stable cases and decreases in height in unstable cases. It is found to depend little upon wind speed; it increases slowly with increasing roughness, and varies primarily with lapse rate (decreasing as the lapse rate becomes more unstable).

Pasquill (1962) suggested certain stability classes which have proven convenient for wind profile and diffusion studies. They are defined in Table 6-2 on the following page.

## TABLE 6-2. RELATION OF TURBULENCE TYPES TO WEATHER CONDITIONS

A— Extremely unstable conditions
B— Moderately unstable conditions
C— Slightly unstable conditions
D— Neutral conditions*
E— Slightly stable conditions
F— Moderately stable conditions

| Surface wind speed, m/sec | Daytime insolation | | | Nighttime conditions | |
|---|---|---|---|---|---|
| | Strong | Moderate | Slight | Thin overcast or ≥4/8 cloudiness† | ≤3/8 cloudiness |
| <2 | A | A–B | B | | |
| 2 | A–B | B | C | E | F |
| 4 | B | B–C | C | D | E |
| 6 | C | C–D | D | D | D |
| >6 | C | D | D | D | D |

*Applicable to heavy overcast, day or night.
†The degree of cloudiness is defined as that fraction of the sky above the local apparent horizon which is covered by clouds.

These classes can be used to summarize data as follows:

## TABLE 6-3. DATA SUMMARY

| Pasquill Class | $\delta T/\delta z$ | $\delta_\varphi$ | p |
|---|---|---|---|
| A | $<-0.6\ ^{o}C/100'$ | $25^{o}$ | .15 |
| B | -0.5 | $20^{o}$ | .17 |
| C | -0.4 | $15^{o}$ | .20 |
| D | -0.2 to -0.3 | $10^{o}$ | .26 |
| E | -0.1 to 0.3 | $5^{o}$ | .39 |
| F | 0.4 to 1.1 | $2.5^{o}$ | .48 |
| (G) | (>1.2) | $(1.7^{o})$ | |

The $\delta T/\delta z$ criteria come from USAEC Safety Guide 23 (1972), and are related to Pasquill classes for moderate winds. They are measured between 10 and 45 m. The $\delta_\varphi$ (vertical-axis vane RMS) values are from Safety Guide 23 and Gifford (1968), and Slade (1965). The p values come from DeMarrais (1959) and apply to the rough Brookhaven site ($z_o \sim 0.5$ to 1.0m).

Golder (1972) provides a more rational way of relating Pasquill classes to the quantities on which the Monin-Obukhov laws are based. He shows how the Pasquill classes are functions of $z_o$ and L (read L' or rather 1/L' for convenient plotting). Figure 6-2 is taken from Golder's report.

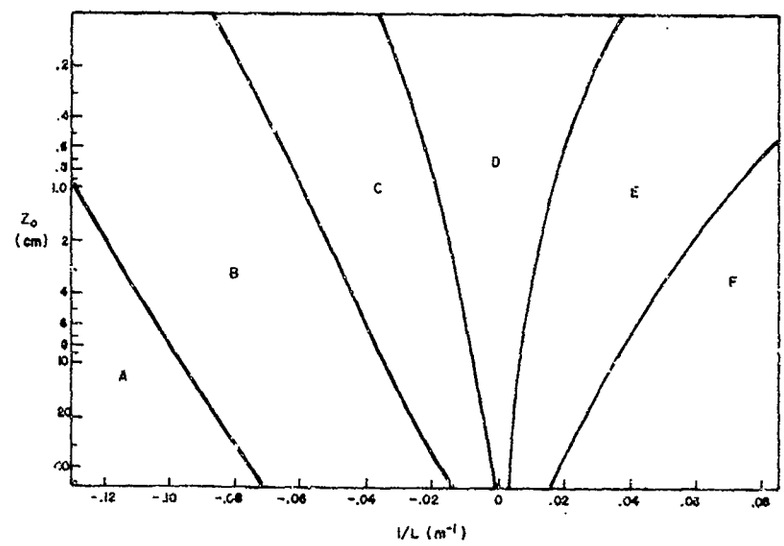


Figure 6-2. 1/L as a Function of Pasquill Classes and $z_o$

Since use of $z_o$ and $L'$ permits one to draw conveniently on the rational and versatile equations based on Monin-Obukhov, it seems preferable to use them instead of the empirical power laws which vary with site and altitude.

ε vs Height

The dissipation rate $\epsilon$, under steady state conditions, is equal to the mechanical production of energy $u^* \partial U/\partial z$ plus the buoyant production $gH/(C_p \rho T)$ less the flux divergence $1/\rho (\partial F_{E_m}/\partial z)$ where $F_{E_m}$ is the upward flux of total turbulent kinetic energy per unit area.



There is considerable controversy about magnitude of the flux divergence term. The observations and theory cited by various authors for unstable conditions vary from the concept that the flux divergence term fully cancels the buoyant production term to the concept that the flux divergence term is negligible. Thus all formulations fit:

$$\epsilon = u^{*2} \frac{\partial U}{\partial z} + C_1 \frac{gH}{C_p \rho T} \qquad (6\text{-}15)$$

with the value of the coefficient being between 0 and 1. G. Briggs (at NOAA Environmental Research Laboratories, Oak Ridge, Tennessee) has recently reviewed all the available evidence and concluded that $C_1 = 1/3$ gives the best fit with observations, and that with this value Eqn. (6-15) works reasonably up to 2/3 of the total depth of the mixed region.

Using the methods discussed by Hanna, Hutchison, and Gifford (1969), and setting $C_1 = 1/3$, Eqn. (6-15) can be transformed to

$$\varepsilon = \frac{u^{*3}}{kz} \frac{1-\frac{1}{3}R_i(1-18R_i)^{\frac{1}{4}}}{(1-18R_i)^{\frac{1}{4}}} \qquad (6\text{-}16)$$

It should be noted that the turbulence intensity function commonly of interest is $\varepsilon^{1/3}$, not $\varepsilon$, which minimizes the accuracy demands on the $\varepsilon$ vs $z$ equations. Taking the neutral approximation, with $R_i = 0$, Eqn. (6-16) becomes

$$\varepsilon^{\frac{1}{3}} = u^* k^{-\frac{1}{3}} z^{-\frac{1}{3}} \qquad (6\text{-}17)$$

If we have already ascertained $z_o$ and we measure $U_1$ at height $z_1$, then from Eqn. (6-11)

$$u^* = U_1 k / (\ell n\, z_1/z_o) \qquad (6\text{-}18)$$

and so

$$\varepsilon^{\frac{1}{3}} = \frac{U_1 k^{\frac{2}{3}}}{z^{\frac{2}{3}} \ell n\, z_1/z_o} \qquad (6\text{-}19)$$

The inverse relation between $\varepsilon$ and $z$ is not inconsistent with the $\varepsilon$ observations from many sources summarized by Ball (1961). Ball examined data from 10cm to 10 km, covering various roughnesses, winds, and stabilities, and although his summary plot shows a wide scatter the ground-related turbulence points have a $z^{-1}$ tendancy.

In the next section, where we consider total vertical energy, there is further discussion about obtaining $\varepsilon^{1/3}$ in non-neutral conditions. The conclusion is that Eqn. (6-17) is probably adequate in conditions well away from neutral.

An excellent, recent review of $\epsilon$ vs z is given by Pasquill (1972). One of his main points is that surface roughness variability in the horizontal, which makes even many field research sites "non-ideal", can have a bigger effect on the $\epsilon$ vs z relationship than the difference between specific formulas.

Energy vs Height

Lumley and Panofsky (1964) state that for neutral conditions in the surface boundary layer, the total turbulent energy $\bar{e}$ should be proportional to $u^{*2}$ and thus be given by

$$\bar{e} = CU^2/(\ln z/z_o)^2 \qquad (6\text{-}20)$$

where the dimensionless constant C is of order one. The few available data are not in exact accord with Eqn. (6-20), and the authors note that although the nearby $z_o$ may determine the vertical motions, the $z_o$ far upstream can have an important bearing on the other components.

As to the vertical component of turbulent energy, $\sigma_w$, containing all frequencies, the Monin-Obukhov theory indicates for a range of stabilities that

$$\sigma_w = Au^* \qquad (6\text{-}21)$$

where A has a value probably near 1.3 in the neutral case, but slightly different values for other $R_i$ or z/L. Combining Eqns. (6-8) and

(6-21) gives, for neutral situations,

$$\sigma_w = \frac{kAU}{\ln z/z_o} = \frac{0.5U}{\ln z/z_o} \qquad (6\text{-}22)$$

In stable air $\sigma_w$ decreases with height; in unstable air it slowly increases.

The value of A found by Monin (1962), corrected by $\times 1.5$ as discussed by Lumley and Panofsky (1964), is given for approximately various stabilities in terms of $z/L'$ . The form shown by Panofsky (1970) is somewhat different, but since it represents more data we will use it. Putting it in equation form:

$$A = 1.3 - 0.3\, z/L' \qquad (6\text{-}23)$$

This is a fair approximation for $-1.2 < z/L' < 0.3$ ,

If one uses a vertical angle vane (horizontal axis) to measure turbulence, its RMS value $\sigma_\theta$ in radians will be related to the RMS of vertical velocity $\sigma_w$ by

$$\sigma_\theta = \sigma_w/U \qquad (6\text{-}24)$$

if we assume angles are small so the sine is the same as the angle. Then from Eqns. (6-22) and (6-24) we see, for the neutral case,

$$\sigma_\theta = 0.5/\ln z/z_o \qquad (6\text{-}25)$$

In neutral stability, (or any strong wind condition) $\sigma_\theta$ is independent of U . Also, note that by measuring $\sigma_\theta$ at a certain height $z_1$, $z_o$ is readily obtained from Eqn. (6-25).

Equations which require knowledge of $L'$ may not be particularly convenient since $L'$'s calculation from $R_i$ requires observing both wind and temperature at two heights and performing long-term averaging to obtain the needed gradients. In the practical case it may be more suitable to estimate H or $L'$ or $R_i$ . This is what AeroVironment Inc. did in developing its General Concentration Model whose application is described by the AV staff (1972). They used the method suggested by Panofsky and McCormick (1960), who postulated on the basis of similarity theory as applied to the constant flux layer that $\sigma_w$ should be a function of height, the rate of energy supplied by mechanical turbulence, and the rate of supply of convective energy. This approach has the further advantage of covering the free convection range as well as stabilities closer to neutral. The basic equation is:

$$\sigma_w = A_2 \left[ z\left(u^{*2} \frac{\partial U}{\partial z} + \frac{\delta g H}{\rho C_p T}\right) \right]^{\frac{1}{3}} \qquad (6\text{-}26)$$

where $A_2$ and $\delta$ are constants (assumed to be $A_2 = 1.25$, $\delta \approx 2.4$). Using Eqns. (6-12) and (6-26), one than has $\sigma_w$ as a function of H , $\Psi(z/L')$, $z_o$, and U . Next, various forms of stability dependent $\Psi$ as proposed by Panofsky et al (1960) and McVehil (1962) were assumed in Eqn. (6-26). The scale length L' is related to heat flux and friction velocity (eqn. (6-2)). The friction velocity further couples the mean wind and L' through the diabatic wind equation (Eqn. 6-12)). The unique way in which these parameters are related to one another makes it possible to determine $\sigma_w$ as a function of wind for given values of $z_o$ and H , although not in closed form. The results were plotted by AV in the form of $\sigma_w$ vs U at 10m for families of $z_o$ and H values. The

roughness dependence was removed by using a roughness reduced velocity $U_r = U_o(\ell n 10/z_o)/(\ell n 10/z_r)$ where $U_r$ is the wind speed at 10m corresponding to the roughness $z_r$. The "universal roughness reduced curves" provided a simple summary for computer storage giving quantitatively $\sigma_w = DU_r$ for the appropriate strong winds, $\sigma_w = CH^{1/3}$ for $H > 0$ and $U_r < BH^{1/3}$ (positive H but very low winds), and $\sigma_w = 0$ for $H < 0$ and $U_r < -AH^{1/3}$ (negative H and very low winds). For U and $\sigma_w$ in m/sec, $z_r$ in m, and H in cals/cm$^3$/min, the constants are A = 13.2, B = 5.7, C = 0.87, and D = 0.125.

The similarity in the derivations of Eqns. (6-21) and (6-26), (and the uncertainty in each) suggests that one will not have much larger errors if one sets

$$\epsilon^{\frac{1}{3}} = \frac{A_3 u^*}{k^{\frac{1}{3}} g^{\frac{1}{3}}} \qquad (6\text{-}27)$$

where the coefficient $A_3$ is assumed to be a weak function of $z/L'$. The variation of $A_3$ should be less than the cube root of the variation of A with $z/L'$ (Eqn. (6-23)) since the coefficient $C_1$ in Eqn. (6-15) is so much smaller than the $\delta$ in Eqn. (6-26). $A_3 = 1$ at $z/L' = 0$, the neutral case. The implication here is that $A_3$ will be within 5% of unity even for $z/L' = -1$. Since the controversy about the magnitude of constants involves indeterminancies much greater than 5%, the temporal variability of $\epsilon^{1/3}$ certainly exceeds 10%, and $z_o$ has local variations, for practical purposes well into the free convection range we can probably set $A_3 = 1$. Eqn. (6-17), the neutral approximation, is deemed adequate in non-neutral cases; it may be as suitable as any other simple equation.

For the RMS lateral velocity $\sigma_v$, or the RMS angular variations of a direction vane with a vertical axis, $\sigma_\varphi$, the situation becomes more

complex because of the increasingly large energies at increasingly large wavelengths (or periods) which are suppressed in the vertical turbulence covered above.

For the neutral case, various data suggest we can use as a first approximation

$$\sigma_v = 2\ u^* \qquad (6\text{-}28)$$

in analogy to Eqn. (6-21), but even in smooth terrain we should use a large $z_o$ to infer an "effective" u* such as 1m because large eddies dominate the quantity. There is always the problem that $\sigma_v$ depends on the sampling time used to derive it -- if longer wavelengths (times) are included, measured $\sigma_v$ is larger. In non-neutral conditions everything gets very complex. There is no complete theory relating $\sigma_w$ to U, $z_o$, $R_i$, primarily because the instability aloft above the surface layer can have a large effect on the large scale lateral motions down low. Table III tries to summarize some of the data (note $\sigma_\varphi \sim \sigma_v/U$), and many other compilations are available (see, for example, Slade 1968, Pasquill, 1962, and Lumley and Panofsky 1964).

To summarize from the last reference: "$\sigma_v$ increases with increasing wind speed, at constant stability, particularly in stable air. It further is generally much larger in unstable air for the same wind speed, with the exception of low-wind speed inversions in which a gradual drift of wind direction may produce large standard deviations."

For the longitudinal component, $\sigma_u$, in anology to Eqns. (6-21) and (6-28), we find in the neutral case $\sigma_u \sim u^*$, with the constant of proportionality empirically set at 2.5. The relative variation of $\sigma_u$ with stability is a bit less than given for $\sigma_w$ in Table III. Panofsky (1970), provides the latest summary plot of the constant of proportionality for $\sigma_u \sim u^*$ and $\sigma_v \sim u^*$, which we summarize in a later section.

## Spectra and Scales of Turbulence

The high frequency end of the atmospheric turbulence horizontal spectrum, the inertial subrange, in neutral and turbulent conditions, fits the "-5/3 law":

$$S(k_1) = b\,\varepsilon^{\frac{2}{3}}\,k_1^{-5/3} \tag{6-29}$$

where $k_1$ is wave number in radians per unit length, $\epsilon$ is the dissipation rate, $S(k_1)$ is the energy per unit wave number, and b is 0.50 for longitudinal spectra and 0.66 for lateral spectra. If $k_1$ is the wave number in cycles per unit length, b is 0.15 for longitudinal spectra. (See the review by Panofsky, 1970, and Pasquill, 1972). There is still controversy about the value of constants. Franzen (1973) considers $b_2 = 0.55$ as the best estimate, and suggests that the relation between $b_2$ and von Karman's k makes the latter take the value 0.35.

With the shape of the high frequency end of the spectrum known, it is possible to derive the intensity factor, $\epsilon$, from any measurement which depends only on wavelengths within the inertial subrange. For example, we can obtain $\epsilon^{1/3}$ from the $\sigma_\theta$ or $\sigma_\varphi$ signals where only high frequencies (in the inertial subrange) are used in the "sigma meter" giving the averages of $\theta$ or $\varphi$ resulting in $\sigma_\theta$ or $\sigma_\varphi$ (here we will call it $\sigma_{\tau_3}$). The filter characteristic time $\tau_3$ must be

$$\tau_3 < 0.44\, z/U \tag{6-30}$$

(see MacCready and Jex, 1964); for accuracy it is safest for $\tau_3$ to be even considerably shorter than Eqn. (6-30). Then the authors find

$$\varepsilon^{\frac{1}{3}} = 0.62\, U^{\frac{2}{3}}\, \tau_3^{-\frac{1}{3}}\, \sigma_{\tau_3} \tag{6-31}$$

for $\epsilon$ in $cm^2\ sec^{-3}$, U in m/sec, $\tau_3$ in seconds, and $\sigma_{\tau_3}$ in degrees.

$\epsilon^{1/3}$ can also be derived from high frequency wind speed fluctuations (see Franzen, 1965). The sensor must have a very short response distance to permit the measurement.

For the whole spectrum of vertical velocity up to z = 50m, Panofsky (1970) notes for neutral and moderately unstable cases that the spectra can be normalized to the following equation for neutral and moderately unstable air:

$$\frac{k_1 S(k_1)}{u^{*2}} = \frac{3.36f}{1+10f^{5/3}} \qquad (6\text{-}32)$$

where $f = k_1 z$, and $u^{*2}$ can be replaced by $3.6\,\sigma_w^2$. Note here $k_1$ is in terms of cycles (not radians) per unit length, and f is a frequency normalized by height.

$k_1 S(k_1)$ has a maximum value of $0.43\,u^{*2}$ for $k_1 z \sim 0.3$, that is, for a wavelength about 3 times the height. In stable air the peak shifts to higher values.

More recently, Pasquill has examined the $S(k_1)$ spectrum in much greater detail. He considers the scale $\lambda_m$, the wavelength of the peak of a $k_1 S(k_1)$ curve, where $\lambda_m$ is the wavelength of maximum power input, expressible also in corresponding wave number by $\lambda_m = (K_{1m})^{-1}$. The situation can be summarized as follows:

a. In neutral flow $\lambda_m/z$ is between 2 and 4, and effectively constant with height in the first 20m or so. The best evidence tends toward the value 2.

b. The effect of thermal stratification is to increase or decrease the scale in unstable or stable conditions, and in effect to increase or decrease the height range with effectively linear increase.

Pasquill also discusses the Eulerian length scale, $\ell_E$, derived from correlation coefficients. Since this depends rather strongly on the large wavelengths, for which measurement (averaging) is difficult, the relative variability of $\ell_E$ is even greater than that for $\lambda_m$. Summary "b" above holds for $\ell_E$ as well as $\lambda_m$.

In final summary, for maximum accuracy the scale constants in Eqn. (6-32) should be adjusted as a function of stability. However, we feel that for our practical application Eqn. (6-32) as it stands is probably adequate.

The Total Boundary Layer

Hanna (1969) examined many different methods for estimating $h_T$, the height of the mixed region constituting the total boundary layer. He found it impossible to relate $h_T$ to quantities measured simply near the surface, such as $u^*$, U, $U_z$ (the geostrophic wind), together with the Coriolis parameter. The best formula for $h_T$ larger than about 150m was found so be that of Laikhtman (1961), with the constant of proportionality altered to fit observations:

$$h_T(U_z, \Delta\theta') = 0.75\, U_z \left(\frac{g\Delta\theta'}{T\Delta z}\right)^{-\frac{1}{2}} \qquad (6\text{-}33)$$

where $\Delta\theta'/\Delta z$ is the average vertical gradient of potential temperature through the boundary layer. Quoting from Hanna, when a complete vertical temperature sounding is available, "$h_T$ is the lowest level which the vertical gradient of temperature exhibits a discontinuity.

For example, during well-mixed afternoon periods when an adiabatic layer near the ground is capped by a relatively stable inversion layer, $h_T$ corresponds to the level of the base of the inversion layer. During a clear, calm night-time period where there is a ground based inversion, $h_T$ corresponds to the top of the strong inversion layer." For the altitudes studied, $\Delta\theta'$ was always positive (conditions always stable over this layer).

The conclusion is that temperature measurements aloft are needed to establish $h_T$ with any reliability. With such measurements, $h_T$ can be taken directly from the sounding. Eqn. (6-33) may be of some slight help if a partial $\Delta\theta'/\Delta z$ is given.

## Empirical Values of $z_o$

The surface boundary layer equations are based on a picture of flat terrain with the roughness everywhere the same. The equations, however, are used for approximating reality in actual terrain, which can be considered as an assemblage of areas each with a different representative $z_o$, all being averaged together to give a final net effect. One effect of a change of roughness can be seen from the analysis by Panofsky (1968). He found that if wind blows over a surface whose roughness length abruptly changes to $z_o$ (at $x = 0$), then below the height $z_1$ where

$$z_1 = 0.8\, z_o\, (x/z_o)^{0.8} \qquad (6\text{-}34)$$

the boundary layer similarity laws can be applied based on the new $z_o$. This whole subject of changing and patchy roughness is extensively reviewed by Pasquill (1972). Where small $z_o$ is involved, it

takes about 1 km for the influence to cover the height of concern to us (70m) for neutral conditions, and much more for stable conditions. For larger $z_o$, or for unstable cases, the influence establishes itself more quickly. For patchy roughness, the situation is obviously complex, and the reader is referred to Pasquill's paper.

Some representative values of roughness are given below:

| | |
|---|---|
| Smooth snow | 0.005 to 0.1 |
| Mown grass | 2.0 |
| Long grass (60-70m) | 6 |
| Open Country (O'Neill) | 7,8 |
| Cotton Field | 50 |
| San Jose, suburb | 60 |
| London, urban | 78 |
| Philadelphia | ~90 to 240, depending on wind direction |
| Brookhaven tower (in woods) | 100 |

## 6.4 A REVIEW OF OPERATIONAL EQUATIONS

Preliminary. Find $z_o$, $R_i$, $L'$, $u^*$

Assume one measures U and T at two heights, the subscript (1) referring to the lower at $z_1$ and the subscript (2) referring to the higher at $z_2$. U and T designate averages, averaged over about 10 minutes.

1. In near neutral conditions, preferably with strong winds, calculate $z_o$.

From $U_1$ at $z_1$ and $U_2$ at $z_2$:

$$U = \frac{u^*}{k} \ln z/z_o \qquad (a)$$

leads to

$$\ln z_o = \frac{\frac{U_1}{U_2} \ln z_2 - \ln z_1}{U_1/U_2 - 1} \qquad (b)$$

Second method:

From $\sigma_\theta$ at any height $z$

$$\ln z_o = \ln z - \frac{0.5U}{\sigma_w} \qquad (c)$$

From $\sigma_w$ at any z and U

$$\ln z_o = \ln z - \frac{0.5U}{\sigma_w} \qquad (d)$$

Third method:

Obtain $\epsilon^{1/3}$ from U and $\sigma_\theta$ (or $\sigma_\varphi$) with a very short filter characteristic $\tau_3$ where $\tau_3 < 0.44\ z/U$ . Then

$$\epsilon^{\frac{1}{3}} = 0.62\ U^{\frac{2}{3}} \tau_3^{-\frac{1}{3}}\ \sigma_\theta \qquad (e)$$

Obtain $z_o$ from

$$\ln z_o = \ln z - \frac{Uk^{\frac{2}{3}}}{\epsilon^{\frac{1}{3}} z^{\frac{1}{3}}} \qquad (f)$$

Use all three methods, and note agreement. Also note systematic variation of $z_o$ with azimuth angle $\varphi$ .

2. Calculate $R_i(\bar{z})$

$$R_i(\bar{z}) = (g/T)\ \frac{\theta_2' - \theta_1'}{(U_2 - U_1)^2}\ \bar{z}\ \ln z_2/z_1 \qquad (g)$$

which gives the best finite difference approximation to the formula for Richardson Number where $\bar{z} = (z_1 z_2)^{1/2}$ is the geometric mean of the heights $z_1$ and $z_2$ .

3. Calculate L' at $\bar{z}$ using the appropriate equation shown on Table 6-I.

4. With this L' , and using the $\Psi(z/L')$ relation from Figure 6-1, calculate u* from the height data using

$$U = \frac{u^*}{k} [\ell n\, z/z_o - \psi(z/L')] \qquad (h)$$

Then calculate u* from the height 2 data. The two u* values should be fairly close. Take their average as the best estimate of u* . One could weight the calculation from the lower height more strongly since the z/L' effect is less at low heights, but the calculation from the higher height may be more suitable as a basis for extrapolation.

U vs z

1. Eqn. (h) gives U vs z for all heights in the surface boundary layer.

$\epsilon$ vs z

1. Calculate $R_i$ for all the heights of interest from z/L' from the Table 6-I equations

2. At these heights, calculate $\epsilon^{1/3}$ by

$$\epsilon^{1/3} = \frac{u^*}{k^{1/3} z^{1/3}} \frac{[1-1/3\, R_i(1-18R_i)^{1/4}]^{1/3}}{(1-18R_i)^{1/12}} \qquad (i)$$

3. As an operational alternative, ignore the $R_i$ effects (which tend to be small) and just assume

$$\varepsilon^{\frac{1}{3}} = \frac{u^*}{k^{\frac{1}{3}} z^{\frac{1}{3}}} \qquad (j)$$

which is the equivalent of

$$\varepsilon^{\frac{1}{3}} = \frac{1}{2^{\frac{1}{3}}} \frac{U_1 k^{\frac{2}{3}}}{\ell n\, z_1/z_o} \qquad (k)$$

If $U_1$ is measured at $z_1$, and $z_o$ is known, Eqn. (k) gives $\epsilon$ vs $z$. If only $\epsilon^{1/3}$ is measured at $z_1$, Eqn. (j) then shows

$$\varepsilon^{\frac{1}{3}} = \varepsilon_1^{\frac{1}{3}} \left(\frac{z_1}{z}\right)^{\frac{1}{3}} \qquad (l)$$

$\sigma_w$ vs $z$

1. Use $\sigma_w = (1.3 - 0.3\, z/L')\, u^*$ (m)

2. For neutral cases, thus $\sigma_w = \dfrac{0.5U}{\ell n\, z/z_o}$ (n)

and is constant with height.

3. Equivalently, $\sigma_\theta = 0.5/\ell n\, z/z_o$ (o)

4. If H can be estimated rather than $R_i$ or $L'$, use the algorithm provided in the discussion below Eqn. (6-26).

## $\sigma_v$ and $\sigma_u$ vs z

1. Consider $\sigma_v \sim u^*$ and $\sigma_u \sim u^*$, with the constants of proportionality being functions of stability as summarized on Figure ! of Panofsky (1970). The constant is about 2.5 for all stabilities for $\sigma_u$, while for $\sigma_v$ it is about 1.5 for stable cases and exceeds 3 for unstable. The relations for any given case are found to be poor because the energy yielding $\sigma_u$ and $\sigma_v$ is not closely tied to local small-scale $z_o$ and so similarity laws are really inapplicable. If accuracy of $\sigma_v$ and $\sigma_u$ is required, they should be measured directly at one point and extrapolated upward and downward by physical reasoning and empirical results from various prior studies.

## Vertical Turbulence Spectra

1. For neutral and moderately unstable cases,

$$\frac{k_1 S(k_1)}{u^{*2}} = \frac{3.36f}{1+10f^{5/3}} \qquad (p)$$

where $k_1$ is wave number in radians per cm, $f = k_1 z$, $S(k_1)$ is the power spectral density, and $u^{*2}$ can be replaced by $0.6\sigma_w^2$. $k_1 S(k_1)$ has maximum of $0.43u^{*2}$ at $k_1 z \sim 0.3$. In stable air this peak shifts to higher values of $k_1$.

## 6.5 AN APPROACH TO AN OPERATIONAL DATA SYSTEM

The system must be fully automatic, requiring no manual inputs. For eventual operational application it should provide information on mean air flow profiles and turbulence throughout a "target" volume about 1 km long, 300m wide, and of thickness tapering from ~70m at one end to 50m at the other. For initial research purposes where one is evaluating monitoring and forecast schemes, the volume of interest can be a bit smaller (especially as regards length).

For the system which is to aid in wake forecasting, the atmospheric characteristics it presents are estimates of future conditions where "future" means a few seconds up to several hundred seconds. Conceptually, the forecast could be rather accurate if an extensive observational system were set up and an associated extensive computational system. The observational setup would have to cover all the air which, for the period of prediction, would move into the target volume. For a strong wind of 20m/sec, a forecast period of 200 seconds, and considering the vertical and horizontal variations of the wind, for one wind direction observations as far as 2000m from the target would be needed, and from heights up to about 500m and cross-wind dimensions of 1 km or so. To cover all wind directions and speeds, obviously a dense three-dimensional network extending out several km in all directions would be required. Even with such a network and an elegant computational scheme, small-scale turbulence could not be forecast in detail.

For simplicity, atmospheric motions are usually divided into two scales of motion: (1) mean motion, explicitly described, and (2) turbulent motion, described only in the form of statistical averages. Actually, the two scales form parts of one continuum. For vortex-wake transport and decay, it is customary to consider that the air's mean motion provides the medium for specifying drift, while the turbulence determines the decay mechanism and speed.

However, the whole motion of the wake evolves in some tens of seconds or a hundred seconds or so, which can be a time down in the turbulent eddy scale rather than the mean scale. To be specific, in unstable conditions the mean vertical wind at 50m over a flat surface may be zero and yet an individual vortex may spend its minute of life in air rising at 2m/sec. Similarly, there may be no crossflow component of vertical shear in the mean, but for the evolution of an individual vortex system the shear may be considerable.

Such considerations force one into some important practical conclusions with respect to forecasting vortex-wake characteristics.

1. Forecasting, to be of practical value, must be for a period of 10 minutes or more -- enough time so total terminal traffic flow can actually be adjusted to the anticipated conditions. Since there is no chance of forecasting individual eddies over such a time interval, the meteorological forecast is limited to providing only mean values -- especially the most important limits of mean flow conditions and turbulence statistics. The forecasting data base must be at least 10 minutes, and experience at the site may show 30 minutes or even 60 minutes to be better.

2. For the monitoring of conditions in the ILS localizer beam near the middle marker, one wants to establish the mean flow, turbulence, and thermal stability throughout the Lagrangian parcel of air in which the observed vortex moves and did move. The prohibition against research aircraft and high towers in this region means direct measurements cannot be made. Indirect probing, say by doppler lidar for velocity and passive IR for temperature, are not deemed practical at the present stage of development. Thus one must do the best one can by extrapolations from surface (or low tower) measurements.

All such considerations seem to force the design of an operational system along the following lines. The suggested system:

a. is directed especially toward the evaluation of wake-vortex transport-decay forecasts,

b. involves some redundancies since the system, applied to the specific site, utilizing the not-entirely-satisfactory theoretical relations of the surface boundary layer, should in itself permit crosschecks,

c. should itself receive some evaluation and calibration by specific pibal releases and measurements from a test aircraft moving along the ILS path, and

d. is more complex than the minimum which might suffice in future years for operational airport uses.

The system consists of a network of tower-mounted meteorological sensors with appropriate data storage and real-time computing and display.

Tower #1 will be 50m high (70m would be even better) and hopefully can be located within 2 km of the test volume where upwind surface conditions are not dissimilar from conditions upwind of the test volume. An existing airport control tower can perhaps be used, especially if a small meteorological tower is superimposed on it, but one must take account of the disturbance of a fat tower on U and $\varphi$ (azimuth) measurements.

At $z$ = 10, 20, 35, and 50m there should be measurements of U, $\varphi$ and T , from which 10 minute averages are derived.

Towers #2, 3, 4, and 5 will each be just 10m high, instrumented only at the top, where U, $\zeta$, and $\sigma$ (elevation angle) will be monitored. The towers should be put at the corners of a square with 500m sides straddling the landing path with the downwind side centered on the middle marker. The measurements will be processed to include 10 minute averages of U, $\zeta$, and $\sigma_\theta$, as well as higher frequency data to be discussed below.

Desirable, but not absolutely essential, measurements would be $\theta$ at z = 20m and z = 5m on Tower #1, and T at z = 2m and 10m on Towers #2-5. A monostatic acoustic sounder giving information on low altitude layering during stable conditions would also be helpful. It would be located someplace within the square of Towers #2-5.

Tower #1 is essential to give meaningful stability information, for which Towers #2-5 are presumed low. It also can give this information aloft (near the 60m height of the glide slope over the middle markers). This stability information tends to characterize conditions over a large area, hence Tower #1 need not be right at the test volume. In strongly stable conditions, vertical shears aloft in speed and direction can also be monitored from Tower #1.

$\Delta$T measurements on all the low towers may be found useful if the relative sensor accuracy is 0.1C and careful averaging over all towers is done. This cannot give accurate $R_i$ or L' measurements, but can at least categorize the more extreme stabilities and instabilities where the neutral-case equations may not suffice.

Tower #2-5 are used first to derive mean $z_o$ characteristics for the area. Then, for operational forecasts, they provide U and $\zeta$ information from which meaningful average U vs $\zeta$ are derived to use as inputs to calculate U vs z, $\epsilon^{1/3}$ vs z, $\sigma_w$ vs z, and vertical turbulence spectra vs z. From the high frequency ends of $\sigma_\theta$ and $\sigma_{\tau_3}$ (evaluated by sigma meter) one also can calculate $\epsilon^{1/3}$ at 10m, and

from the low frequency sigma meter evaluation of $\sigma_\theta$ one derives $\sigma_w$ at 10m. These provide useful redundancy. Upcurrents and downcurrents are estimated from the convergences and divergences measured using the U and $\zeta$ values of Towers #2-5. For the area defined by Towers #2-5, instantaneous components of wind perpendicular to the sides of the square will show the convergence-divergence situation. A similar calculation for the area defined by any three of the towers can give clues as to centering of the up or down current, if such is desired.

The research/evaluation system suggested here is presumably much more complex than an eventual operational system will be. After the "calibration" of the site which the use of this system provides, a final operational system could conceivably be as simple as (a) a single anemometer at 5m or 10m, (b) one measure of a quantity related to heat flux -- a temperature between 2m (or ground) and 10m -- and (c) something to indicate the height of stable layers, such as an automated short-range acoustic sounder. For the critical stable cases some direct observations of stability and wind shear from a tower to at least 50-60m is highly desirable, even if the tower is a few miles from the operational site. The acoustic sounder should at least be able to show the height above which turbulence is low, and thus illuminate critical hazard conditions. Radiation measurements are so poorly coupled to heat flux or stability-instability that they are not recommended.

The system detailed in this section does not give as much detail as one might want for checking the accuracy of monitoring system. Such detail could only come from indirect probing, as with a doppler lidar which is considered not yet fully operational, or from a network of tall towers, which is inappropriate as long as the tests are located at an airport. Even though this system is not perfect for case studies of monitoring devices, the system will likely be found satisfactory for that purpose.

# 7. SUMMARY

The general factors relating aircraft wing geometry to the vorticity shed from the wing are presented. The rollup of the resulting vortex sheet into the classical wake consisting of a pair of contra-rotating trailing vortices is described, and a set of operational equations for principal wake characteristics is presented.

The wake encounter hazard with respect to a following aircraft is discussed. Axial and normal encounter danger factors are developed. These factors relate the aerodynamic response and control characteristics of the following aircraft to the wake characteristics of the generating aircraft. It is recommended that the axial danger factor D be used as a primary criterion for determining hazardous encounter situations.

The general conditions relating to the transport of a vortex pair are reviewed. The effects on the vortex pair dynamics due to vorticity generation and re-distribution are discussed. Vorticity generation is caused by density variation in the fluid. Vorticity re-distribution results from the diffusing vortex cores and the entrainment of mass and the detrainment of vorticity at the boundaries of the recirculation cells surrounding each vortex. In general, this diffusion of the vortex cores results in departure from the classical equations describing the motion of the vortex pair. However it is pointed out that this is a relatively slow process, and usually, before it becomes significant, the vortex pair has experienced one of several decay mechanisms (linking, core bursting).

The effects of (crosswind) wind shear are examined. In this case the geometry of the vortex recirculation cells is drastically altered. The upwind cell increases in size and the downwind cell shrinks. This effect increases with shear, and the probable effects that wind shear might have on banking of the vortex pair and core bursting are discussed.

Previous experimental and theoretical works in the area of wake descent into a stratified atmosphere are discussed. The conclusion is that at the present there seems to be no model that adequately describes the phenomenon of vorticity generation. A new theory for the descent of a wake into a weakly-stratified atmosphere is developed. For the condition of weak stratification (large Brunt Vaisala times) and fast wake descents (time for wake to descend one vortex span) — a situation which normally occurs in practice — the theory concludes that the vortices will draw closer together with a consequent increase in descent speed. Thus the effect of stable stratification alone (without entrainment) is to increase descent speed.

A discussion of the effects of entrainment alone (without buoyancy) is given. It appears that entrainment will definitely retard wake descent, however the magnitude and mechanism of entrainment is controversial.

The general concepts regarding Crow Instability are discussed. A new theory is developed as an extension of the Crow Stability Theory which assumes an atmospheric turbulent input to the growth of the instability. The vortices are treated as a pair of linear oscillators with a random forcing function assumed to be that corresponding to the one-dimensional, transverse energy spectrum within the Komolgorov inertial subrange. The "time-to-linking" is found from the new theory as a function of the vortex parameters, $\Gamma_o$ and $b_o$, and the turbulence dissipation rate, $\epsilon$. This correlates very well with available flight test data.

Core bursting is discussed with respect to global invariants of core development. The nature and precise mechanism of vortex breakdown is still controversial. It is generally agreed that breakdown is always associated with adverse pressure gradients. The conditions for breakdown are related principally to the swirl ratio and the magnitude of the axial flow, both parameters being a function of the developing core flow. The exact nature of the dissipative processes in influencing the develop-

ment of the core is still not known, but plays an important role in the core flow. and hence in the time required for breakdown.

The final section shows how to determine the atmospheric dynamic parameters from general meteorological information, using such concepts as Kolmogorov's hypothesis and Monin-Obukhov Similarity. Operational equations are presented, and a projected design for an operational meteorological data system is given.

# 8. CONCLUSIONS

The general thrust of this report is concerned with the still unsolved problems of vortex descent and decay in a real atmosphere. Considerable theoretical progress has been made in certain aspects of this problem, in that new analytical results have been developed for

1) Time-to-linkage in a turbulent environment.

2) Descent in a stratified flow.

3) Cell shapes in sheared flow.

These theoretical results can only be validated by experiment, and a major recommendation is that the appropriate data be obtained. The analyses developed here and the specific problems identified, will provide the proper basis for sound experiments designed to resolve some of these difficulties.

For the important area of core bursting, the conclusion is that still no definite operational criteria exist and that more experimental and theoretical research is required. It is possible, however, that natural core bursting seldom occurs in the vortex wakes of large aircraft and thus an operational criteria is not a practical necessity. Further flight test, and examination of existing test data is necessary to establish this hypothesis.

The problem of the solitary vortex, and the possibility that this is caused by a sheared crosswind is raised in this report. This appears to be an important operational consideration, more experimental data here is badly needed. It is likely that further analysis, continuing the sheared cell-shape developed in this report, would assist in understanding this phenomenon.

The turbulent entrainment in the descending vortex pair is discussed at length. Here again, experiments are needed, and the report defines appropriate parameters which would be essential in designing the proper tests to unambiguously determine the turbulent mechanisms.

For the wing aerodynamics defining the vortex configuration, the aircraft dynamics defining the hazard, and the meteorology defining the atmospheric dynamics, this report gives specific operational equations which can be used in predictive models. It is believed that in these fields the state of the art is sufficiently well developed that engineering calculations can be made with reasonable confidence.

An assessment of the situation with respect to the prediction of vortex wake descent and decay is as follows:

1) Wing aerodynamics defining vortex configuration, aircraft dynamics defining hazard, and meteorology defining atmospheric dynamics are reasonably well understood.

2) Vortex descent and decay in a stratified flow is still not properly understood.

3) Crow Instab lity is well understood, and equations presented here give a rational approach to predicting time-to-linkage as a function of turbulence.

4) Core-bursting is still very poorly understood and qualitative equations are lacking, however core bursting may not be as important as Crow Instability for vortices from large aircraft.

5) Unsymmetric effects causing vortex tilting and unsymmetric breakdown, resulting in a long-lived sclitary vortex have been observed; and are not understood. These may be very important for hazard prediction.

6) Further analytical research and flight test experimentation is very definitely required to resolve the problems above, both at altitude and in ground effect. This report defines a basis for the rational and effective design of continued research.

## 9. REFERENCES


AeroVironment Staff, 1972: Air Quality Analysis and Impact Study Routes 85 and 87 in the San Jose Area, AeroVironment Inc., Tech. Report AV FR 232, prepared for State of California Division of Highways.

Andrews, W. H. , G. H. Robinson, and R. R. Larson, 1972: Exploratory Flight Investigation of Aircraft Response to the Wing Vortex Wake Generated by Jet Transport Aircraft, NASA TN D-6655.

Ball, F. K., 1961: Viscous Dissipation in the Atmosphere. J. Meterol., 18, 553.

Batchelor, G. K., "Axial Flow in Trailing Line Vortices", J. Fluid Mech., Vol. 20, Part 4, pp. 645-658, 1964.

Betz, A., 1933: Behavior of Vortex Systems, NACA Tech. Report No. 713.

Bilanan, A. J., and S. E. Widnall, 1973: Aircraft Wake Dissipation by Sinusoidal Instability and Vortex Breakdown. AIAA Paper 73-107.

Birkhead, J. L., J. Shwartz, and M. P. Tulin, 1969: Penetration of a Density Discontinuity by a Turbulent Vortex-Pair, Hydronautics, Inc., Tech. Report 231.

Bisgood, P. L., R. L. Maltby, and F. W. Dee, 1971: Some work at the RAE on the Behaviour of Vortex Wakes. In Aircraft Wake Turbulence and its Detection (Ed. J. H. Olsen, et al.), Plenum Press, 171-206.

Burnham, D. C., 1972: Effect of Ground Wind Shear on Aircraft Trailing Vortices. AIAA J., 10, 1114-1115.

Chevalier, H., 1973: Flight Test Studies of the Formation and Dissipation of Trailing Vortices. J. Aircraft, 10, 14-18.

Chigier, N. A., and V. R. Corsiglia, 1972: Wind-Tunnel Studies of Wing Wake Turbulence. AIAA Paper 72-41.

Condit, P. M., and P. W. Tracy, 1971: Results of the Boeing Company Wake Turbulence Test Program. In Aircraft Wake Turbulence and its Detection (Ed. J. H. Olsen, et al.), Plenum Press, 473-508.

Costen, R. C., 1972: Drift of Buoyant Wing-tip Vortices. J. Aircraft, 9, 406-412.

Crow, S. C., 1970: Stability Theory for a Pair of Trailing Vortices: AIAA J., 8, 2172-2179.

Crow, S. C., 1971: Panel Discussion. In Aircraft Wake Turbulence and its Detection (Ed. J. H. Olsen, et al.), Plenum Press, 577-583.

Crow, S. C., and J. H. Olsen, 1969: The Duration of Trailing Vortices, 747 and 707, BSL Tech. Comm., 008.

Darwin, C., 1953: Note on Hydrodynamics. Proc. Camb. Phil. Soc., 49, 342.

DeMarrais, G. A., 1959: Wind Speed Profiles at Brookhaven National Laboratory. J. Meteorol., 16.

FAA Task Force, 1971: Vortex Wake Turbulence Flight Tests Conducted During 1970. FAA Report No. FAA-FS-71-1.

Fiedler, F., and H. A. Panofsky, 1972: The Geostrophic Drag Coeffieient and the "Effective" Roughness Length. Quart. J. Roy. Meteorol. Soc., 98, 213-220.

Frenzen, P., 1965: Determination of Turbulence Dissipation by Eulerian Variance Analysis. Quart. J. Roy. Meteor. Soc., 91, 28-34.

Frenzen, P., 1973: The Observed Relation Between the Kolmogorov and von Karman Constants in the Surface Layer. Boundary Layer Meteorology, 4, to be published.

Golder, D., 1972: Relations Among Stability Parameters in the Surface Layer. Boundary Layer Meteorology, 3, 47-58.

Gifford, F. A., Jr., 1968: An Outline of Theories of Diffusion in the Lower Layers of the Atmosphere. In Meteorology and Atomic Energy (Ed. D. H. Slade), USAEC, Division of Technical Information, Document No. TID-24190, Oak Ridge, Tennessee.

Gradshteyn, I. S., and I. M. Ryzhik, 1965: Tables of Integrals, Series, and Products, Academic Press, New York.

Hanna, S. R., 1969: The Thickness of the Planetary Boundary Layer. Atmospheric Environment, 3, 519-536.

Hanna, S. R., B. A. Hutchison, and F. A. Gifford, Jr., 1969: Spread of Small Plumes, U. S. Dept. of Commerce, ESSA, Tech. Memorandum ERLTM-ARL 15.

Harvey, J. K., and F. J. Perry, 1971: Flowfield Produced by Trailing Vortices in the Vicinity of the Ground. AIAA J., 9, 1659-1660.

Houbolt, J. C., 1971: Aircraft Response to Turbulence Including Wakes. In Aircraft Wake Turbulence and its Detection (Ed. J. H. Olsen, et al.), Plenum Press, 509-522.

Kuhn, G. D., and J. N. Nielsen, 1972: Analytical Studies of Aircraft Trailing Vortices. AIAA Paper 72-42.

Laikhtman, D. L., 1961: Physics of the Boundary Layer of the Atmosphere. Translated by the Israel Program for Scientific Translations, Jerusalem, 1964. Available from the Office of Technical Services, U. S. Dept. of Commerce, Washington, D. C., 200 pp.

Lamb, H., 1932: Hydrodynamics, Sixth Ed., Cambridge University Press.

Landahl, M. T., and S. E. Widnall, 1971: Vortex Control. In Aircraft Wake Turbulence and its Detection (Ed. J. H. Olsen, et al.), Plenum Press, 137-155.

Lighthill, M. J., 1965: Group Velocity. J. Inst. Maths. Applics., 1,1.

Lissaman, P. B. S., 1973: Analysis of High Aspect Ratio Jet Flap Wings of Arbitrary Geometry. NASA CR-2179.

Lumley, J. L., and H. A. Panofsky, 1964: The Structure of Atmospheric Turbulence, Interscience Publishers, John Wiley and Sons, New York.

MacCready, P. B., 1962: The Inertial Subrange of Atmospheric Turbulence. J. Geophysical Research, 67, 1051-1059.

MacCready, P. B., 1966: Operational Application of a Universal Turbulence Measuring System. AIAA Paper 66-364.

MacCready, P. B., and H. R. Jex, 1964: Turbulent Energy Measurements by Vanes. Quart. J. Roy. Meteor. Soc., 90, 198-203.

Mager, A., 1972: Dissipation and Breakdown of a Wing Tip Vortex. J. Fluid Mech., 55, 609-628.

Maxworthy, T., 1972: The Structure and Stability of Vortex Rings. J. Fluid Mech., 51, 15-32.

McVehil, G. E., Jr., 1962: Wind Distribution in the Diabatic Boundary Layer. Ph. D. thesis. Dept. of Meteor., Pennsylvania State University.

Monin, A. S., 1962: Empirical Data on Turbulence in the Surface Layer of the Atmosphere. J. Geophysical Research, 67, 3103.

Mowbray, D. E., and B. S. H. Rarity, 1967: A Theoretical and Experimental Investigation of the Phase Configuration of Internal Waves of Small Amplitude in a Density Stratified Liquid. J. Fluid Mech., 28.

Munk, M. M., 1924: Isoperimetrische Aufgaben aus der Theorie des Fluges. Translated as NACA TR 191.

Owen, P. R., 1970: The Decay of a Turbulent Trailing Vortex. Aero. Quarterly, 19, 69-78.

Panofsky, H. A., 1968: A Survey of Current Thought on Wind Properties Relevant for Diffusion in the Lowest 100 m. Symp. on the Theory and Measurement of Atmos. Turb. and Diffusion in the Planetary Boundary Layer (SC-M-191-May 1968).

Panofsky, H. A., 1970: The Structure of Atmospheric Shear Flows. Aerodynamics of Atmospheric Shear Flows. AD 702 659.

Panofsky, H. A., and R. A. McCormick, 1960: The Spectrum of Vertical Velocity Near the Surface. Quart. J. Roy. Meteorol. Soc., 86, 495.

Panofsky, H. A., A. K. Blackadar, and G. E. McVehil, 1960: The Diabatic Wind Profile. Quart. J. Roy. Meteorol. Soc., 86, 390.

Pasquill, F., 1962: Atmospheric Diffusion, D. Van Nostrand, New York.

Pasquill, F., 1972: Some Aspects of Boundary Layer Description. Quart. J. Roy. Meteorol. Soc., 98, 469-494.

Richards, J. M., 1963: Experiments on the Motions of Isolated Cylindrical Thermals Through Unstratified Surroundings. Int. J. Air. Wat. Poll., 7, 17-34.

Rose, R., and F. W. Dee, 1965: Aircraft Vortex Wakes and Their Effects on Aircraft. ARC CP No. 795.

Saffman, P. G., 1972: The Motion of a Vortex Pair in a Stratified Atmosphere. Studies in Applied Mathematics, 51, 107-119.

Scorer, R. S., and L. J. Davenport, 1970: Contrails and Aircraft Downwash. J. Fluid Mech., 43, 451-464.

Slade, D. H., 1965: Dispersion Estimates from Pollutant Releases of a Few Seconds to Eight Hours in Duration. Tech. Note 2-ARL-1, Air Resources Lab., ESSA, U. S. Dept. of Commerce, Wash., D. C.

Slade, D. H., Editor, 1968: Meteorology and Atomic Energy (see Gifford, F. A., Jr., 1968 reference).

Smith, T. B., and K. M. Beesmer, 1959: Contrail Studies for Jet Aircraft. Meteorology Research, Inc., Final Report to USAF Cambridge Research Center, No. AFCRC-TR-59-251. AD 217 188.

Smith, T. B., and P. B. MacCready, Jr., 1963: Aircraft Wakes and Diffusion Enhancement. Meteorology Research, Inc., Final Report, Part B., to Dugway Proving Ground, Cont. DA-42-007-CML-545.

Smith, T. B., and M. A. Wolf, 1963: Vertical Diffusion from an Elevated Line Source Over a Variety of Terrains. Meteorology Research, Inc., Report, Part A, to Dugway Proving Ground, Cont. DA-42-007-CML-545. AD 418 599.

Spreiter, J. R., and A. H. Sacks, 1951: The Rolling Up of the Trailing Vortex Sheet and Its Effect on the Downwash Behind Wings. J. Aero. Sci. 18, 21-72.

Squire, H. B., 1954: The Growth of a Vortex in Turbulent Flow. Aero. Res. Council, Imperial College, London. No. 16,666, 1-5.

Tennekes H., and J. L. Lumley, 1972: A First Course in Turbulence, MIT Press, Cambridge, Mass.

Thwaites, B., 1960: Incompressible Aerodynamics, Oxford University Press.

Tombach, I. H., 1971: Transport of a Vortex Wake in a Stably Stratified Atmosphere. In Aircraft Wake Turbulence and Its Detection (Ed. J. H. Olsen, et al.), Plenum Press, 41-56.

Tombach, I. H., 1972: Transport and Stability of a Vortex Wake. Meteorology Research, Inc., Final Report to AFOSR, Cont. F44620-70-0032.

Tombach, I. H., 1973: Observations of Atmospheric Effects on the Transport and Decay of Trailing Vortex Wakes. AIAA Paper 73-110.

Tsang, G., 1971: Laboratory Study of Line Thermals. Atmospheric Environment, 5, 445-471.

Tulin, M. P., and J. Shwartz, 1971: The Motion of Turbulent Vortex - Pairs in Homogeneous and Density Stratified Media. Hydronautics, Inc., Tech. Report 231-15. AD 723 184.

Turner, J. S., 1960: A Comparison between Buoyant Vortex Rings and Vortex Pairs. J. Fluid Mech., 7, 419-432.

U. S. AEC, Safety Guide 23, 1972: Onsite Meteorological Program, USAEC Div. of Reactor Licensing, Wash., D. C., 13 pp.

Woodward, B., 1959: The Motion in and Around Isolated Thermals. Quart. J. Roy. Meteor. Soc., 85, 144-151.

Yih, C. S., 1969: Stratified Flows. Annual Review of Fluid Mechanics, 1, Annual Reviews, Palo Alto.

Zwieback, E. L., 1964: Trailing Vortices of Jet Transport Aircraft During Takeoff and Landing. Douglas Aircraft Company, prepared for FAA, Cont. No. FA-WA-4106.

## 10. BIBLIOGRAPHY

### 1. Vortex Generation, Motion and Decay


Acharya, Y. V. G., and Krishnamurthy, K., "Investigations on Vortex Flows", National Aeronautical Laboratory (India), TN AS-28-65, September 1965.

Barcilon, A. I., "Vortex Decay Above a Stationary Boundary", J. Fluid Mech., Vol. 27, Part 1, pp. 155-175, 1967.

Batchelor, G. K., "Axial Flow in Trailing Line Vortices", J. Fluid Mech., Vol. 20, Part 4, pp. 645-658, 1964.

Betz, A., "Behavior of Vortex Systems", NACA TM 713, June 1932.

Birkhead, J. L., J. Shwartz, and M. P. Tulin, 1969: Penetration of a Density Discontinuity by a Turbulent Vortex-Pair, Hydronautics, Inc., Tech. Report 231-21.

Burnham, D. C., 1972: Effect of Ground Wind Shear on Aircraft Trailing Vortices. AIAA J., 10, 1114-1115.

Burnham, D., J. Hallock, R. Kodis, and T. Sullivan: Vortex Sensing Tests at NAFEC. Dept. of Transportation Tech. Report No. DOT-TSC-FAA-72-2, 1972.

Chervinsky, A., "Similarity of Turbulent Axisymmetrical Swirling Jets", AIAA Journal, Vol. 6, No. 5, pp. 912-914, May 1968.

Chigier, N. A., and Chervinsky, A., "Experimental Investigation of Swirling Vortex Motion in Jets", J. Applied Mech., June 1967.

Chigier, N. A., and V. R. Corsiglia, 1972: Wind-Tunnel Studies of Wing Wake Turbulence. AIAA Paper 72-41.

Costen, R. C., 1972: Drift of Buoyant Wing-tip Vortices. J. Aircraft, 9, 406-412.

Crow, S. C., and J. H. Olsen, 1969: The Duration of Trailing Vortices, 747 and 707, BSL Tech. Comm., 008.

de Moufville, Albert, "The Dying Vortex", Proc. Fifth Mid-Western Conference on Fluid Mechanics, 1957, University of Michigan Press, Ann Arbor, 1957.

Dergarabedian, Paul, and Fendell, Francis, "Parameters Governing the Generation of Free Vortices", The Physics of Fluids, Vol 10, No. 11, November 1967.

Donaldson, C. duP., "Decay of an Isolated Turbulent Vortex", presented at Boeing/AFOSR Aircraft Wake Turbulence Symposium, Seattle, Washington, September 1970.

_____, and Sullivan, Roger D., "Decay of an Isolated Vortex", A. R. A. P. Tech. Memo 70-6, presented at Boeing/AFOSR Aircraft Wake Turbulence Symposium, Seattle, Washington, September 1970.

Earnshaw, P. B., "An Increment in Total Head in the Neighborhood of a Leading-Edge Vortex", Royal Aircraft Establishment TR No. 66218, July 1966.

Fage, A., and Simmons, L. F. G., "An Investigation of the Airflow Pattern in the Wake of an Aerofoil of Finite Span", Philosophical Transactions of the Royal Society of London, Vol. 225, No. A632, pp. 303-330, 1925.

Fragoyannis, George B., "A Contribution to the Theory of Jet-Wakes and Vortices in Free and Confined Surroundings", USAAVLABS Technical Report 66-69, November 1966.

Gibbons, J. E., and Mollo-Christensen, E., "Behavior of a Trailing Vortex in a Favorable Pressure Gradient", AIAA Journal, Vol. 1, No. 3, pp. 705-706, March 1963.

Gortler, H., "Decay of Swirl in an Axially Symmetrical Jet", Publicado en la Revista Mathematica Hispano Americana, 4a Serie Tomo XIV Nums 4y5.

Granger, Robert, "Steady Three-Dimensional Vortex Flow", J. Fluid Mech., Vol. 25, Part 3, pp. 557-576, 1966.

Grow, Terence L., "The Effect of Wing Geometry and Lower Surface Boundary Layer on the Rolled-up Tip Vortex", M. S. Thesis, Dept. of Aerospace Engr., The Penna. State University, June, 1967.

Hall M. G., "A Numerical Method for Solving the Equations for a Vortex Core", Aeron. Res. Center R&M, No. 3467, May 1965.

Hilton, W. F., "Longitudinal Flow in a Trailing Vortex", Aeron. Res. Comm. R&M No. 1858, August 1938.

Hoffman, E. R., and Joubert, P. N., "Turbulent Line Vortices", J. Fluid Mech., Vol 16, Part 3, pp. 395-411, July 1963.

Jordan, P. F., "Span Loading and Formation of Wake", presented at Boeing/AFOSR Aircraft Wake Symposium, Seattle, Washington, September 1970.

Kiang, R. L., "Sub-Scale Modeling of Aircraft Trailing Vortices", presented at Boeing/AFOSR Aircraft Wake Turbulence Symposium, Seattle, Washington, September 1970.

Kinney, R. B., "Universal Velocity Similarity in Fully Turbulent Rotating Flows", J. Applied Mech., June 1967.

Kuchemann, D., "Report on the I. U. T. A. M. Symposium on Concentrated Vortex Motions in Fluids", J. Fluid Mech., Vol. 21, Part 1, pp. 1-20, 1965

Kuhn, G. D., and J. N. Nielsen, 1972: Analytical Studies of Aircraft Trailing Vortices. AIAA Paper 72-42.

Lee, Shao-Lin, "Axisymmetrical Turbulent Swirling Jet", J. Appl. Mech., Paper No. 64-WA/APM-39, 1964.

Lusby, William A., "A Study of the D. ay of a Trailing Vortex", M. S. Thesis, Dept. of Aerospac. Engr., The Penna. State University, June 1963.

MacCready, Paul B., Jr., "An Assessment of Dominant Mechanisms in Vortex-Wake Decay", presented at Boeing/AFOSR Aircraft Wake Turbulence Symposium, Seattle, Washington, 1970.

McCormick, B. W., Tangler, J. L., and Sherrieb, H. E., "On the Structure of Trailing Vortices", AIAA J. of Aircraft, Vol. 5, No. 3, May-June 1968.

_____, "On Cavitation Produced by a Vortex Trailing from a Lifting Surface", ASME J. of Basic Engr., pp. 369-379, September 1962.

_____, "A Study of the Minimum Pressure in a Trailing Vortex System", Ph. D. Thesis, Dept. of Aerospace Engr., The Penna. State University, June 1954.

Madden, S. J., Jr., and R. B. Harlan: A Program to Analyze and Model Trailing Vortices on Airports. Measurement Systems Laboratory Final Report Prepared for U. S. Dept. of Transp., Report No. RN-69, 1971.

McMahon, T. A., and Widnall, S. E., "Vortex Wake Rollup and Vorticity Concentration Behind an Airfoil", MIT, ASRL TR 143-1, June 1967.

_____, "Review of the Vortex Wake Rollup Problem", MIT ASRL TR 145-1, June 1967.

Newman, B. G., "Flow in a Viscous Trailing Vortex", Aeronautical Quarterly, Vol. X, May 1959.

Nielsen, J. N., and Schwind, R. G., "Decay of a Vortex Pair Behind an Aircraft", presented at Boeing/AFOSR Aircraft Wake Turbulence Symposium, Seattle, Washington, September 1970.

Owen, P. R., "The Decay of a Turbulent Trailing Vortex", The Aero. Quarterly, Vol. XXI, February 1970.

_____, "The Decay of a Turbulent Trailing Vortex", Aero Res. Counc. 25818, 1964.

Parks, P. C., "A New Look at the Dynamics of Vortices with Finite Cores", presented at Boeing/AFOSR Aircraft Wake Turbulence Symposium, Seattle, Washington, September 1970.

Piercy, N. A. V., "On the Vortex Pair Quickly Formed by Some Aerofoils", The J. of the Roy. Aeron. Soc., Vol 27, pp. 488-500, 1923.

Piziali, R., and Trenka, A., "An Experimental Study of Blade Tip Vortices", Technical Report, Cornell Aeronautical Lab., No. AC-2647-S-1, January 1970.

Ragsdale, R. G., "Applicability of Mixing Length Theory to a Turbulent Vortex System", NASA TN D-1051, August 1961.

Rouse, H., and Hsu, H. C., "On the Growth and Decay of a Vortex Filament", Proc. First Natl. Congress of Appl. Mech., 1951.

Saffman, P. G., "The Velocity of Viscous Vortex Rings", presented at Boeing/AFOSR Aircraft Wake Turbulence Symposium, Seattle, Washington, September 1970.

Saffman, P. G., 1972: The Motion of A Vortex Pair in a Stratified Atmosphere. Studies in Applied Mathematics, 51, 107-119.

Spreiter, J. R., and A. H. Sacks, 1951: The Rolling Up of the Trailing Vortex Sheet and its Effect on the Downwash Behind Wings. J. Aero. Sci. 21-72.

Squire, H. B., "The Growth of a Vortex in Turbulent Flow", 16, 666. Aeronautical Research Council, 1954.

Timm, G. K., "Survey of Experimental Velocity Distributions in Vortex Flows with Bibliography", Boeing Scientific Research Labs., Flight Sciences Lab. Rept. No. 126, November 1967.

Ting, L., "Studies in the Motion and Decay of Vortices", presented at Boeing/AFOSR Aircraft Wake Turbulence Symposium, Seattle, Washington, September 1970.

Titcher, I. M., and Taylor, A. J., "Experiments on the Growth of Vortices in Turbulent Flow", Aeron. Res. Counc. Report No. FM2379, March 1956.

Tombach, I. H., "Transport of a Vortex Wake in a Stably Stratified Atmosphere", presented at Boeing/AFOSR Aircraft Wake Turbulence Symposium, Seattle, Washington, September 1970.

Tombach, I. H., 1972: Transport and Stability of a Vortex Wake. Meteorology Research, Inc., Final Report to AFOSR, Cont. F44620-70-C-0032.

Tulin, M. P., and J. Shwartz, 1971: The Motion of Turbulent Vortex-Pairs in Homogeneous and Density Stratified Media. Hydronautics, Inc., Tech. Report 231-15. AD 723 184.

Turner, J. S., 1960: A Comparison Between Buoyant Vortex Rings and Vortex Pairs. J. Fluid Mech., 7, 419-432.

Wilson, D. J., M. R. Brashears, E. A. Carter, and K. R. Shrider: Wake Vortex Avoidance System. Lockheed Missiles and Space Company, Inc. Report Prepared for Dept. of Transp., Report No. FAA-RD-72-108.

Zwiebach, E. L., "Trailing Vortices of Jet Transport Aircraft During Takeoff and Landing", Douglas Aircraft Company, 1964, prepared for FAA contract No FA-WA-4306.

## 2. Vortex Control


Baronti, P. O., and Elzweig, S., "Fog Formation and its Dispersal by Trailing Vortices", presented at Boeing/AFOSR Symposium on Aircraft Wake Turbulence, Seattle, Washington, September 1970.

Corsiglia, V. R., Jacobsen, R. A., and Chigier, N., "An Experimental Investigation of Trailing Vortices Behind a Wing with a Vortex Dissipator", presented at Boeing/AFOSR Symposium on Aircraft Wake Turbulence, Seattle, Washington, September 1970.

Corsiglia, V. R., Jacobsen, R. A., and Chigier, N. A., "An Experimental Investigation of Wing Trailing Vortices with Dissipation", presented at Boeing/AFOSR Symposium on Aircraft Wake Turbulence, Seattle, Washington, September 1970.

Landahl, M. T., and Widnall, S. E., "Vortex Control", presented at Boeing/AFOSR Symposium on Aircraft Wake Turbulence, Seattle, Washington, September 1970.

Ludwieg, H., "Zur Erklärang der Instabilität der uber angestellten Deltaflügeln auftretenden freion Wirkbelkerne", Z. Flugw., 10, [illegible]2, 1962.

Menkes, J., and Abernathy, F. H., "An Estimate of the Power Required to Eliminate Trailing Vortices by Suction", presented at Boeing/AFOSR Symposiumon Aircraft Wake Turbulence, Seattle, Washington, September 1970.

McCormick, B. W., and Padakannaya, R., "The Effect of a Drooped Wing Tip on its Trailing Vortex System", presented at Boeing/AFOSR Symposium on Aircraft Wake Turbulence, Seattle, Washington, September 1970.

Rinehart, Stephen A., "Study of Modification of Rotor Tip Vortex by Aerodynamic Means", Rochester Applied Science Associates, Inc., Report 70-02, January 1970.

Spencer, R. H., Sternfeld, H., Jr., and McCormick, B. W., "Tip Vortex Core Thickening for Application to Helicopter Rotor Noise Reduction", USAAVLABS Technical Report 66-1, September 1966.

## 3. Stability of Vortex Pairs or Filaments


Bilanin, A. J., Widnall, S. E., Aircraft Wake Dissipation by Sinusoidal Instability and Vortex Breakdown. AIAA Paper 73-107. Jan. 1973.

Crow, Steven C., "Stability Theory for a Pair of Trailing Vortices", AIAA Paper No. 70-53, New York, January 1970.

Dee, F. W., and Nicholas, O. P., "Flight Measurements of Wing-Tip Vortex Motion Near the Ground", Aero. Res. Counc. Current Paper 1065. 1969.

Jensen, R., "A Theoretical and Experimental Study of Wake Instabilities," M. S. Thesis, Masschusetts Institute of Technology, Dept. of Aeronautics and Astronautics, to be Submitted, 1972.

MaxWorthy, T., The Structure and Stability of Vortex Rings. J. Fluid Mech., 51, 15-32, 1972.

Olsen, J. H., "Towing Tank Observations of Wake Instabilities", presented at Boeing/AFOSR Symposium on Aircraft Wake Turbulence, Seattle, Washington, September 1970.

Widnall, S. E., Bliss, D., and Zalay, A., "A Theoretical and Experimental Study of the Stability of a Vortex Pair", presented at Boeing/AFOSR Symposium on Aircraft Wake Turbulence, Seattle, Washington, September 1970.

## 4. Vortex Breakdown


Benjamin, T. Brooke, "Theory of the Vortex Breakdown Phenomenon", J. Fluid Mech., Vol. 14, pp. 543-629, 1962.

Bossel, H., "Inviscid and Viscous Models of the Vortex Breakdown Phenomenon", Ph.D. Dissertation, Univ. of Calif., Berkeley-Aeronautical Sciences Division, August, 1967.

Bossel, Hartmut, H., "Vortex Breakdown Flowfield", The Physics of Fluids, Vol. 12, No. 3, March 1969.

Cassidy, John J., and Falvey, Henry T., "Observations of Unsteady Flow Arising after Vortex Breakdown", J. Fluid Mech., Vol. 41, Part 4, pp. 727-736, 1970.

Ellle, B. J., "On the Breakdown at High Incidences of the Leading-Edge Vortices on Delta Wings", J. Roy. Aero. Soc., 64, 596.

Hall, M. G., "The Structure of Concentrated Vortex Cores", in Progress in the Aeronautical Sciences, Vol. Vii, D. Kucheman, Pergamon Press, 1966.

Harvey, J. K., "Some Observations of the Vortex Breakdown Phenomenon", Part II. Aero. Dept., Imperial College, Rep. no. 103. 1960.

Jones, J. P., "The Breakdown of Vortices in Separated Flow", Dept. Aero. Astro., Univ. of Southampton, Re. no. 140. 1960.

Lambourne, N. C., and Bryer, D. W., "The Bursting of Leading-Edge Vortices—Some Observations and Discussion of the Phenomenon", Ministry of Aviation, Aeronautical Research Council R. &M. No. 3282, 1961.

Landahl, M.T., "Wave Mechanics of Breakdown", to appear inthe Journal of Fluid Mechanics.

Leibovich, S., "Wave Motion and Vortex Breaddown", Cornell University, AIAA Paper No. 69-645, 1969.

Ludwieg, H., "Contribution to the Explanation of the Instability of Vortex Cores Above Lifting Delta Wings", Aero. Versuchsanstalt, Gottingen, Rep. AVA/61 a 01. 1961.

Mager, A., Dissipation and Breakdown of a Wing Tip Vortex. J. Fluid Mech., 55, 609-628, 1972.

Sarpkaya, T., "On Stationary and Traveling Vortex Breakdown", J. F. M., Vol. 45, Part 3, 15 February 1971.

Scorer, R. S., and Davenport, L. J., "Contrails and Aircraft Downwash", J. Fluid Mech., Vol. 43, Part 3, pp. 451-464, 1970.

Squire, H. B., "Analysis of the Vortex Breakdown Phenonemon", Part I. Aero. Dept., Imperial College, Rep. no. 102. 1960.

Wentz, William H., Jr., and Kohlman, David L., "Wind Tunnel Investigations of Vortex Breakdown on Slender Sharp-Edged Wings", Univ. of Kansas Center for Research, Inc., Engr. Sciences Div., Report FRL-68-013, November 1968.

## 5. Flight Measurements, Including Detection and Visualization


Andrews, W. H., Flight Evaluation of the Wing Vortex Wake Generated by Large Jet Transports", Boeing/AFOSR Symposium on Aircraft Wake Turbulence, Seattle, Washington, September 1970.

Andrews, W. H., G. H. Robinson, and R. R. Larson, Exploratory Flight Investigation of Aircraft Response to the Wing Vortex Wake Generated by Jet Transport Aircraft, Report No. NASA TN D-6655, 1972.

Bisgood, P. L., Maltby, R. L., and Dee, F. W., "Some Work on the Behavior of Vortex Wakes at the Royal Aircraft Establishment", presented at Boeing/AFOSR Symposium on Aircraft Wake Turbulence, Seattle, Washington, September 1970.

Caiger, B., and Gould, D. G., "An Analysis of Flight Measurements in the Wake of a Jet Transport Aircraft", presented at Boeing/AFOSR Symposium on Aircraft Wake Turbulence, Seattle, Washington, September 1970.

Chevalier, H., Flight Test Studies of the Formation and Dissipation of Trailing Vortices. J. Aircraft, 10, 14-18, 1973.

Child, R., "Recent Experiments on Wave Vortex Behavior of a Hovering Helicopter Rotor", presented at Boeing/AFOSR Symposium on Aircraft Wake Turbulence, Seattle, Washington, September 1970.

Dunham, R. E., Jr., "Photographs of Vortex Motion", presented at Boeing/AFOSR Symposium on Aircraft Wake Turbulence, Seattle, Washington, September 1970.

Easterbrook, C. C., and Joss, W. W., "The Utility of Doppler Radar in the Study of Aircraft Wing Tip Vortices", presented at Boeing/AFOSR Symposium on Aircraft Wake Turbulence, Seattle, Washington, September 1970.

FAA Task Force, Vortex Wake Turbulence Flight Tests Conducted During 1970. FAA Report No. FAA-FS-71-1, 1971.

Garodz, L., "Measurements of Boeing 747, Lockheed C5A and Other Aircraft Vortex Wake Characteristics by Tower Fly-By Technique", presented at Boeing/AFOSR Symposium on Aircraft Wake Turbulence, Seattle, Washington. September 1970.

Goodman, T., "Visualization of Wing Tip Vortices", presented at Boeing/AFOSR Symposium on Aircraft Wake Turbulence, Seattle, Washington, September 1970.

Hale, R. W., "A New Approach for Visualizing Complex Airfoil Airflows", presented at Boeing/AFOSR Symposium on Aircraft Wake Turbulence, Seattle, Washington, 1970.

Huffaker, R. M., Jelalian, A., Keene, W., Sonneschein, C., and Thomson, J.A.L., "Application of Laser Doppler Systems to Vortex Measurement and Detection", presented at Boeing/AFOSR Symposium on Aircraft Wake Turbulence, Seattle, Washington, September 1970.

Kerr, T. H. and Dee, F. W., "A Flight Investigation into the Persistence of Trailing Vortices Behind Large Aircraft", Aero Res. Counc. Current Paper, 489. 1960.

Kraft, Christopher, C., Jr. "Flight Measurements of the Velocity Distribution and Persistence of the Trailing Vortices of an Airplane", NACA Tech. Note 3377, March 1955.

May, Donald, Monroe, "The Development of a Vortex Meter", M. S. Thesis, Dept. of Aerospace Engr., The Penna. State University, June 1964.

Olin, J. G., and Kiland, R. B., "Split-Film Anemometer Sensors for Three-Dimensional Velocity-Vector Measurements", presented at Boeing/AFOSR Symposium on Aircraft Wake Turbulence, Seattle, Washington, September 1970.

Smith, T. B., and K. M. Beesmer, Contrail Studies for Jet Aircraft. Meteorology Research, Inc., Final Report to USAF Cambridge Research Center, No. AF 19 (604) - 2038. AD 217 188, 1959.

Smith, T. B., and P. B. MacCready, Jr., Aircraft Wakes and Diffusion Enhancement. Meteorology Research, Inc., Final Report, Part B, to Dugway Proving Ground, Cont. DA-42-007-CML-545, 1963.

Tombach, I. H., Observations of Atmospheric Effects on the Transport and Decay of Trailing Vortex Wakes. AIAA Paper 73-110, 1973.

## 6. Interaction with Aircraft


Andrews, W. H., "Flight Evaluation of the Wing Vortex Wake Generated by Large Jet Transports", presented at Boeing/AFOSR Symposium on Aircraft Wake Turbulence, Seattle, Washington, September 1970.

(Anonymous), "Pilot Alert: Wake Turbulence", The AOPA Pilot, pp. 52-55, November 1970.

Attwooll, V. W., "The Effects of Trailing Vortices on the Safe Capacity of Air Routes and Airports", RAE Technical Memorandum No. 6702/2, June 1967.

Bennett, W. J., "State of the Art Survey for Minimum Approach, Landing, and Takeoff Intervals as Dictated by Wakes, Vortices, and Weather Phenomena", The Boeing Company, Report No. RD-6-4, January 1964.

Bleviss, Z. O., "Theoretical Analysis of Light Plane Landing and Takeoff Accidents Due to Encountering the Wake of Large Aircraft", Report No. SM-18647, Douglas Company, 1954.

Condit, P. M., and Tracy, P. W., "Results of the Boeing Company Wake Turbulence Test Program", presented at Boeing/AFOSR Symposium on Aircraft Wake Turbulence, Seattle, Washington, September 1970.

Conner, A. B., and O'Bryan, T. C., "A Brief Evaluation of a Helicopter Wake as a Potential Operational Hazard to Aircraft", NASA TN D-1227, March 1962.

Crow, S. C., Panel Discussion. In Aircraft Wake Turbulence and its Detection (Ed. J. H. Olsen, et al.), Plenum Press, 577-583, 1971.

Downie, Don, "The Horizontal Tornado", The AOPA Pilot, pp. 48-51, November 1970.

Hackett, J. E., and Theisen, J. G., "Vortex Wake Development and Aircraft Dynamics", presented at Boeing AFOSR Symposium on Aircraft Wake Turbulence, Seattle, Washington, September 1970.

Houbolt, J. C., "Aircraft Response to Turbulence Including Wakes", presented at Boeing/AFOSR Symposium on Aircraft Wake Turbulence, Seattle, Washington, September 1970.

Johannes, R. P., "Aircraft Wake Turbulence Controllability Experiment", presented at Boeing/AFOSR Symposium on Aircraft Wake Turbulence, Seattle, Washington, September 1970.

Jones, W. P., and Rao, B. M. , "Airloads and Moments on an Aircraft Flying Over a Pair of Inclined Trailing Vortices", presented at Boeing/AFOSR Symposium on Aircraft Wake Turbulence, Seattle, Washington, September 1970.

Jones, W. P., and Rao, B. M., "Wing-Vortex Interaction", Texas A. & M. University, Texas Engineering Experiment Station, January 1970.

McGowan, William A., "Trailing Vortex Hazard", Society of Automotive Engineers, Business Aircraft Meeting, Wichita, Kansas, April 1968 (No. 680220).

McGowan, William A., "Calculated Normal Load Factors on Light Airplanes Traversing the Trailing Vortices of Heavy Transport Airplanes", NASA TN D-829, May 1961.

Reeder, John P., Zalovcik, John A., and Dunham, R. Earl, Jr., "Vortex Wakes and Their Influence on Aircraft Terminal Area Separation Requirements", NASA Report to Dept. of Transportation Advisory Committee on Air Traffic Control, Group I, January 1969.

Rose, R., and Dee, F. W., "Aircraft Vortex Wakes and Their Effects on Aircraft", Aero. Res. Counc. Current Paper 795. 1965.

Rudhman, Wylie E., "A Numerical Solution of the Unsteady Airfoil with Application to the Vortex Interaction Problem", M. S. Thesis, Dept. of Aerospace Engr., The Penna. State University, December 1970.

Sforza, Pasquale M., "Aircraft Vortices: Benign or Baleful?" Space/Aeronautics, April 1970.

Surendraiah, Makam, "An Experiment al Study of Rotor Blade-Vortex Interaction, M. S. Thesis, Dept. of Aerospace Engr., The Penna. State University, December 1969.

Thelander, J. A., "Separation Minimums for Aircraft Considering Disturbances Caused by Wake Turbulence", McDonnell Douglas Aircraft Company, Report prepared for DOT Air Traffic Control Advisory Committee, Group I - Team D ( Wake Turbulence), January 15, 1969.

Werle, H., "Sur l'eclatement des tourbillons d'apex d'une aile delta aux faibles vitesse". Res. Aero., Paris, no. 74, 23.

Wetmore, Joseph W., "Aircraft Trailing Vortices - A Hazard to Operations", Astronautics & Aeronautics, December 1964.

Wetmore, Joseph W., and Reeder, John P., "Aircraft Vortex Wakes in Relation to Terminal Operations", NASA TN D-1777, April 1963.